MUTANT HUNTINGTIN-MEDIATED ALTERATIONS OF N-METHYL-D-ASPARTATE RECEPTOR CURRENTS AND DOWNSTREAM EVENTS UNDERLYING ENHANCED EXCITOTOXICITY IN HUNTINGTON'S DISEASE

by

HERMAN BRIAN FERNANDES

B.Sc., McMaster University, 1997
M.Sc., University of British Columbia, 2001

A THESIS SUBMITTED IN PARTIAL FULFILLMENT OF
THE REQUIREMENTS FOR THE DEGREE OF

DOCTOR OF PHILOSOPHY

in

THE FACULTY OF GRADUATE STUDIES

(Neuroscience)

THE UNIVERSITY OF BRITISH COLUMBIA

August 2007

ABSTRACT

Expansion of a CAG repeat in the Huntington disease (HD) gene results in progressive neuronal loss, particularly of medium-sized spiny neurons of the striatum (MSNs). Previous studies suggest that increased activity of N-methyl-D-aspartate (NMDA) receptors (NMDARs) and altered mitochondrial function contribute to selective neuronal degeneration. Here I utilized MSNs obtained from transgenic mice expressing human huntingtin (htt) on a yeast artificial chromosome (YAC) to study alterations in NMDAR function and possible downstream consequences, particularly in regards to altered calcium (Ca^{2+}) handling and mitochondrial function.

I examined the relationship between the length of the polyglutamine (polyQ) repeat in mutant htt (mhtt) and NMDAR currents in MSNs *in vitro*. I found that NMDAR current density was significantly enhanced in YAC72 MSNs compared to wild type (WT), YAC18, YAC46 and YAC128 MSNs, and that there was a trend toward larger NMDAR current density with increasing polyQ length for YAC18, YAC46 and YAC72 MSNs. This increase was selective for NMDARs and occurred in a neuronal type-specific fashion. The mechanism for increased NMDAR current in YAC72 MSNs appears due to a mhtt-mediated increase in trafficking of NMDARs to the plasma membrane.

While NMDA-induced apoptosis is enhanced in YAC128 MSNs, I found the initial steps in the intrinsic apoptotic pathway, including NMDAR current and cytosolic Ca^{2+} loading, are similar to those observed in WT MSNs. In contrast, the NMDAR-mediated Ca^{2+} load triggered a significantly greater depolarization of mitochondria in YAC128 MSNs, suggesting that NMDAR signaling via the mitochondrial apoptotic

pathway is altered. YAC128 MSNs demonstrated impaired cytosolic Ca^{2+} clearance following NMDA application, a difference that was not apparent following depolarization-evoked Ca^{2+} entry. Inhibitors of the mitochondrial permeability transition (mPT) reduced peak cytosolic Ca^{2+} and mitochondrial depolarization evoked by NMDA in YAC128, but not WT, MSNs. Hence, in contrast to YAC models with moderate CAG expansions, enhanced NMDA-induced apoptosis in YAC128 MSNs is largely due to augmented mitochondrial sensitivity to Ca^{2+}-induced activation of the mPT.

These findings suggest that the CAG repeat length can influence the mechanism by which mhtt enhances NMDAR-mediated excitotoxicity. However, as signaling pathways activated by strong NMDAR stimulation converge on mitochondria in all YAC HD models, bolstering mitochondrial function and/or inhibiting the mPT represent possible therapeutic targets.

TABLE OF CONTENTS

LIST OF TABLES

LIST OF FIGURES

LIST OF ABBREVIATIONS

3-NP, 3-nitropropionic acid

ADP, adenosine diphosphate

AM, acetoxymethyl

AMPA, α-amino-3-hydroxy-5-methyl-4-isoxazole-propionic acid

AMPAR, AMPA receptor

ANOVA, analysis of variance

ANT, adenine nucleotide translocase

APV, 2-amino-5-phosphonovalerate

ATP, adenosine 5'-triphosphate

AUC, area under the curve

BAPTA, 1,2-bis(2-aminophenoxy)-ethane-N,N,N',N'-tetraacetic acid

BDNF, brain-derived neurotrophic factor

BkA, bongkrekic acid

BSA, bovine serum albumin

BSS, balanced salt solution

C6R, caspase-6 resistant

CaBP, calbindin

cAMP, cyclic adenosine 5'-monophosphate

CBP, CREB binding protein

CCCP, carbonyl cyanide 3-chloro-phenylhydrazone

CGN, cerebellar granule neuron

CHO, Chinese hamster ovary

C/N ratio, CCCP/NMDA ratio

CNS, central nervous system

COS, Simian fibroblasts (CV-1 cells) transformed by SV40

CPN, cortical pyramidal neuron

CREB, cAMP response element binding protein

CsA, cyclosporin A

DARPP-32, dopamine- and cAMP-regulated phosphoprotein 32 kDa

$\Delta\Psi_m$, mitochondrial membrane potential

DNA, deoxyribonucleic acid

DRPLA, dentatorubral pallidoluysian atrophy

d.i.v., days *in vitro*

DMSO, dimethyl sulfoxide

EAA, excitatory amino acid

EC50, effective concentration to achieve 50% of maximal response

EPSC, excitatory post-synaptic current

ER, endoplasmic reticulum

FPL, FPL64176

GABA, γ-aminobutyric acid

GAD-65, glutamic acid decarboxylase

GluR, glutamate receptor

HAP-1, huntingtin-associated protein-1

HBSS, Hank's balanced salt solution

HD, Huntington's disease

HEK293 cells, human embryonic kidney 293 cells

HEPES, (N-[2-hydroxyethyl]piperazine-N'-[2-ethanesulfonic acid])

HIP-1, huntingtin-interacting protein-1

htt, huntingtin

IFN, ifenprodil

iGluR, ionotropic glutamate receptor

$\mathbf{I_{peak}}$, peak current

$\mathbf{IP_3}$, inositol 1,4,5-trisphosphate

$\mathbf{IP_3R}$, IP3 receptor

$\mathbf{I_{ss}}$, steady-state current

$\mathbf{K_d}$, dissociation constant

mGluR, metabotropic glutamate receptor

mhtt, mutant htt

MK-801, dizocilpine or (5R, 10S)-(+)-5-methyl-10,11-dihydro-5H-dibenzo[a,d]cyclohepten-5,10-imine hydrogen maleate

mPT, mitochondrial permeability transition

mRNA, messenger RNA

MSN, medium-sized spiny neuron of the striatum

NCX3, Na^+/Ca^{2+} exchanger isoform 3

NF-κB, nuclear factor kappa-B

NII, neuronal intranuclear inclusion

NMDA, N-methyl-D-aspartate

NMDAR, NMDA receptor

NR1, NMDAR subunit-1

NR2, NMDAR subunit 2

P, postnatal day

polyQ, polyglutamine

PSD-95, post-synaptic density protein 95 kDa

REST/NRSF, repressor element 1 (RE1)-silencing transcription factor (REST)/neuron-restrictive silencer factor (NRSF)

Rhod-123, rhodamine-123

RNA, ribonucleic acid

ROI, region of interest

SBMA, spinal bulbar muscular atrophy

SCA, spinocerebellar ataxia

SEM, standard error of the mean

TTX, tetrodotoxin

UV, ultraviolet

VDAC, voltage-dependent anion channel

VGCC, voltage-gated calcium channel

V_H, membrane holding potential

WT, wild type

YAC, yeast artificial chromosome

ACKNOWLEDGEMENTS

I would like to thank Dr. Lynn Raymond for many things, including her knowledge, insight, dedication, and for her supportive yet 'hands-off' style of supervision that allowed me to explore and expand my limits and abilities as a scientist. I would also like to thank the other members of my supervisory committee, including Drs. Ken Baimbridge, John Church, and Blair Leavitt for their guidance, ideas and help carrying out the various aspects of my research. I wish to particularly thank Drs. Church and Baimbridge for the use of their equipment and lab resources to carry out all of the imaging experiments presented here.

A number of other people in the lab have also provided help and support along the way. Bo Li gave me valuable advice while learning the patch-clamp technique, and Nansheng Chen shared with me the secrets of the theta-tube. Jacqueline Shehadeh, Mannie Fan, Tao Luo, Lily Zhang and Esther Yu all helped me with cell culture as well as other day-to-day matters too numerous to mention. Drs. Timothy Murphy, Cath Cowan, Austen Milnerwood, and Andy Shih, as well as Lavan Sornarajah, whiled away many an hour with me discussing ideas, enriching the quality of my work and work experience by their contributions.

I would also like to thank our collaborators, Drs. Michael Hayden, Blair Leavitt, and Rona Graham for providing and replenishing the transgenic mice which were essential to my project. Dr. Gordon Rintoul provided both analysis tools and valuable input regarding my work, and Drs. Claire Sheldon and Tony Kelly provided technical assistance. Lastly, I would like to thank the other members of the Kinsmen Labs for good times… good times.

DEDICATION

This work is dedicated to my former girlfriend and now wife Amanda, for her unconditional and endless patience and support throughout my graduate degrees.

I would also like to thank my family and friends for their support and sense of humour while I slowly but surely progressed towards finally finishing my education – for now....

Chapter 1

Introduction

1.1 Huntington's Disease

Huntington's disease (HD) is an inherited, progressive neurodegenerative disorder, with a prevalence of ~5-10 per 100 000 people (Vonsattel and DiFiglia, 1998). This genetic, autosomal dominant disease is caused by a mutation in exon 1 of the IT15 gene, resulting in the expansion of a CAG repeat (HDCRG, 1993) encoding a polyglutamine (polyQ) region in the protein huntingtin. Normal individuals have 35 or fewer CAG repeats (Kremer et al., 1994), while 36 or more CAG repeats results in the eventual development of the disease (Rubinsztein et al., 1996). HD is one of nine currently identified neurodegenerative diseases resulting from the expansion of a CAG tract within the coding region of nine different genes reviewed in (Tobin and Signer, 2000; Ross, 2002), which include spinocerebellar ataxia (SCA) 1, 2, 3, 6, 7, 17, spinal bulbar muscular atrophy (SBMA), and dentatorubral pallidoluysian atrophy (DRPLA).

1.1.1 Clinical Features of HD

The clinical presentation of HD includes a range of motor, cognitive and mood (emotional) changes. The age of onset generally occurs between the ages of 35-50, progressing over 15-20 years until death (Hayden, 1981). Motor symptoms include choreiform involuntary movements, postural imbalance, uncoordinated voluntary movements and dysphagia, followed at later stages by akinesia and rigidity. Depression is a common symptom, and patients often display personality changes such as apathy and

flashes of temper. Generally, emotional and cognitive changes precede the motor symptoms (Harper, 1996; Paulsen et al., 2001). Cases of juvenile-onset HD also occur and these cases have a somewhat different clinical presentation, with symptoms including bradykinesia, rigidity, dystonia, and often the presence of epileptic seizures (Vonsattel and DiFiglia, 1998). In contrast to the adult-onset form of HD, juvenile-onset patients often have little or no chorea (Brandt et al., 1996).

Expanded CAG regions show increased instability, particularly when passed via the paternal germline, with expansions in CAG length occurring more often than reductions. This produces the phenomenon known as anticipation, where the CAG repeat number tends to increase in subsequent family generations (Myers et al., 1982; Duyao et al., 1993). The age of onset of symptoms generally correlates inversely with the length of the CAG expansion (Andrew et al., 1993; Brinkman et al., 1997; Stine et al., 1993). Most adult-onset cases have CAG repeat lengths of 40-50, whereas juvenile-onset cases have somewhat longer CAG expansions (>60) (Brandt et al., 1996).

1.1.2 Neuropathology in HD

The pattern of neurodegeneration in HD is particularly selective for the medium-sized spiny neurons (MSNs) of the striatum, which normally project to other areas of the basal ganglia, specifically the substantia nigra and globus pallidus (Graveland et al., 1985), and make up approximately 95% of neurons in the striatum (Surmeier et al., 1988). In an extensive study characterizing postmortem HD brains, the highest degree of degeneration was found in the caudate and putamen (Vonsattel et al., 1985). The authors of this study used a five-point grading system (0-4) to describe striatal neuropathology in

ascending order of severity, correlating closely with the extent of clinical disability. For example in grade 0 HD brains no discernable neuropathological changes could be seen; in grade 1 brains there are only microscopic neuropathological changes (50% loss of neurons in the caudate nucleus) evident. The more severe cases showed increasing neuronal loss within the caudate as well as other striatal regions; for example, grade 4 brains show >95% neuronal loss in the caudate, as well as extensive neuronal losses in the putamen, globus pallidus and nucleus accumbens, accompanied by increasing numbers of astrocytes through grades 2-4 (Vonsattel et al., 1985).

MSNs are the first population of neurons to die, and generally show the greatest losses in numbers (Vonsattel and DiFiglia, 1998). In the early stages of HD, the subpopulation of MSNs expressing enkephalin and projecting to the external segment of the globus pallidus (the indirect basal ganglia pathway) die first, followed by the substance P-expressing MSNs (Richfield et al., 1995) that project to the internal segment of the globus pallidus (the direct basal ganglia pathway). Notably, the large aspiny cholinergic and nitric oxide synthase-containing interneurons are relatively spared (Ferrante et al., 1985; Ferrante et al., 1987). In later stage HD cases, a number of brain regions display atrophy, or a loss in cross-sectional area. The caudate and putamen show approximately 60% area loss whereas other brain regions (e.g. substantia nigra, globus pallidus, thalamus, hippocampus) display lesser atrophy of 20-30% in later stages (de la Monte et al., 1988; Cowan and Raymond, 2006). Hence, the striatum undergoes the greatest extent of neuronal loss, and in the most severe cases (grade 4) this results in a significant decrease in neuronal density despite the concurrent regional atrophy.

A loss of cortical neurons and volume also occurs in more advanced cases of HD, particularly loss of the large pyramidal neurons in layers III, V and VI which project directly to the striatum (Cudkowicz and Kowall, 1990; Hedreen et al., 1991).

1.1.3 Huntingtin: Distribution, Cellular Roles and Function

The protein huntingtin (htt) is widely distributed throughout many tissues of the body (Strong et al., 1993) and throughout most brain regions (Landwehrmeyer et al., 1995b) although there is no particular enrichment of the protein in the striatum (Sharp et al., 1995). Expansion of the CAG repeat region of the HD gene to produce polyglutamine expanded, mutant htt (mhtt) does not appear to alter the tissue distribution of the protein (Aronin et al., 1995). Htt is a 350 kDa cytosolic protein and can be found in the soma and throughout the dendrites as well as in synaptic terminals (Aronin et al., 1995).

To this point the function of htt is unknown. It has been found associated with membrane-bound organelles including mitochondria (Choo et al., 2004) and vesicular membranes (DiFiglia et al., 1995; Velier et al., 1998). Htt is also found in the nucleus, and this has implications for a possible role in gene transcription for both the normal and mutant forms (Kegel et al., 2002). Htt expression is essential for normal development, as disruption of the endogenous htt protein results in embryonic lethality (Leavitt et al., 2001; Nasir et al., 1995; Zeitlin et al., 1995). However, mhtt retains at least some of the developmentally required functionality of the wild type protein, as expression of mhtt can rescue the lethal suppression of endogenous htt expression (Leavitt et al., 2001).

In the context of the yeast artificial chromosome (YAC) mouse model, it could also be said that a function of htt is to prevent neuronal death, as overexpression of human htt with 18 glutamine repeats is neuroprotective against a variety of toxic insults in primary MSN cultures (Leavitt et al., 2006; Shehadeh et al., 2006), and endogenous murine htt counters the pro-apoptotic effects of human mhtt in YAC46 mice (Leavitt et al., 2001). Additionally, normal htt was found to have an anti-apoptotic effect against a number of pro-apoptotic stimuli in cloned striatal cells, acting upstream of caspase-3 activation (Rigamonti et al., 2000).

One controversy in the HD field revolves around the functions of htt and mhtt, specifically whether HD represents a gain of function of the mutant protein, or a loss of function of the normal protein. Several lines of evidence exist to support both sides of this argument. Conditional inactivation of endogenous htt in the brain of mice produced a progressively severe limb-clasping behaviour when picked up by the tail, a behaviour commonly observed in HD mouse models; this was accompanied by motor deficits progressing to hypoactivity and death by 13 months, with obvious striatal degeneration (Dragatsis et al., 2000). Additionally, mhtt retains at least some required activity of htt, as it can rescue the embryonic lethality of endogenous htt disruption in mice (Leavitt et al., 2001). These observations support the idea that the loss of htt function is sufficient to cause HD-like pathology. However, the case can also be made that this last observation supports a toxic gain of function in mhtt; since the mutant protein has been shown to retain some semblance of physiological function, an additional toxic function could be conferred by the mutation and would be necessary to produce the pathological changes associated with HD. Furthermore, HD shows a pattern of dominant inheritance,

suggesting that one copy of the mutant allele is sufficient; but again, this does not exclude a 'loss of htt function' component to the disease. Several clinical studies (Wexler et al., 1987; Myers et al., 1989; Durr et al., 1999) suggest that homozygous HD appears clinically identical to heterozygous HD, and as the normal allele does not improve disease phenotype, this suggests that normal htt function does not play a role in the development or progression of HD. However, methodological weaknesses in these studies render this evidence inconclusive (Cattaneo et al., 2001), and another study suggests that phenotype and disease progression are altered in HD patients with two mutant alleles compared to heterozygous HD patients (Squitieri et al., 2003). Overall, it is likely that both gain and loss of htt function contribute to the overall development and progression of HD.

1.1.4 Model Systems for the Study of HD

1.1.4.1 Heterologous Expression Systems

The simplicity and degree of control possible in heterologous expression systems made them an ideal starting point for examining the basis of mhtt-mediated toxicity. For example, the HEK293 cell line has been used extensively to study ionotropic glutamate receptor-mediated toxicity and function in the absence of htt (Monyer et al., 1992; Cik et al., 1994; Anegawa et al., 1995; Anegawa et al., 2000; Raymond et al., 1996), as well as the influence of overexpression of both htt and mhtt on N-methyl-D-aspartate receptor (NMDAR) function and excitotoxicity (Chen et al., 1999b; Zeron et al., 2001). Other cell lines such as COS and CHO cells have been used to also study NMDAR function and

toxicity (Boeckman and Aizenman, 1996; Anegawa et al., 2000; Rameau et al., 2000). The finding that expression of mhtt along with NMDARs composed of NR1 and NR2B subunits enhanced NMDAR current amplitude (Chen et al., 1999b), similar to subsequent observations in acutely dissociated and cultured MSNs (Zeron et al., 2002; Zeron et al., 2004), was the genesis for studies of NMDAR-mediated excitotoxicity in our laboratory (Zeron et al., 2001; Zeron et al., 2002; Zeron et al., 2004; Shehadeh et al., 2006) and indeed for the work presented here.

1.1.4.2 Mouse Models of HD

A number of different mouse models have been established as tools to provide insights into the pre-symptomatic changes, pathogenic mechanisms, progression of disease pathology, and possible areas of therapeutic intervention in HD. A summary of the relevant mouse models discussed here can be found in Table 1. A comprehensive summary of these and other models can be found courtesy of the Hereditary Disease Foundation (www.hdfoundation.org/PDF/hdmicetable.pdf). Generally speaking, the most commonly used models fall into one of three categories: transgenic mice expressing an N-terminal fragment of human htt containing an expanded CAG region (N-terminal fragment models); transgenic mice that express full length human htt in addition to their own endogenous murine htt (full length models); and knock-in mouse models where an expanded CAG repeat region has been inserted into the endogenous Hdh gene.

The most commonly used N-terminal fragment models are the R6/1 and R6/2 lines, expressing exon 1 of the human HD gene containing 116 and 144 CAG repeats, respectively (Mangiarini et al., 1996), with the R6/2 model showing the more aggressive

disease phenotype. Generally these models both feature early death (approximately 12 months for R6/1, 4 months for R6/2) preceded by an early onset of motor symptoms (as early as 1 month in R6/2) and overall brain atrophy (~20%, Davies et al., 1999) which is apparent prior to neuronal loss (Mangiarini et al., 1996). Another well characterized fragment model expresses an N-terminal fragment of 171 residues, which contains a CAG repeat length of 82 and also dies prematurely, having a lifespan between 2.5 to 11 months (Schilling et al., 1999). In a study comparing striatal gene expression changes mediated by a polyglutamine repeat expansion in the R6/2 and N171-82Q models, both models produce similar changes to striatal gene expression (Luthi-Carter et al., 2000), indicating common pathological changes. Interestingly, both of these models also display striatal resistance to excitotoxins after HD-like symptoms have developed (Hansson et al., 2001; MacGibbon et al., 2002; Jarabek et al., 2004), but they also lack frank striatal neuronal loss, which is inconsistent with the notable striatal degeneration in human postmortem HD brains. Hence one key criticism of these models may be that expression of the full-length htt gene, with all critical regulatory sequences, is required to most accurately reproduce the human disease. However, the aggressive pathology and shortened lifespan make toxic fragment models ideal for therapeutic testing in one sense, as beneficial effects of intervention will be more obvious than in a more discrete phenotype.

Knock-in HD mouse models generally exhibit a late onset of motor symptoms, with a relatively mild disease phenotype and little to no neuropathology evident, aside from predominantly striatal aggregate formation, despite longer CAG repeat lengths ranging from 72 up to 150 (Shelbourne et al., 1999; Wheeler et al., 2000; Lin et al., 2001;

Menalled et al., 2002; Menalled et al., 2003). One particular advantage of these models is the elimination of a key confounding factor in interpreting results from other HD models, that of htt (mutant or otherwise) overexpression. As well, the long lifespan make these models ideal for studying behavioural changes as a proxy for neuronal dysfunction prior to neuronal loss.

Full length models, such as the YAC mouse model (Hodgson et al., 1999; Slow et al., 2003) or the CMV promoter model (Reddy et al., 1998) recapitulate the pattern of selective striatal neuronal loss seen in human HD patients, making them ideal for studying changes in neuronal function that could underlie human disease. Therefore, the work presented here utilizes YAC mouse models of HD, which were developed at UBC in the Hayden lab. Mice in these models generally have a later onset (2-7 months, depending on the htt polyQ repeat length) of the HD motor phenotype, and have a relatively normal length lifespan (Hodgson et al., 1999; Slow et al., 2003; Van Raamsdonk et al., 2005). For this project, we made use of several different lengths of CAG repeat expansions to represent a range of human phenotypes, from non-pathogenic repeat lengths of 18 to sizes correlating to adult (46 repeats) and juvenile (72 or 128 repeats) HD (Hodgson et al., 1999; Slow et al., 2003). In this model, the full length human htt gene with a specific CAG repeat length and all regulatory domains is integrated into a YAC, leaving expression under control of the endogenous human HD promoter. Using this method, expression of transgenic htt is regulated in a developmentally and anatomically appropriate fashion. The expression of transgenic htt in the YAC lines used (YAC18 – line 212, YAC46 – line 668, YAC72 – line 2511, YAC128 – line 55) is approximately one third to one half the endogenous amount and

equivalent across genotypes (Hodgson et al., 1999; Slow et al., 2003); these lines were selected for use to minimize mhtt expression level-related phenomena, specifically differences in phenotype that could be attributed to the amount of transgenic protein expressed (Hickey and Chesselet, 2003; Graham et al., 2006a).

1.1.5 Mechanisms of Cellular Pathology in HD

There are several different mechanisms which have been proposed as the underlying cause of neurodegeneration in HD, based on evidence from a variety of sources including observations gleaned from examination of human brain tissue, study of HD model organisms, *in vitro* experiments in cellular preparations of both neuronal and non-neuronal origin, and *in vitro* experiments using isolated proteins and/or organelles. The work here focuses exclusively on one particular mechanism, the excitotoxicity hypothesis, which will be discussed in depth in a later section. Here I will describe several of the competing hypotheses, several (or all) of which may well act in concert to produce neuronal dysfunction and death in HD.

1.1.5.1 The Toxic Fragment Hypothesis

Both htt and mhtt can be proteolytically cleaved, producing N-terminal fragments which contain the polyQ domain. There is substantial evidence in the literature suggesting that htt is proteolytically targeted by the family of cysteine proteases known as caspases. There are both caspase-3 cleavage sites (residues 513 and 552) and a caspase-6 cleavage site (residue 586), which have been shown to be targeted *in vitro* (Wellington et al., 1998; Wellington et al., 2000). Mutation of these caspase cleavage

sites resulted in reduced apoptosis (both in neurons and non-neuronal cell lines) and protein aggregate formation (Wellington et al., 2000). The identification of htt as being cleaved by apopain (a cysteine protease, also known as caspase-3) led to the hypothesis that HD pathogenesis involved conditions where inappropriate apoptosis occurred, and that the cleavage fragments of mhtt could be the toxic agent (Goldberg et al., 1996). Expression of N-terminal htt fragments containing expanded polyQ regions has been demonstrated to be toxic by a number of studies (Martindale et al., 1998; Hackam et al., 1998; Cooper et al., 1998; Saudou et al., 1998), and it was proposed that proteolytic cleavage of mhtt produces toxic fragments containing expanded polyQ regions which are neurotoxic themselves, and in addition may also stimulate further proteolytic activity (Wellington and Hayden, 1997).

This idea gained further support with the demonstration that htt was proteolytically cleaved by caspase-3 *in vivo* in brains from both HD mouse models (Hodgson et al., 1999; Wellington et al., 2002) and human patients (Kim et al., 2001; Wellington et al., 2002). These N-terminal fragments derived from mhtt have been proposed to be more toxic than full-length mhtt (Wellington et al., 2000), and there may be a tissue-specific component to htt cleavage activity, as both N- and C-terminal htt fragments were found to be enhanced in the striatum of HD versus control brains (Mende-Mueller et al., 2001). This could be a result of enhanced cleavage of htt and/or impaired degradation of htt proteolysis products. Evidence for an increased rate of htt cleavage with increasing polyQ length (Goldberg et al., 1996) supports the idea that mhtt cleavage is enhanced, although other reports dispute this notion, suggesting either that that normal htt is more susceptible to cleavage than mhtt (Dyer and McMurray, 2001) or

that polyQ repeat length does not affect the likelihood of cleavage (Wellington et al., 1998).

It has been reported that htt from both human and mouse brain can also be cleaved by another family of cysteine proteases known as calpains (Kim et al., 2001). Gafni and Ellerby demonstrated that N-terminal htt cleavage fragments found in the caudate of HD patient post-mortem brain were products of calpain cleavage, and confirmed this finding *in vitro*; they did not find similar cleavage fragments in brain tissue from controls (Gafni and Ellerby, 2002). Studies using a chemical model of HD in rats found activated calpain selectively in the striatum, which was associated with the appearance of calpain cleavage products of htt (Bizat et al., 2003); another recent study using the same model found neuroprotection with memantine that coincided with reduced calpain activity (Lee et al., 2006). Further evidence of a role for calpain-mediated cleavage of htt in HD pathology was provided by a study demonstrating increased striatal and cortical calpain activity in a knock-in mouse model of HD, and that mutation of calpain-cleavage sites to produce a cleavage-resistant form of mhtt reduced toxicity in a cell line (Gafni et al., 2004).

Since it is established that (m)htt is a target for proteolytic cleavage, the question becomes how do these fragments of mhtt differ from cleavage products of htt to produce toxic effects?

1.1.5.2 Mhtt Aggregates and Inclusions Contain N-terminal Fragments

It was noted in the R6/2 model of HD that the appearance of neuronal intranuclear inclusions (NIIs) correlates with the onset of symptoms, and these NIIs contain both N-

terminal htt and ubiquitin (Davies et al., 1997). Similar NIIs have also been noted in the striatum and cortex of human brain tissue from HD patients, and N-terminal mhtt fragments were found in dystrophic neurites (Sapp et al., 1999). It appears that smaller htt fragments containing an expanded polyQ region preferentially form NIIs compared to larger fragments, and that the expanded polyQ region increases the susceptibility of cells to toxic stimuli (Hackam et al., 1998; Martindale et al., 1998), further implicating cleavage fragments of mhtt as potential toxic mediators underlying neuronal dysfunction in HD. It is notable that aggregates of mhtt are also ubiquitinated, suggesting that mhtt fragments are targeted for proteasomal degradation but cannot be processed and impair cellular function leading to degeneration (DiFiglia et al., 1997). This hypothesis is supported by the observation that the proteasomal degradation of another protein containing an expanded polyQ region, ataxin-1, is impaired, underlying aggregate formation and appearance of ubiquitinated nuclear inclusions in SCA-1 (Cummings et al., 1999). Hence the presence of aggregates may reflect an inability to process expanded polyQ repeats, leading to cell dysfunction and eventual death (Bence et al., 2001). Recent evidence from HD patient brains supports this deficiency as a factor in human disease development, as decreased proteasomal activity and association of ubiquitin with inclusions is noted particularly in the caudate and putamen in late stages (Seo et al., 2004).

Aside from possible effects on protein degradation, NIIs containing mhtt fragments have also been implicated in interference with transcriptional activity (Kegel et al., 2002), most notably binding to the transcriptional co-activator CREB binding protein (CBP) in models of HD (Nucifora et al., 2001; Steffan et al., 2000) and SBMA and SCA3

(McCampbell et al., 2000). Overexpression of CBP (McCampbell et al., 2000; Nucifora et al., 2001) or the application of HDAC inhibitors (McCampbell et al., 2001) successfully reduced toxicity in these models, implying that transcriptional repression is in part responsible for the toxicity in these disease models (Nucifora et al., 2001; Steffan et al., 2000).

Another possible mechanism for mhtt fragments to mediate toxicity would be through documented interactions with organelle structures, possibly impairing subcellular function. This localization characteristic may be a feature of the expanded polyQ repeat itself (Monoi et al., 2000). Caspase-3 cleavage fragments of mhtt have been shown to preferentially interact with membrane-bound structures (Kim et al., 2001). It has also been reported that fragments of mhtt, but not endogenous or non-pathogenic length htt, become lodged in the membranes of mitochondria from YAC72 mice, possibly compromising their bioenergetic functions (Panov et al., 2002). Another recent study demonstrated that the first 17 amino acids in the N-terminus of mhtt fragments alter association with the ER and Golgi as well as mitochondria, and cause acute dysfunction in isolated mitochondria (Rockabrand et al., 2006). The altered association of htt with these organelles caused by the polyQ expansion may also adversely affect organelle morphology and function (Hilditch-Maguire et al., 2000).

Recent studies concerning variants of the YAC128 HD mouse model provide further controversy regarding the toxic fragment hypothesis. The shortstop mouse (Slow et al., 2005) has a truncated form of htt expressed with an intact polyQ region of 128 repeats, and yet lacks any behavioural symptoms and shows no signs of neurodegeneration, seemingly contradicting the hypothesis that N-terminal mhtt

fragments are toxic on their own. Another interesting finding was that YAC128 mice expressing full length caspase-6 resistant (C6R) mhtt showed a remarkable lack of HD symptoms or neuropathological changes, whereas YAC128 mice expressing full length caspase-3 resistant mhtt resembled YAC128 mice in terms of behaviour, neuropathology, and neuronal toxicity (Graham et al., 2006b). Hence the toxic fragment hypothesis remains a controversial basis for explaining disease development and progression in HD.

1.1.5.3 Mhtt Expression is Associated with Transcriptional Deficiencies

A particularly interesting property of polyQ tracts is their tendency to fold into a β-sheet configuration (Chen et al., 2002), allowing both self-association and association with other proteins containing polyQ stretches through a polar zipper interaction (Perutz, 1994). This tendency underlies aggregation of polyQ-containing proteins, and occurs in proportion to polyQ length (Chen et al., 2001b).

As briefly mentioned earlier (see Section 1.1.5.1), mhtt interacts with a number of transcription factors and nuclear proteins including CBP, Sp1, p53, NF-κB, and several others, with the overall effect generally trending towards reduced transcriptional activity (Sugars and Rubinsztein, 2003). A number of striatal transcriptional and signaling pathways are altered by mhtt in two different HD mouse models, again the overall effect being a reduction in expression of striatal genes required for normal neuronal function (Luthi-Carter et al., 2000); this effect was found to be particularly evident with N-terminal fragments of mhtt (Chan et al., 2002). A recent study found that mRNA profiles in HD patient brains exhibited the greatest changes in the caudate

nucleus, followed by motor cortex and cerebellum, showing a parallel between molecular expression events and neuropathology in the human disease (Hodges et al., 2006).

One particularly well-studied consequence of mhtt-mediated transcriptional repression is the effect on brain-derived neurotrophic factor (BDNF) production, where mhtt expression decreases cortical production of BDNF at the transcriptional level, resulting in poor trophic support of MSNs (Zuccato et al., 2001). This result was noted in both human HD brain tissue as well as transgenic mouse HD models (R6/2 and N171-82Q), and the levels of cortical BDNF mRNA correlated well with HD disease progression in these mice (Zuccato et al., 2005). Normal htt is known to interact with the transcriptional repressor REST/NRSF and retain it in the cytosol, inhibiting its function and thus allowing transcription of BDNF, among other genes (Zuccato et al., 2003). However, mhtt loses this ability to restrict REST/NRSF translocation to the nucleus, resulting in suppression of BDNF transcription (Zuccato et al., 2003). Hence, transcriptional alterations may produce sub-optimal conditions for neuronal survival and promote dysfunction and premature death in HD.

1.1.5.4 Mhtt May Alter Trafficking of Several Cellular Components

As discussed earlier, htt is associated with vesicular membranes, providing possible clues to a physiological role. This is supported by the apparent functions of some its interacting proteins, particularly huntingtin interacting protein 1 (HIP-1) and huntingtin associated protein 1 (HAP-1).

HIP-1 is associated with the clathrin-mediated endocytosis pathway and is enriched on clathrin-coated vesicles (Metzler et al., 2001). HIP-1 is also a homologue of

the yeast protein Sla2p (Wanker et al., 1997), which is essential for appropriate cytoskeletal function (Kalchman et al., 1997). The strength of interaction between htt and HIP-1 is inversely proportional to the polyQ length, hence mhtt may indirectly, through its altered interaction with HIP-1, perturb membrane-cytoskeleton interactions (Kalchman et al., 1997). For example, HIP-1 has been strongly implicated in the normal endocytosis and trafficking of α-amino-3-hydroxy-5-methyl-4-isoxazole-propionic acid receptors (AMPARs; Metzler et al., 2003). Another possible manifestation of the aberrant mhtt-HIP-1 interaction is altered neurotransmitter release, as demonstrated in corticostriatal terminals in symptomatic R6/2 mice (Cepeda et al., 2003), and a reduction in the presynaptic vesicular pool in several transgenic HD mouse models.

The finding of a reduced presynaptic vesicle pool may also be attributed to the effect of mhtt expression on the association of HAP-1 with synaptic vesicles (Li et al., 2003b). HAP-1 also interacts with the cytoskeletal microtubule network via an association with dynactin, and is likely involved in intracellular vesicular transport (Engelender et al., 1997). In an interesting parallel to mhtt-mediated transcriptional inhibition of BDNF production, the transport of BDNF in corticostriatal axons and MSNs is impaired by mhtt, resulting in neurotoxicity (Gauthier et al., 2004; del Toro et al., 2006).

Mhtt also appears to interfere with the trafficking of organelles other than vesicles. A recent report noted that mhtt effectively limited the mobility of mitochondria along cortical neuronal processes, an event attributed to the enhanced ability of full length mhtt to form cytosolic aggregates (Chang et al., 2006). This impairment could reduce the ability of neurons to remove injured mitochondria, provide adequate energy

production at a given site, or prevent adequate and timely buffering of intracellular Ca^{2+} (Chang et al., 2006). Therefore mhtt can impair essential trafficking functions through several mechanisms, each of which may contribute to the underlying neuronal dysfunction in HD.

1.1.6 Summary

These are several of the main hypotheses for the underlying causes of neuronal dysfunction and eventual death in HD. There are several other hypotheses to explain the neuropathological changes seen in both the human condition and the changes in animal models (genetic and chemical models of HD) with substantial supporting evidence. The mechanisms of neuropathology are largely thought to be postsynaptic, and here I have grouped them under the umbrella of the excitotoxicity hypothesis of HD pathogenesis. This categorization best represents the underlying rationale for the research performed in support of this thesis project.

1.2 The Excitotoxicity Hypothesis in HD Pathogenesis

There are many lines of evidence which both directly and indirectly support the role of excitotoxicity in HD, from alterations of NMDAR function to bioenergetic impairment. Here I will provide an overview of evidence supporting the excitotoxicity hypothesis from human patients and *in vivo* and *in vitro* experiments using animal and cellular models. In doing so we will arrive at the hypotheses that we attempt to answer with this body of work.

1.2.1 Excitotoxicity Defined

Excitotoxicity in neurons is a toxic consequence of the actions of excitatory amino acids (EAAs), whether endogenous or exogenous (in the case of some chemical models in animals or *in vitro*). Within the CNS, since glutamate is the major excitatory neurotransmitter, excitotoxicity is generally considered to result from neurons being exposed to glutamate, either for prolonged periods or in excessive concentrations (Lucas and Newhouse, 1957; Olney, 1969). This can result in a number of pathological changes including ion influx, osmotic dysregulation, energy depletion and biochemical changes, eventually leading to cellular death (Sattler and Tymianski, 2001; Mattson, 2003).

Glutamate activates two classes of receptors in neurons: 1) metabotropic glutamate receptors (mGluRs), which exert their effects via coupling to G-proteins; and 2) ionotropic glutamate receptors (iGluRs), which upon binding of the appropriate ligands allow passage of cations through a channel pore formed by the receptor subunits (Dingledine et al., 1999). The most intensely studied of the iGluRs in excitotoxicity is the NMDAR, a subclass of receptor with several key features of relevance to neuronal death, i.e. a relatively high permeability to Ca^{2+} and relatively slow activation and deactivation kinetics.

1.2.2 General Properties of the NMDAR

NMDARs are heteromeric protein complexes, composed of two NR1 subunits and at least two NR2 subunits (Monyer et al., 1994; McIlhinney et al., 1998; Laube et al., 1998), most likely in a tetrameric configuration (Clements and Westbrook, 1991; Laube et al., 1998). Functional NMDARs require a combination of both NR1 and NR2 subunits

(Monyer et al., 1992). There are four different genes that encode the NR2 (NR2A, NR2B, NR2C, NR2D) subunits, and their expression is both developmentally and spatially regulated, on a cellular level as well as a brain-regional level (Ishii et al., 1993; Monyer et al., 1994; Akazawa et al., 1994; Laurie et al., 1997). There are eight possible splice variants of the NR1 subunit, generated at the mRNA level (Sugihara et al., 1992; Hollmann et al., 1993). The combination of NR1 splice variants with different NR2 subunits alters ion channel characteristics (Monyer et al., 1992; Ishii et al., 1993; Flint et al., 1997; Misra et al., 2000; Monyer et al., 1994; Chen et al., 1999a), providing significant potential for functional diversity.

Activation of the NMDAR ion channel complex requires concurrent events: the binding of the co-agonists glutamate and glycine, and depolarization of the plasma membrane. The binding site for glutamate is located on NR2 subunits (Anson et al., 1998; Anson et al., 2000), whereas glycine binds to the NR1 subunit (Kuryatov et al., 1994). Binding of the two co-agonists has the property of negative co-operativity (Regalado et al., 2001), thus ensuring that sufficient concentrations of both co-agonists must be present to activate the channel. Mg^{2+} physically blocks the NMDAR channel pore in a voltage-dependent fashion, requiring depolarization of the plasma membrane to allow channel function (Mayer et al., 1984; Nowak et al., 1984); this is physiologically achieved by the activation of postsynaptic AMPARs by synaptically-released glutamate. Activation of the NMDAR channel under physiological conditions allows for the conductance of cations, predominantly Na^{+} and Ca^{2+} influx accompanied by K^{+} efflux, with the Ca^{2+} component of the current being ~10-18% (Burnashev et al., 1995; Schneggenburger, 1996). Hence NMDARs are a major route for Ca^{2+} influx.

As mentioned above, NR2 subunit expression is both developmentally and spatially regulated. In the mammalian brain, certain brain regions characteristically express particular NR2 subunits (Akazawa et al., 1994; Monyer et al., 1994). In the adult forebrain, the main NR2 subunits expressed are NR2A and NR2B, indicating that the majority of NMDARs in these regions are diheteromers composed of either NR1/NR2A or NR1/NR2B, or are in a triheteromeric configuration of NR1/NR2A/NR2B (Sheng et al., 1994; Li et al., 1998; Chapman et al., 2003). These subunit combinations produce NMDARs that are similar in certain channel properties such as permeability to Ca^{2+}, single channel conductance, and sensitivity to voltage-dependent Mg^{2+} block. However, there are key differences between NR2A and NR2B subunits, both in terms of the functional properties they convey to channels, and how they are distributed on a subcellular level. NR2A and NR2B subunits have differential sensitivity to both agonists and antagonists (Buller et al., 1994; Vicini et al., 1998; Dingledine et al., 1999; Christie et al., 2000), and channel gating properties are altered in a subunit-dependent fashion (Monyer et al., 1994; Vicini et al., 1998). The NR2A receptor is generally expressed within synaptic NMDARs, and this subcellular expression pattern is considered to be a consequence of developmental regulation and synaptic maturation (Sheng et al., 1994; Li et al., 1998; Tovar and Westbrook, 1999; Chapman et al., 2003). In contrast, NR2B receptors appear to predominate at extrasynaptic sites (Li et al., 1998; Stocca and Vicini, 1998; Tovar and Wesbrook, 1999; Barria and Malinow, 2002) and the specificity of this spatial distinction between NR2A and NR2B expression patterns may reflect differential roles in determining cell survival and cell death (Hardingham et al., 2002; Hardingham and Bading, 2003; Liu et al., 2004; Massey et al., 2004). Interestingly the striatum

appears to express higher levels of NR2B relative to other NR2 subunits, compared to other regions of the brain; this pattern of expression is observed in several species, including man (Landwehrmeyer et al., 1995a; Rigby et al., 1996; Ghasemzadeh et al., 1996; Standaert et al., 1999; Kuppenbender et al., 1999; Li et al., 2003a).

1.2.3 The Basis for the Excitotoxicity Hypothesis in HD

Critical evidence to support the idea of excitotoxicity being involved in HD pathogenesis came from studies of post-mortem HD brains, showing a loss of striatal NMDAR binding sites (Young et al., 1988; Albin et al., 1990a; Albin et al., 1990b). These observations even extended to brains from individuals who were pre-symptomatic, indicating that NMDAR-expressing MSNs were at particular risk and loss occurred very early in disease progression, possibly underlying further symptoms. These observations correlate with the selective loss of MSNs in HD patient brains (Graveland et al, 1985).

A survey of transgenic HD mouse models also reveals changes in NMDAR composition and subunit expression. In the R6/2 mouse model, immunostaining of striatal NR2A and NR2B are both decreased in symptomatic mice, although NR1 immunostaining is enhanced (Cepeda et al., 2001b). Other studies in the same model showed that NR1 protein levels in brain homogenates were unchanged at 12 weeks, and striatal NMDAR binding had not changed (Cha et al., 1999). However, in another N-terminal fragment model (N171-82Q, see Section 1.1.4.2 and Table 1), no significant changes in NR1 or NR2B expression relative to controls were found (Jarabek et al., 2004). In the YAC mouse models, striatal NR1 and NR2B expression were similar in WT, YAC46 and YAC72 mice prior to any onset of symptoms (2 mos; Li et al., 2003a),

whereas in the more aggressive YAC128 model, striatal atrophy and neuronal loss were highly correlated with motor dysfunction (Slow et al., 2003). Therefore, while there is an inconsistency between the human disease and transgenic mouse models in terms of early-stage loss of MSNs, it is likely that HD produces a decrease in the overall number of functional NMDARs within the striatum. This may reflect a deficit in neuronal function, which can precede neuronal death (Van Raamsdonk et al., 2005). Changes in NMDAR function will be addressed in a later section.

1.2.3.1 Evidence From Chemical Models of HD Support the Excitotoxic Hypothesis

Several studies have demonstrated that intrastriatal injection of NMDAR agonists results in the selective loss of MSNs while sparing interneurons, reproducing many behavioural and neuropathological characteristics of HD (Schwarcz et al., 1984; Sanberg et al., 1989; Hantraye et al., 1990; Beal et al., 1986; Beal et al., 1991). Additionally, striatal MSNs show increased sensitivity to NMDA-induced swelling (a correlate of current and toxicity) compared with large-sized striatal interneurons, whereas kainate produced similar swelling in both neuronal populations (Cepeda et al., 2001a). Moreover, NMDAR agonists are more effective than other GluR agonists for inducing striatal neuronal excitotoxicity (DiFiglia, 1990). A different means of chemically inducing HD-like symptoms and neuropathology involves the use of inhibitors of mitochondrial complex II. Both malonate and 3-nitropropionic acid (3-NP) can be either injected intrastriatally, or interestingly enough, given systemically to rodents to produce selective degeneration of striatal MSNs (Beal et al., 1993b; Greene et al., 1993; Brouillet et al., 1995; Bogdanov et al., 1998), which can be blocked by NMDAR antagonists

(Greene et al., 1993; Bogdanov et al., 1998). While these models effectively replicate many aspects of advanced HD, they cannot be used to study early presymptomatic changes, which may be critical to understanding disease pathogenesis and dysfunction prior to neuronal death. However, these models do provide further evidence for the excitotoxic involvement of NMDARs in HD pathogenesis, and in the case of mitochondrial complex II inhibitors, implicate mitochondrial dysfunction as a predisposing factor in excitotoxicity in HD.

1.2.4 Alterations of NMDAR Function in HD models

Given the likely involvement of NMDARs in HD pathology, whether causative or not, there has been a great deal of interest addressing the question of whether NMDAR function in HD models is altered, and if so, how? Studies in intact HD animal models, *in vitro* preparations derived from HD model animals, and heterologous systems have been performed to answer this question.

The most direct method to look for potential HD-associated changes in NMDAR function would be observation of NMDAR function through electrophysiological means. A number of studies have demonstrated enhancement of NMDAR currents, in several different transgenic HD mouse models.

1.2.4.1 NMDAR Currents in HD Models

Enhancement of NMDAR currents was observed in MSNs acutely dissociated from striata of both pre-symptomatic and symptomatic R6/2 mice (Starling et al., 2005). The same study also observed decreased sensitivity of NMDAR currents to Mg^{2+} block in

a subpopulation of MSNs which had significantly larger NMDAR currents, possibly reflecting an alteration of NMDAR subunit composition. This observation extended to MSNs from pre-symptomatic mice, indicating altered NMDAR function prior to any apparent onset of symptoms. NMDA-evoked currents in striatal slices taken from both pre-symptomatic and symptomatic R6/2 mice are increased over WT, whereas in the same mice AMPA-evoked currents are actually smaller, indicating a process selective for NMDARs (Cepeda et al., 2001b). Later studies in this same model demonstrated that this enhancement of NMDAR current is specific for the striatum, as cortical NMDAR-mediated currents were not enhanced (Andre et al., 2006). These enhanced striatal NMDAR currents also explain an earlier observation of enhanced swelling of MSNs in R6/2 striatal slices compared to slices from WT animals in response to exogenous NMDA application, an observation which was also confirmed with MSNs in slices from a knock-in HD mouse model with a polyQ length of 94 (Levine et al., 1999). Similar observations were also documented in another N-terminal fragment model of HD (with a polyQ length of 100 contained within the N-terminal third of the human htt gene), showing significant enhancement of NMDAR peak currents and current density in MSNs from striatal slices (Laforet et al., 2001).

Our lab has reported similar changes in NMDAR function in the YAC mouse models of HD. Acutely dissociated MSNs from 6-11 week old YAC72 animals had increased NMDAR peak current densities relative to those in MSNs from WT animals (Zeron et al., 2002). This age corresponds to the pre-symptomatic period in these animals, indicating that aberrant NMDAR activity may be present prior to, and possibly play a causative role in, any noticeable behavioural changes associated with HD. As

these data were obtained using exogenously applied NMDA and stimulating presumably extrasynaptic NMDARs, subsequent studies focused on possible changes in synaptic NMDAR properties produced by mhtt. Synaptic NMDAR currents recorded from MSNs in corticostriatal slices from YAC72 mice were also found to be enhanced compared to those recorded from WT mice, and this enhancement was found to reflect a postsynaptic NMDAR-selective mechanism (Li et al., 2003a; Li et al., 2004), suggesting that mhtt preferentially modulates NMDAR function.

1.2.4.2 The NR2B-Selective Hypothesis of Mhtt-Mediated Enhancement of NMDAR Function

The first demonstration of an effect of mhtt on NMDAR function was in a study where NMDARs, composed of either NR1/NR2A or NR1/NR2B, were expressed in conjunction with full length human htt containing either 15 or 138 polyQ repeats (Chen et al., 1999b). The authors observed that mhtt enhanced the responses of NMDARs composed of NR1/NR2B, whereas NR1/NR2A NMDARs were not differentially affected by the presence of htt or mhtt (Chen et al., 1999b). These results were underscored by a later finding that mhtt selectively enhanced apoptotic cell death in HEK cells co-transfected with NR1/NR2B (Zeron et al., 2001), indicating a possible preferential modulation of NR2B-containing NMDARs by mhtt (the NR2B-selective hypothesis).

The possibility that the NR2B subunit could be necessary for selective modulation by mhtt is not surprising, considering that the adult striatum is enriched in NR2B (as mentioned previously). In the same paper that demonstrated enhanced NMDAR currents in acutely dissociated MSNs from YAC72 mice, the authors found that greater than 50%

of the NMDAR current was mediated by NR1/NR2B NMDARs (Zeron et al., 2002). This work provided several other supporting lines of evidence for a specialized role for NR2B in mhtt-mediated changes in NMDAR function. In conjunction with enhanced NMDAR currents in YAC72 MSNs NMDA-induced apoptosis was enhanced in YAC72 vs. WT MSNs, but there was no differential effect observed in cerebellar granule neurons (CGNs), which did not express NR2B under the culture conditions used. The NR1/NR2B selective antagonist ifenprodil (IFN) effectively reduced apoptosis in both WT and YAC72 MSNs (Zeron et al., 2002), providing further evidence of the important role that this particular NMDAR subunit combination may play in mediating mhtt-enhanced excitotoxic cell death in MSNs.

1.2.4.3 Neurotoxicity as an Indicator of PolyQ Length-Dependent Alterations in NMDAR Function by Mhtt

Building on the aforementioned studies in support of the NR2B-selective hypothesis (Chen et al., 1999b; Zeron et al., 2001; Zeron et al., 2002), the influence of the polyQ length in mhtt on neurotoxicity, and in particular apoptosis, was further examined. Cultured YAC72 MSNs were more susceptible to NMDA-induced toxicity than WT MSNs, although no difference was observed between the two genotypes in response to AMPA application (Zeron et al., 2002), supporting observations of selective enhancement of NMDAR currents in corticostriatal slices (Li et al., 2003a; Li et al., 2004) and correlating electrophysiological observations with neurotoxicity (Zeron et al., 2002). Additionally, it was found that the enhancement of apoptosis by mhtt in YAC46 and YAC72 MSNs was proportional to the length of the polyQ repeat (Zeron et al.,

2002). This observation was further bolstered by a subsequent study demonstrating that rates of NMDA-induced apoptosis induction were maximal and equivalent in YAC72 and YAC128 MSNs when saturating concentrations of NMDA were used, with YAC128 MSNs showing enhanced sensitivity to apoptosis at subsaturating concentrations of NMDA (Shehadeh et al., 2006). An IFN-sensitive enhancement of glutamate-induced apoptosis in YAC128 relative to WT MSNs was also reported by another group (Tang et al., 2005).

1.2.5 Downstream Consequences of NMDAR Activation in Cells Expressing Mhtt

A recent paper by our lab illustrated how polyQ length influences the induction of apoptosis in MSNs (from YAC HD mice) in response to a number of noxious stimuli that increase intracellular Ca^{2+}, and found that YAC128 MSNs are generally more sensitive to most toxic stimuli; however, the most effective inducer of neuronal apoptosis relative to control YAC18 MSNs was NMDAR activation (Shehadeh et al., 2006). This finding illustrates how the presence of mhtt may preferentially affect the relationship between intense NMDAR stimulation and the resultant intracellular Ca^{2+} elevations in a manner that results in neuronal death.

1.2.5.1 Ca^{2+} Homeostasis is Affected by Mhtt

A number of damaging events can ensue from an excessive amount of free cytosolic Ca^{2+}, which is a downstream consequence of NMDAR activation in MSNs in the presence of mhtt (Zeron et al., 2004; Tang et al., 2005; Shehadeh et al., 2006). These could include inappropriate enzyme activation (i.e. calpains, calcineurin, other Ca^{2+}-

regulated enzymes) and mitochondrial dysfunction (elaborated on below) which in turn has a number of toxic consequences. There is evidence from several HD models that the regulation of intracellular Ca^{2+} is altered in several ways, although not always predictably. For example, resting Ca^{2+} levels are elevated in MSNs from R6/2 mice (Hansson et al., 2001), hippocampal neurons in YAC72 mice and an immortalized cell line derived from striatal neurons from a knock-in HD mouse model (Seong et al., 2005). On the other hand, in studies using primary MSN cultures from YAC mice resting Ca^{2+} levels were equivalent between WT, YAC46 and YAC72 MSNs (Zeron et al., 2004) and WT, YAC18 and YAC128 MSNs (Tang et al., 2005). The former study found that stimulation of NMDARs in mhtt-expressing MSNs resulted in elevated Ca^{2+} levels relative to controls. Additionally, the latter study by Tang et al., (2005) in YAC128 MSNs found increased cytosolic Ca^{2+} levels in YAC128 MSNs following glutamate stimulation that were attributed in part to enhanced IP_3 receptor-mediated Ca^{2+} release from the ER, downstream of mGluR1/5 activation, as mhtt was found to sensitize the IP_3 receptor (IP_3R) (Tang et al., 2003). Hence not only does mhtt appear to enhance NMDAR activity, and subsequently Ca^{2+} influx via NMDARs (Zeron et al., 2004), but it may also enhance the probability of intracellular Ca^{2+} release. Similar findings of mhtt-enhanced NMDAR-mediated Ca^{2+} entry in MSNs have been found in N-terminal fragment HD models, including the R6/2 (Cepeda et al., 2001b) and tgHD100 mice (Laforet et al., 2001). Importantly, these findings of altered Ca^{2+} regulation in YAC HD mice have been observed in MSNs obtained from early postnatal mice (Zeron et al., 2004; Tang et al., 2005), implying that these changes are present at birth and may over time increase the risk of neuronal dysfunction and death.

Shehadeh et al., (2006) compared the toxic effects of Ca^{2+} influx via both NMDAR and non-NMDAR routes, and the findings raised two particularly important points to consider: 1) the route of Ca^{2+} entry could play a significant role in determining the extent of toxicity; 2) The level of toxicity produced by NMDAR activation in the presence of mhtt may be proportional to cytosolic Ca^{2+} elevations.

Addressing the first point, previous work suggests that mitochondria preferentially buffer Ca^{2+} entering via NMDARs, the so-called privileged access hypothesis (Peng and Greenamyre, 1998; Sattler et al., 1998). As NMDAR activation and consequent Ca^{2+} entry are increased in MSNs expressing mhtt, the possible consequences of this preferential pathway include enhanced mitochondrial stress, free radical generation, loss of adenosine 5'-triphosphate (ATP)-generating capability, and generalized mitochondrial dysfunction, which could result in the eventual activation of the intrinsic apoptotic pathway. The finding that NMDA application was a more potent inducer of apoptosis than other means to raise intracellular Ca^{2+}, such as treatment with Ca^{2+} ionophores or membrane depolarization, is consistent with this hypothesis.

As to the second point, evidence from our lab has shown that NMDAR currents (Zeron et al., 2002; Zeron et al., 2004) and Ca^{2+} influx downstream of NMDAR activation (Zeron et al., 2004) are both enhanced in YAC72 compared to WT MSNs, correlating with enhanced apoptosis levels in YAC72 MSNs compared to controls (Zeron et al., 2002; Shehadeh et al., 2006). This difference in apoptosis was abolished by using the competitive NMDAR antagonist 2-amino-5-phosphonovalerate (APV) to reduce NMDAR-mediated Ca^{2+} influx in YAC72 MSNs down to a level equivalent to that seen in WT MSNs. This indicated that the enhanced level of neurotoxicity produced by

NMDAR activation in the presence of mhtt is due to the augmentation of NMDAR function by mhtt in YAC72 MSNs (Shehadeh et al., 2006). A relationship where increased cytosolic Ca^{2+} corresponded to increased neuronal death following stimulation with glutamate was also found with YAC128 MSNs (Tang et al., 2005).

1.2.6 Mitochondrial and Bioenergetic Impairment in HD

Given the influence that mhtt exerts on both NMDAR function and subsequent Ca^{2+} entry and regulation, it follows that by virtue of these changes mitochondrial responses will also be affected. While there is direct evidence of this, there is also evidence that mhtt may independently impair mitochondrial function via different mechanisms.

Mitochondria have an electrochemical gradient across their inner membrane established by the active extrusion of H^+ ions, in order to couple re-entry of protons to oxidative phosphorylation in the generation of ATP. Mitochondria may also utilize this gradient to drive the uptake of Ca^{2+} from the cytosol in situations where local concentrations exceed ~ 1 μM (Nicholls and Ward, 2000). During this process the mitochondrial membrane potential ($\Delta\Psi_m$) is dissipated; under normal conditions it is re-established through continued activity of active H^+ transport, but excessive mitochondrial depolarization is associated with increased risk of apoptotic neuronal death (Schinder et al., 1996). NMDAR activation in YAC46 and YAC72 MSNs has been shown to produce enhanced mitochondrial depolarization, associated with increased cytosolic Ca^{2+} levels and apoptosis as noted earlier (Zeron et al., 2004; Shehadeh et al., 2006). Compounding this is the observation that mitochondria isolated from HD patients, as well as from

YAC72 mice, tend to have a reduced resting $\Delta\Psi_m$ and depolarize to a greater extent when stressed (Sawa et al., 1999; Panov et al., 2002), and that expression of mhtt may reduce the ability of mitochondria to re-establish baseline $\Delta\Psi_m$ (Oliveira et al., 2006). These observations demonstrate that mhtt-mediated changes in NMDAR function can have negative consequences to neuronal health beyond altered activity of the receptor itself.

Ca^{2+} cycling between the mitochondria and cytosol occurs normally as a consequence of physiological activity, such as during synaptic activity. However, under conditions where excessive concentrations of Ca^{2+} are achieved, such as during an excitotoxic stimulus, mitochondrial Ca^{2+} uptake leads to pathological activation of a conductance known as the mitochondrial permeability transition (mPT; White and Reynolds, 1996; Crompton, 1999; Dubinsky and Levi, 1998), which is associated with apoptotic neuronal death processes ((Marchetti et al., 1996; Nicholls and Budd, 1998; Brustovetsky et al., 2002). The mPT is formed by the association of several mitochondrial membrane proteins, including the voltage-dependent anion channel (VDAC), adenine nucleotide translocase (ANT), and cyclophilin D to create a pore with a conductance of ~1.5 kDa, allowing the movement of ions and small proteins out of the mitochondria (Bernardi et al., 1994; Petit et al., 1996; Green and Reed, 1998). Activation of the mPT short-circuits $\Delta\Psi_m$, preventing ATP generation and allowing the release of Ca^{2+} and apoptotic factors into the cytosol (Green and Reed, 1998; Crompton, 1999; Duchen, 2004; Orrenius, 2004). NMDA-induced mPT activity has been previously observed in murine MSNs (Alano et al., 2002), and inhibitors of mPT formation have been shown to prevent NMDA-induced apoptosis in YAC HD MSN culture preparations including YAC46 and YAC128 (Zeron et al., 2004; Tang et al., 2005). The release of

cytochrome c from mitochondria has been shown to occur following NMDAR stimulation in primary MSN cultures from YAC128 mice (Tang et al., 2005), indicating induction of the mPT and intrinsic apoptotic pathway.

A number of observations, from alterations in energy status indicators to direct physical interactions, in both human HD patients and HD models, have indicated that mhtt may directly impair mitochondrial function. Reduced levels of cAMP have been reported in the cerebrospinal fluid, brain tissues and lymphoblasts of HD patients (Cramer et al., 1984; Gines et al., 2003), and striata of HD knock-in mice (Wheeler et al., 2000) while lactate levels seem to be increased (Jenkins et al., 1993; Koroshetz et al., 1997), possibly indicating a shift to greater reliance on glycolytic ATP generation. Consistent with this idea are observations of reduced cAMP generation and decreased ATP:ADP (Gines et al., 2003; Seong et al., 2005) accompanied by reduced mitochondrial ATP levels (Seong et al., 2005) in a cell line (ST*HdH*^{Q111}) derived from MSNs from a knock-in HD mouse model. Other studies of human HD brain tissue have noted decreased enzyme activity in a number of electron transport chain components, including complexes II, III and IV (Brennan et al., 1985; Beal, 1995; Gu et al., 1996; Browne et al., 1997) as well as other enzymes (i.e. aconitase) involved in mitochondrial ATP generation (Tabrizi et al., 1999). Studies on mitochondria isolated from both human and YAC HD mice are more depolarized at rest, and are more sensitive to imposed Ca^{2+} loads, which may be due to direct interactions between mhtt (or polyQ)-containing protein fragments and mitochondria (Panov et al., 2002; Choo et al., 2004). Other studies which have focused on mitochondrial function, by the use of either mitochondrial toxins (Sawa et al., 1999; Shehadeh et al., 2006) or conditions where mitochondria are solely relied upon for

energy production (Oliveira et al., 2006), indicate that mitochondrial function is impaired by expression of mhtt. Indeed, defects in mitochondrial complex II have been noted in HD patient brains and MSNs expressing HttN171-82Q (Benchoua et al., 2006). Lastly, the aforementioned studies using systemic inhibitors of mitochondrial complex II to mimic HD pathology in animal models (Beal et al., 1993a; Brouillet et al., 1993; Palfi et al., 1996) broadly illustrate that mitochondrial dysfunction, either alone or in conjunction with upstream alterations in NMDAR function and Ca^{2+} handling changes, may impact neuronal survival in the context of HD.

1.3 Research Hypotheses and Goals

The results of this thesis project have been divided into three chapters, each representative of a different phase of the project, correspondingly driven by changing hypotheses along the way.

Our initial goal was to characterize the electrophysiological properties of NMDARs in primary cultures of MSNs from YAC HD mice, with several hypotheses inherent in the objectives, as described in Chapter 3: 1) We wanted to correlate NMDAR current amplitudes within primary MSN cultures to the observed NMDA-induced apoptosis, and hypothesized that the amplitude of NMDAR currents would correlate with increasing polyQ lengths in the YAC HD mice, thus explaining enhanced neurotoxicity with increasing polyQ length. Characterization of NMDAR current in the YAC HD mouse model had not been done in cultured primary MSNs, which was the preparation used for many of the toxicity studies (Zeron et al., 2002; Graham et al., 2006b; Shehadeh et al., 2006). We started with WT, YAC18, YAC46 and YAC72 mice (Hodgson et al.,

1999), with the later addition of YAC128 mice as that model became available (Slow et al., 2003) for testing. 2) We hypothesized that any enhancement of NMDAR activity that could be correlated to increased apoptosis would be selective for NMDARs and not other glutamate receptors, and that there would be neuronal-type specificity to explain selective striatal loss in HD. 3) Given the possibility of an NR2B-related component to augmentation of NMDAR function by mhtt, we hypothesized that mhtt might alter the subunit composition of NMDARs in a striatal-specific fashion. 4) Having examined the relationship between polyQ length and NMDAR current density in the various YAC HD mouse lines and finding a significant difference, we then attempted to address the underlying mechanisms for this observation.

Given the findings regarding the characterization of NMDAR properties in MSNs from HD mice described in Chapter 3, our overall objective for the experiments outlined in Chapters 4 and 5 was to explain the enhanced sensitivity to NMDAR-mediated apoptosis in YAC128 MSNs in the absence of enhanced NMDAR function. Using fluorescent imaging techniques, the hypotheses investigated were as follows: 1) Ca^{2+} homeostasis was altered in YAC128 MSNs, and our hypothesis was that resting Ca^{2+} levels or responses to NMDAR-mediated Ca^{2+} entry would be augmented in a toxic fashion. 2) Although we did not find any genotypic differences in the magnitude of Ca^{2+} responses, we did observe a difference in recovery rate from an intracellular Ca^{2+} load. We hypothesized that YAC128 MSNs could have a generalized defect in Ca^{2+} handling, and designed experiments to address this possibility. 3) Having observed mitochondrial membrane potential changes downstream of NMDAR and cytosolic Ca^{2+} changes in YAC46 and YAC72 MSNs (Zeron et al., 2004), we hypothesized that a similar event in

YAC128 MSNs could perhaps explain their enhanced rates of NMDAR-mediated apoptosis. To address this question, we simultaneously monitored changes in cytosolic Ca^{2+} and $\Delta\Psi_m$, and attempted to define the relationship between the two parameters.

This thesis describes a transition of hypotheses that were initially focused on describing broad trends to provide a unifying theory describing neurotoxicity in YAC HD mouse models. Subsequently my research became focused on neurotoxic events within one particular HD mouse model, the YAC128 model, which exemplified enhanced neuronal apoptosis via a mechanism contrary to our initial hypotheses.

Chapter 2

Materials and Methods

2.1 Animals

Primary striatal neuronal cultures were prepared from offspring of breedings between two homozygous yeast artificial chromosome (YAC) transgenic mice on a pure FVB/N strain background (Hodgson et al., 1999; Slow et al, 2003). YAC46 (line 668), YAC72 (line 2511) and YAC128 (line 55) mice expressed full length human mhtt containing 46, 72 or 128 glutamine repeats. These mice were compared to both FVB/N WT mice and in some experiments compared against YAC18 (212 line) mice, which express full length human htt but contain a non-pathogenic number (18) of glutamine repeats. All mice were bred and maintained according to Canadian Council on Animal Care (CCAC) and UBC Animal Care guidelines.

2.2 Primary Neuronal Cultures

2.2.1 Preparation of Primary Striatal Neurons

Primary MSN cultures were prepared as previously described (Zeron et al., 2004; Shehadeh et al., 2006). Briefly, sterile poly-D-lysine (low molecular weight, MW 30-70K, 50 μg/ml) coated glass coverslips (12 mm; Paul Marienfeld GmbH & Co. KG, Lauda-Königshofen, Germany) were placed in 24-well plates, and allowed to dry prior to culturing. Striata were dissected from postnatal day 0-1 (P0-P1) mice in Hank's Balanced Salt Solution (HBSS) on ice and then digested in warmed (37°C) papain solution (HBSS,

40 U/ml papain) for ten minutes. Cells were pelleted by centrifugation, then further dissociated using a series of reducing bore-size Pasteur pipettes in warmed trypsin inhibitor solution (containing Neurobasal media, 0.25% bovine serum albumin, 0.25% trypsin inhibitor, 20 μg/ml DNAse) and subsequently transferred to warmed serum-free plating media containing Neurobasal medium with 2% B27 without supplements, 2 mM L-glutamine, and 1% penicillin/streptomycin.

Neurons were plated at a density of approximately 5.0×10^5 cells/well (1.0×10^6 cells/ml), and incubated (37°C, 5% CO_2) for 9-12 days. In order to maintain the cells, every 4-5 days half of the medium was replaced with fresh medium. Approximately 80-90% of cells cultured in this serum-free medium have the characteristics of medium-sized spiny neurons (MSNs), as evidenced by morphology, DARPP-32 staining, and/or staining for the GABAergic neuronal marker glutamic acid decarboxylase-65 (Hansson et al., 1999; Kovacs et al., 2001; Shehadeh et al., 2006). In all experiments measurements were taken only from cells with morphological features consistent with MSNs, including an ovoid soma with a short diameter of approximately 10 μm and 2-4 short projecting processes (Shi and Rayport, 1994).

2.2.2 Preparation of Primary Cortical Neurons

Primary cortical neuronal cultures were occasionally prepared in parallel from the same animals used for MSN cultures, and in largely similar fashion with a few differences. Cells obtained from cortical tissue were plated in Neurobasal medium with a composition identical to that used for MSN cultures, except for a lower concentration of L-glutamine (0.5 mM) used in the plating medium. Cortical neurons were plated at a

density of 3.0 x 10^5 cells/well (5.0 x 10^5 cells/ml), and incubated (37°C, 5% CO_2) for 4-21 days. In order to maintain the cells, every 4-5 days half of the medium was replaced with fresh medium. In all experiments measurements were taken only from cells with morphological features consistent with cortical pyramidal neurons (CPNs), including a general pyramidal (triangular) somatic structure with prominent neurites (de Lima et al., 1997).

2.2.3 Preparation of Primary Cerebellar Granule Neurons

Primary cultures of cerebellar granule neurons (CGNs) were prepared to provide a control for the selectivity of IFN for NR1/NR2B-containing NMDARs. CGNs prepared in the manner described here express NMDARs that lack NR2B by 9 d.i.v. (Vallano et al., 1996), and thus NMDAR currents in these cells should not be sensitive to IFN antagonism (see Results, Figure 7B). Coverslips (12 mm) were prepared as described for MSN cultures. Cerebella were dissected from P7-P9 mice in HBSS on ice, and then digested for 15 min in a warmed (37°C) papain solution (HBSS, 60 U/ml papain). Cells were pelleted and resuspended in trypsin inhibitor solution (same composition as that used for MSN cultures), and passed through either polished Pasteur pipettes or a 5 ml plastic culture pipette with a standard yellow 100 µl plastic tip on the end. After several passes, the cell suspension was placed on ice for 2-3 minutes, during which time clumps of non-dissociated tissue settled to the bottom. The supernatant (containing single cells) was carefully removed with a pipette, DNAse (final concentration 20 µg/ml) was added, and the suspension was centrifuged to produce a pellet. After the cells were resuspended in ice-cold HBSS they were centrifuged at 4°C for 15 min @ 2000 RPM through 40.5%

Percoll. The resulting cell pellet was resuspended in cerebellar plating media (Basal Medium Eagle with Earle's salts from Invitrogen, containing 10% heat-inactivated fetal bovine serum, 1% penicillin/streptomycin, 2 mM L-glutamine, 25 mM KCl, 17 mM D-glucose), re-spun for 1 min, and the resulting pellet resuspended in warmed (37°C) cerebellar plating medium. CGNs were plated at a density of 5.0 x 10^5 cells/well (1.0 x 10^6 cells/ml), and incubated (37°C, 5% CO_2) for 8-10 days.

2.3 Electrophysiological Experiments

All MSNs were used for electrophysiological analysis at 9-11 days *in vitro* (d.i.v.); CPNs were used at 4-7 d.i.v., whereas CGNs were recorded from between 8-10 d.i.v. Coverslips with cultured neurons were placed in the recording chamber on the stage of an inverted microscope (Axiovert 100, Carl Zeiss, Thornburg, NY). Intracellular recording solution contained: 115 mM $CsMeSO_3$, 10 mM HEPES, 10 mM BAPTA, 4 mM Mg-ATP, 20 mM K_2-creatine phosphate, and 50 U/ml creatine phosphokinase, titrated to pH 7.25 using CsOH and with an osmolarity of 309-310 mosm. Extracellular recording solution contained: 167 mM NaCl, 2.4 mM KCl, 1.8 mM $CaCl_2$, 10 mM HEPES, 10 mM D-(+) glucose, titrated to pH 7.3 using NaOH and with an osmolarity of 325 mosm. Both intracellular and extracellular solutions were filtered prior to use. In all experiments, 50 μM glycine and 0.3 μM tetrodotoxin (TTX; to block voltage-gated sodium currents) were added to all extracellular solutions. Superfusion of neurons with different agonist solutions was achieved using a gravity-fed solenoid system attached to a theta tube. Currents were sampled at 5 kHz and acquired and analyzed using pCLAMP

software and an Axopatch 200A amplifier (Axon Instruments, Foster City, CA). Current amplitude measurement and kinetics fittings were performed using Clampfit software.

2.3.1 Measurement of Current Density, Steady-State to Peak Ratio, Ifenprodil Sensitivity

Primary neuronal cultures were prepared as described, and whole-cell currents were recorded under voltage clamp (V_H = -60 mV; except where otherwise noted). All currents were leak-subtracted prior to analysis. NMDAR currents were elicited by a 4s application of 1 mM NMDA. This was repeated twice at 60s intervals, for a total of 3 separate trials. Peak current density was calculated by dividing the peak current amplitude by the cell capacitance, thus normalizing current to cell surface area (allowing comparisons between cells with potentially different membrane surface areas). NMDAR steady-state to peak current ratios (I_{ss}/I_{peak}) were calculated by averaging NMDAR currents over the last 200 ms prior to cessation of NMDA application (to get a measure of steady-state current) and then dividing by the peak current amplitude and expressing the ratio as a percentage. This was done for each cell using the first and second trials (to minimize any effect of rundown), so that the I_{ss}/I_{peak} expressed for each cell is an average of two responses.

The NMDA stimulation paradigm was then repeated in the presence of 3 μM ifenprodil (IFN), for a total of 3 trials. The percentage of current inhibited by IFN was calculated by dividing the average peak NMDAR current of the last two responses in the presence of IFN by the peak NMDAR current prior to IFN application. IFN was washed

out, and the stimulation paradigm repeated to monitor recovery of NMDAR current from IFN block.

2.3.2 Kainate Stimulation

In some experiments, 1 mM kainate was used instead of 1 mM NMDA to assess possible changes in AMPA/kainate receptor current density. Kainate was used because it activates AMPARs in a non-desensitizing fashion (Hollmann and Heinemann, 1994), making it easier to accurately measure peak current. Measurements of IFN sensitivity or I_{ss}/I_{peak} were not carried out in these experiments.

2.3.3 Electrophysiological Measurement of NMDAR Insertion to the Plasma Membrane

Whole-cell patch clamp recordings were performed under voltage clamp (V_H = -80 mV, to minimize any possibility of MK-801 dissociation) on cultured striatal MSNs as described above. NMDAR-mediated current was evoked by bath application of saturating (1 mM) concentrations of NMDA. To irreversibly block all surface NMDARs, 5 μM MK-801 (a use-dependent, open-channel blocker) was co-applied with 1 mM NMDA for 9 s immediately following a 1 s application of NMDA alone. During this period whole-cell NMDA current could be observed to decay to pre-NMDA application levels (see Results, Figure 10A). Thirty seconds following initial blockade, this protocol was repeated to ensure complete block of all surface NMDA receptors. After extensive washout of MK-801, subsequent recovery of NMDAR-mediated current was measured for as long as possible at 5 min intervals by stimulating three times with a 500 ms

application of 1 mM NMDA, 30 seconds apart. The three responses at each 5 min interval were recorded and averaged, and expressed as an average Area Under the Curve (AUC) for the NMDA-evoked current, normalized to cell capacitance (pF) to obtain a measure of integrated current density, which over time could be interpreted as integrated current recovery (or density of NMDARs) per unit of cell membrane. The integrated NMDA-evoked current over 500 ms was used in order to circumvent the effect of noise and difficulty in accurately discriminating peak amplitudes of these relatively small whole-cell currents.

2.4 Visualization of Relative Changes in Cytosolic Free Ca^{2+} and Mitochondrial Membrane Potential ($\Delta\Psi_m$)

Measurements were taken at room temperature (20-21°C) from primary cultures of age-matched WT or YAC128 MSNs between 9 and 11 d.i.v. Neurons were loaded with the acetoxymethyl (AM) esters of Fura-2, Fura-FF or MagFura-2 by incubation at 32°C for 45 min in 6.7 μM of indicator dye in balanced salt solution (BSS, containing 139 mM NaCl, 3.5 mM KCl, 2 mM $NaHCO_3$, 10 mM HEPES, 3 mM Na_2HPO_4–$7H_2O$, 1.8 mM $CaCl_2$, 11 mM D-glucose, 50 μM glycine, pH adjusted to 7.35) containing 0.05% bovine serum albumin. The coverslips were then transferred to BSS alone for 15 min before each experiment to ensure hydrolysis of the fluorophore. Experiments were performed using a Zeiss Attofluor digital fluorescence imaging system as previously described (Abdel-Hamid and Baimbridge, 1997).

Neurons were superfused continuously with BSS at 2.4 ml/min. Regions of interest (ROIs) were sized and placed over the soma of cells that morphologically resembled MSNs. Cells were stimulated with varying concentrations (100 or 500 μM) of

NMDA or 50 mM KCl + 5 μM FPL 64176 (FPL), with 50 μM glycine in all experiments; other compounds were added where indicated. Exposure of cells to 50 mM KCl was achieved by replacing BSS (during the stimulation period) with a high KCl solution containing: 70 mM NaCl, 50 mM KCl, 2 mM $NaHCO_3$, 10 mM HEPES, 3 mM Na_2HPO_4–$7H_2O$, 1.8 mM $CaCl_2$, 11 mM D-glucose, 50 μM glycine, pH adjusted to 7.35. Cells that morphologically resembled MSNs and responded to NMDA or KCl/FPL application with an increase in cytosolic Ca^{2+} were used in the analysis.

Data conversion calculations and analysis were performed using Microsoft Excel macros created in Microsoft Visual Basic by Dr. Gordon Rintoul. For estimation of relative changes in cytosolic Ca^{2+}, the mean peak F_{334}/F_{380} response for each cell was calculated by averaging over a 30s period around the maximal peak response during application of NMDA or KCl/FPL, after subtraction of mean baseline F_{334}/F_{380} for a 30s period before stimulus application. The resulting values from each cell were then used to calculate an overall mean value for that experiment; mean and standard error for each treatment group were calculated from the means of each experiment for that treatment group (i.e., n is the number of experiments). Estimates of cytosolic calcium recovery were made by expressing the mean F_{334}/F_{380} value every 5 min following NMDA or KCl/FPL washout as a percentage of the maximal peak F_{334}/F_{380} response.

Changes in $\Delta\Psi_m$ were assessed by single wavelength imaging of rhodamine-123 (rhod-123) fluorescence. This dye is preferentially sequestered in mitochondria (on the basis of their negative transmembrane potential relative to the cytosol) where its fluorescence is quenched due to dye stacking. A loss of $\Delta\Psi_m$ results in the redistribution of rhod-123 back into the cytosol, producing an increase in overall cell fluorescence. The

absolute magnitude of the fluorescence change is dependent on several factors (including variability in dye-loading and de-esterification times, and changes in the intensity of the UV light source over time) that vary from experiment to experiment, not the least of which are the health of the cells and consequent mitochondrial polarization that day, and which other dyes, if any, are present. Hence the maximum fluorescence measured using rhod-123 should ideally be compared in experiments performed on the same day under the same conditions. Importantly, maximum mitochondrial depolarization is only achieved using protonophores or other measures to directly dissipate $\Delta\Psi_m$. When other stimuli are used that result in loss of $\Delta\Psi_m$, unless they are compared within the same experiment to a stimulus that produces maximum depolarization, it is not possible to accurately assess the relative mitochondrial depolarization achieved using different stimuli between different experiments. This caveat can also be extended to data sets from experiments performed on different days; hence, genotoype-paired experiments were performed wherever possible (the notable exception being those experiments where mPT inhibitors were used, as paired cultures were not reliably available).

In some experiments the initial loading of Ca^{2+} indicator (either Fura-2 or Fura-FF) was followed immediately by an addition of 26.3 mM rhod-123 to the loading buffer to achieve a final concentration of 5.0 μM rhod-123. Fifteen minutes after the addition of rhod-123, coverslips were transferred to BSS alone, at room temperature. Dual imaging experiments were then performed where both cytosolic Ca^{2+} and $\Delta\Psi_m$ were monitored simultaneously under the same conditions and in the same age-matched and paired (except for experiments using mPT inhibitors) WT and YAC128 MSNs. The same chamber and imaging system were used as described above, and the same stimulation and

measurement paradigm with the addition of an excitation (488 nm) and emission (>510 nm) cycle for rhod-123. Data for $\Delta\Psi_m$ were expressed as the background-corrected change in fluorescence compared with baseline ($\Delta F/F_0$). The mean peak $\Delta F/F_0$ during NMDA application (calculated by averaging over a 30 s period around the peak response) was calculated from measurements for all responding neurons during stimulus (NMDA or KCl/FPL) application in each experiment. The resulting means from each experiment were then used to calculate an overall mean and standard error (based on n's reflecting number of experiments) for each treatment group.

2.4.1 Determination of Resting $\Delta\Psi_m$

To get an approximate measurement of resting $\Delta\Psi_m$ in intact MSNs, MSNs were loaded with rhod-123 and visualized as described above. In some experiments, MSNs were co-loaded with Fura-FF for two reasons: 1) to help visualize neuronal soma, and 2) to allow for monitoring of Ca^{2+} release from mitochondria. The mitochondrial protonophore CCCP (5 μM) was applied, resulting in maximal depolarization of $\Delta\Psi_m$ and release of accumulated rhod-123 (Toescu and Verkhratsky, 2000). The relative fold-increase in rhod-123 fluorescence following application of CCCP provides a rough indication of the degree of depolarization achieved, and in doing so allows indirect measurement of the relative resting $\Delta\Psi_m$ prior to depolarization.

2.4.2 Calculation of CCCP/NMDA (C/N) Ratio to Determine Efficiency of Mitochondrial Ca^{2+} Uptake

For some experiments, mitochondrial Ca^{2+} content was measured following NMDA application by depolarizing mitochondria using 5 μM CCCP, causing mitochondria to release accumulated free Ca^{2+} into the cytosol. In order to isolate this source of Ca^{2+} influx to the cytosol (and exclude Ca^{2+} entry from the extracellular space), neurons were superfused with a Ca^{2+}-free BSS (same composition as normal BSS above, except 1.8 mM $CaCl_2$ is replaced by 0.9 mM $MgCl_2$) for 2 min prior to the addition of CCCP, during the washout of NMDA. We used previously established methods to determine the efficiency of mitochondrial Ca^{2+} uptake (Brocard et al., 2001). The area under the curve (AUC) of Ca^{2+} responses (during stimulus application) was measured, in serial fashion, in response to a 1-min exposure to 500 μM NMDA (N) followed 2 min later by a 1-min application of CCCP (C; to release free Ca^{2+} accumulated by mitochondria). The regions where AUC measurements were performed were limited to periods during NMDA or CCCP application, i.e. a 60 s region in each case. The C/N ratio was then calculated.

2.4.3 Quantifying the Temporal Relationship Between Increases in Ca^{2+} and Loss of $\Delta\Psi_m$

To calculate the lag time between initial changes in cytosolic Ca^{2+} and $\Delta\Psi_m$, experiments using the dye pair of Fura-2 (due to high sensitivity at low $[Ca^{2+}]$) and rhodamine-123 were analyzed. The time bases for both variables were aligned and the initiation of fluorescence changes for each variable were recorded. The start time for a

fluorescence change was defined as the initial data point in a series of at least five data points that successively increased in a positive direction, following NMDA application. Increases in Ca^{2+} were observed to always be initiated prior to changes in $\Delta\Psi_m$.

2.5 Data Analysis

All data are presented as means ± standard error of the mean (SEM), unless otherwise noted. T-tests, one-way, two-way and Repeated Measure ANOVAs followed by Bonferroni post-test were performed using GraphPad Prizm statistical analysis software.

For imaging experiments, ANOVAS were used where experiments using WT and YAC128 MSNs could be age-matched and performed on the same days (the majority of experiments), allowing for variability in dye-loading and de-esterification times, and changes in the intensity of the UV light source over time, to be accounted for equally in all genotype and treatment groups within and across culture batches. Where experiments for both genotypes could not be performed on the same day (those using mPT inhibitors), unpaired t-tests were used to analyze data within genotype only, in order to assess the effects of treatment. All Ca^{2+} imaging data were baseline-subtracted prior to analysis.

For statistical purposes, the number of experiments (n) was considered to be the number of cells tested for electrophysiological experiments, and the number of individual coverslips used for imaging experiments. For all data sets, cells from at least 3 different litters of pups (culture batches) were used, so n is theoretically representative of results from a number of different mice. The number of experiments carried out was not dependent on achieving a given result; in fact, most significant differences found were

apparent with low n's. Rather, the numbers of experiments performed were largely determined by the birth rate of pups of the relevant genotypes, using the minimum standard of the results of at least 3 separate litters per genotype being incorporated into the overall data set. In certain data sets, for example as represented in Figures 8 and 9, this approach limited the size of n as these data were obtained towards the end of experimental protocols where cells died prematurely. Hence, in these cases, it may be desirable for n to be increased.

2.6 Materials

Acetoxymethyl esters of Fura-2, Fura-FF, and MagFura-2, as well as rhodamine-123 were purchased from Invitrogen Canada Inc. (Burlington, ON). TTX was purchased from Alomone labs (Israel). Neurobasal medium, B27 with no added supplements, HBSS, and penicillin/streptomycin were purchased from Invitrogen Canada Inc. (Burlington, ON). All other chemicals were purchased from Sigma Aldrich Canada (Oakville, ON).

Chapter 3

NMDAR Function in the YAC Mouse Models of HD

Our laboratory previously reported that co-expression of NR1/NR2B-containing NMDARs with mhtt (htt138, 138 polyQ) in HEK293 cells led to an enhancement of NMDAR-mediated current density (Chen et al., 1999b). Quantification of NMDA-induced apoptosis in primary MSN cultures from WT, YAC46 and YAC72 MSNs showed that the presence of full-length mhtt significantly increased NMDAR-mediated apoptosis in a polyQ length-dependent fashion (Zeron et al., 2002). In this paper the authors noted that YAC72 MSNS acutely dissociated from the striata of 6-11 week old YAC72 mice had enhanced NMDAR peak current densities, a phenomenon similar to that observed in the studies using transfected HEK cells as noted above. Since these results were obtained in two distinct neuronal preparations, our first question here was to determine whether the same enhancement of NMDAR current occurred in the primary MSN culture preparation, and whether these changes were specific to NMDAR activity or a symptom of a broader alteration in neuronal function which also affected other ionotropic glutamate receptors. Secondly, we wondered whether any changes that were observed could be correlated to the length of the polyQ repeat region in htt. A parallel question would be whether any changes in NMDAR function seen would be specific to the population of neurons most at risk in HD, the MSN, or would different neuronal subtypes also be affected in a similar fashion? And finally, we set out to determine what mechanism(s) underlie any functional changes observed.

3.1 NMDAR Current Density in Neuronal Primary Cultures

In order to investigate whether any relationship existed between htt polyQ length and NMDAR-mediated current, we established primary cultures of striatal MSNs from early postnatal mice on a FVB/N strain background (WT) or from YAC transgenic mice expressing full-length human htt containing various polyQ lengths: YAC18 (18Q, line 212), YAC46 (46Q, line 668), YAC72 (72Q, line 2511), and YAC128 (128Q, line 55). The generation and characterization of these different YAC transgenic mouse lines have been previously described (Hodgson et al., 1999; Slow et al, 2003; Leavitt et al., 2006).

The first set of experiments sought to establish whether cultured early postnatal MSNs from YAC mice expressing mhtt with various polyQ lengths showed increased NMDA-evoked current. Figure 1 illustrates a typical MSN (in this case WT) whole-cell current evoked by the application of a saturating (1 mM) concentration of NMDA while under voltage clamp (V_H = -60 mV). Note that upon application of NMDA the current rapidly reaches peak amplitude, and then proceeds to decay toward a steady-state plateau in the continued presence of agonist. The measurements of both peak current amplitude (I_{peak}) and steady-state current (I_{ss}) are demonstrated here. Comparing NMDAR peak current density (I_{peak} normalized to the cell capacitance) across genotypes, we found that NMDAR peak current density generally increased with longer htt polyQ length, up to 72Q (YAC18 vs. YAC72, $^{**}P<0.01$; YAC46 vs. YAC72, $^{*}P<0.05$; One-way ANOVA, Bonferroni post-test, Figure 2). Similar to previously reported results with acutely dissociated MSNs from ~2-month old mice (Zeron et al., 2002), YAC72 MSNs exhibited significantly increased NMDAR peak current density vs. WT MSNs ($^{*}P<0.05$, One-way ANOVA, Bonferroni post-test, Figure 2). This enhancement of current was specific to

NMDA receptors, as activation of the other classes of non-NMDA ionotropic glutamate receptors by bath application of kainate (an agonist at both AMPA and kainate receptors) showed no significant difference in current density between WT and YAC72 MSNs (Figure 3). It should be noted that the mean cell capacitance was not significantly different across all genotypes of cultured MSNs studied (12.6 ± 1.8 pF, n=42 for WT; 15.5 ± 2.3 pF, n=13 for YAC18; 15.1 ± 1.2 pF, n=11 for YAC46; 12.1 ± 0.9 pF, n=16 for 72Q; and 13.2 ± 0.9 pF, n=20 cells for YAC128).

Interestingly, NMDAR peak current density was not increased in YAC128 MSNs vs. WT (Figure 2), despite the fact that primary cultures of YAC128 MSNs exhibit enhanced sensitivity to NMDA-induced apoptosis (Shehadeh et al., 2006). This observation formed the basis for Chapters 4 and 5, which describe our attempts to resolve this paradox.

To determine whether other neuronal populations expressing mhtt would also have enhanced NMDAR current, we assessed NMDAR current density in primary cultures of CPNs taken from the same mice used to prepare our MSN cultures. Since there were no significant differences in NMDAR current density between YAC46 and WT or YAC18 MSNs, we chose not to pursue these recordings in YAC46 CPNs. As Figure 4 illustrates, we found similar NMDA-evoked peak current densities in cultured CPNs from WT, YAC18, YAC72 and YAC128 mice. This observation suggests that neither the overexpression of non-pathogenic htt nor (m)htt polyQ length serve to regulate NMDAR activity in CPNs. Hence, htt polyQ length-dependent potentiation of NMDAR current is neuronal-type specific and may contribute to enhanced excitotoxic

striatal vulnerability in the YAC72 mice as well as in human HD expressing htt with moderate repeat lengths.

3.2 NMDAR Desensitization

The level of desensitization of NMDAR current could play a significant role in determining the total charge transfer and Ca^{2+} influx that occurs during NMDAR activation, possibly influencing the vulnerability of MSNs to excitotoxicity. To determine whether mhtt, in addition to increasing peak NMDAR current density, decreased desensitization (i.e. resulted in a higher I_{ss}) of NMDARs as an alternate mechanism to enhance excitotoxicity, we examined I_{ss}/I_{peak} ratios across genotypes in both MSNs (Figure 5) and CPNs (Figure 6). We found that desensitization of NMDAR currents recorded from YAC transgenic MSNs was not significantly different regardless of mhtt polyQ length; however, NMDAR currents in YAC18 MSNs desensitized significantly less than those in WT MSNs (WT vs. YAC18, $^{**}P<0.01$; One-way ANOVA, Bonferroni post-test). No significant differences in NMDAR desensitization were found between genotypes in CPNs.

3.3 NR1/NR2B-Containing NMDARs

NMDARs are composed of both NR1 and NR2 subunits, and it is the NR2 subunits that define NMDAR channel properties including peak open probability, single-channel conductance, and desensitization (reviewed in Cull-Candy et al., 2001). As well, since mhtt significantly enhanced NMDAR currents and NMDA-induced apoptosis in NR1/NR2B-expressing HEK cells (but not in HEK cells expressing NR1/NR2A), we

hypothesized that an mhtt-influenced alteration of NMDAR subunit composition could play a role in enhanced excitotoxicity in YAC72 MSNs (Zeron et al., 2002).

To probe NMDAR subunit composition, we conducted our whole-cell patch clamp recordings in both MSNs and CPNs in the absence and presence of 3 μM IFN, an NR1/NR2B-selective antagonist of NMDARs (Williams, 1993). As illustrated in Figure 7, IFN blocked a significant proportion of NMDAR current in MSNs (Figure 7A), but had no effect on NMDAR current in cultured CGNs (Figure 7B), which do not express NR2B under the culture conditions used (see Methods). As summarized in Figure 8, NR1/NR2B-containing NMDARs mediated the majority of current in MSNs, and this proportion was similar across genotypes. Similar observations were made regarding NR1/NR2B-containing NMDARs in CPNs (Figure 9), with no significant difference between genotypes.

Together, these results indicate that mhtt likely does not alter the subunit composition of NMDARs expressed at the plasma membrane. It should be noted that the proportion of current mediated by NR2B-containing NMDARs was generally less in CPNs compared with MSNs of the same genotype, significantly so for both WT and YAC72 (**$P < 0.01$ for wt and *$P<0.05$ for YAC72 by unpaired t-test, percentage of IFN-sensitive current in CPNs vs. MSNs within genotypes).

3.4 Shift of NMDAR Expression in YAC72 MSNs to the Surface of the Plasma Membrane

Although we found an increase in NMDAR current density in YAC72 MSNs, the overall level of protein expression of NR1 and NR2B subunits in striatal tissue of YAC72

mice is not increased above that in striatal tissue from WT mice (Li et al., 2003a). Therefore, it is unlikely that the increase in NMDAR current density in YAC72 MSNs is simply a function of greater amounts of NMDAR proteins. However, in other experiments we found that the expression pattern of NR1 and NR2B was shifted in YAC72 MSNs such that a greater proportion (approximately 50% increase in surface:internal NR1 expression, $*P<0.01$ by one-way ANOVA, Bonferroni post-test and approximately 30% increase in surface:internal NR2B expression, $*P<0.05$ by one-way ANOVA, Bonferroni post-test) was expressed at the plasma membrane than in WT or YAC18 MSNs, while the total amount of NR1 expressed is similar across genotypes (Fan et al., 2007). Hence, a greater number of surface NMDARs could explain the enhanced current in YAC72 MSNs.

One possible mechanism to explain the shift in NMDAR expression pattern towards the plasma membrane is that the rate of forward trafficking (towards the plasma membrane) of NMDARs is enhanced. To determine whether the insertion of NMDARs into the plasma membrane occurred at a faster rate in YAC72 MSNs vs. WT MSNs, I utilized an electrophysiological approach similar to that described previously (Lan et al., 2001; Tovar and Westbrook, 2002; Mu et al., 2003; Lin et al., 2004), monitoring the recovery of NMDAR-mediated current following functional blockade of surface receptors by the use-dependent, irreversible NMDAR antagonist MK-801 (electrophysiological silencing). All surface NMDARs were first fully stimulated and then blocked by application of a saturating (1 mM) concentration NMDA, first alone and then in conjunction with MK-801 (see Methods, Figure 10A). Once 'silenced', surface NMDARs remain inactivated for the duration of the experiment as MK-801 binding to

the NMDAR channel is expected to be irreversible under the voltage-clamp conditions used (Huettner and Bean, 1988). Therefore, any subsequent NMDA-evoked current reflects the insertion of new NMDA receptors (or ones that were not on the surface during 'silencing') to the plasma membrane.

Following NMDAR block by MK-801, NMDA-evoked current was monitored at 5 min intervals (as in Figure 10B), and quantified as described (see Methods). The recovery of NMDAR current was ~3-, 3-, and 2-fold higher in YAC72 compared with WT MSNs at 5, 10 and 15 min following MK-801 washout, respectively (Figure 11), a difference that was significant at the 10- and 15-minute time points ($*P< 0.05$, $**P< 0.01$ respectively by two-way ANOVA followed by Bonferroni post-test). This difference in the rate of NMDAR current recovery indicates a faster rate of insertion of NMDARs to the plasma membrane from membrane proximal intracellular pools in YAC72 MSNs.

3.5 Summary

Taken together, these observations suggest that NMDAR current density is enhanced in early postnatal cultured MSNs expressing mhtt with a polyQ length up to a certain ceiling, beyond which other competing mechanisms may prevent the enhancement of NMDAR current. Since these cells are obtained from very early postnatal mice, this would suggest that mhtt-mediated mechanisms that result in the potentiation of NMDAR activity are present at birth, and are selectively expressed in MSNs (and not other neuronal types). Hence this functional alteration may serve as an ongoing source of neuronal stress, possibly underlying a cumulative insult, which renders MSNs vulnerable in HD.

Chapter 4

Aberrant Cytosolic Ca^{2+} Handling in the YAC128 Mouse Model of HD

YAC128 mice, carrying a more extreme CAG expansion than the other YAC HD mouse models described earlier, show an accelerated phenotype and significant striatal neurodegeneration by 6-12 months (Slow et al., 2003). Here we wanted to examine the events downstream of NMDAR activation, specifically regulation of cytosolic Ca^{2+}, preceding the previously reported (Graham et al., 2006b) enhanced NMDA-induced apoptosis in YAC128 compared with WT MSNs. As shown in Chapter 3, the NMDAR current density of MSNs from YAC transgenic mice containing full-length human (m)htt generally correlates to the length of the polyQ repeat region in the human (m)htt transgene. However, this relationship is clearly not intact for polyQ lengths of 128, despite MSNs from this line of mice (YAC128 line 55) showing enhanced NMDA-mediated excitotoxicity to the same maximal level as that seen in YAC72 MSNs (Shehadeh et al., 2006). Having previously documented events downstream of enhanced NMDAR activation in YAC72 MSNs which predictably lead to an apoptotic endpoint, namely enhanced peak cytosolic Ca^{2+} and mitochondrial membrane depolarization (Zeron et al., 2004), we followed the same line of investigation with YAC128 MSNs to resolve the discrepancy between normal NMDAR currents and enhanced NMDA-induced neurotoxicity.

Therefore, the goal was to explain the apparent paradox: mhtt expression in YAC128 MSNs does not increase the NMDAR peak current density as it does in YAC72 MSNs or affect desensitization (and hence the integrated NMDAR current) or NMDAR

subunit composition, yet NMDA exposure induces apoptosis more efficiently in YAC128 than in WT MSNs (Graham et al., 2006b), and indeed produces the largest enhancement of apoptosis in YAC128 MSNs relative to YAC18 controls of any stimulus (Shehadeh et al., 2006).

4.1 Considerations Regarding NMDA Concentration Used for These Studies

Given the results presented in Chapter 3, enhanced excitotoxicity in YAC128 MSNs in the absence of increased NMDAR current could result from impaired Ca^{2+} homeostasis and/or mitochondrial dysfunction. Therefore, I began to investigate these events by comparing cytosolic Ca^{2+} changes as a predictable consequence of NMDAR activation. For several reasons we decided that 500 μM NMDA was an appropriate agonist concentration for maximally stimulating NMDARs in the majority of these experiments. The EC_{50} for sustained glutamate stimulation of recombinant NR1/NR2B NMDARs in HEK cells was found to be ~20 μM (Chen et al., 2001a), and NMDA is a less efficacious NMDAR agonist with a higher EC_{50} than glutamate (Sather et al., 1992; Banke and Traynelis, 2003). Furthermore, in a series of experiments measuring cytosolic Ca^{2+} changes in cultured rat MSNs, Alano et al (2002) found that NMDA concentrations on the order of 500 μM - 1 mM were required to induce maximal Ca^{2+} responses. Lastly, our own previous results confirmed that 500 μM NMDA was sufficient to achieve maximal apoptosis induction in cultured MSNs (Zeron et al., 2004), while 100 μM NMDA was insufficient (Shehadeh et al., 2006). As the goal of these experiments was to examine changes in cytosolic Ca^{2+} (and also mitochondrial function, as described later in Chapter 5) that would explain enhanced apoptosis in YAC128 MSNs, we thought it most

appropriate to use an NMDA concentration proven to most efficiently induce such an endpoint.

4.2 Resting and NMDA-Induced Changes in Cytosolic Ca^{2+} in YAC128 MSNs

We initially hypothesized that YAC128 MSNs would have a higher resting Ca^{2+} level, which could possibly indicate a stress-induced change (Hansson et al., 2001) or pre-existing mitochondrial impairment (Xiong et al., 2002) leaving cells more vulnerable to further insult. Alternatively, an equivalent concentration of NMDA under the aforementioned conditions could produce a larger increase in cytosolic Ca^{2+} in YAC128 than seen in WT MSNs. To address this question, I performed fluorescence imaging of cytosolic free Ca^{2+} levels in MSNs using the high-affinity calcium dye Fura-2. An example of a typical experiment is shown in Figure 12, depicting how and when measurements for resting (basal) Ca^{2+} levels and peak cytosolic Ca^{2+} were performed. Representative mean responses (one experiment each for WT and YAC128) to a 5 min application of 500 μM NMDA are illustrated in Figure 13. Also shown in this experiment (Figure 12) is the application of the Ca^{2+} ionophore 4Br-A23187, to illustrate the maximal fluorescence signal in this experiment and demonstrate that our responses were not saturated by NMDA-induced Ca^{2+} influx.

Contrary to our hypothesis, we found similar basal cytosolic Ca^{2+} levels, as reflected in similar F_{334}/F_{380} ratios ($P>0.05$ by paired t-test) for WT and YAC128 MSNs (Figure 14A). Furthermore, the maximal peak cytosolic Ca^{2+} evoked as a consequence of the application of either 100 μM NMDA or 500 μM NMDA was not significantly different ($P>0.05$ by paired t-test) between WT and YAC128 MSNs (Figure 14A), as

expected from the similar whole-cell current densities evoked by 1 mM NMDA (Figure 2). As the relatively high affinity of Fura-2 for free Ca^{2+} (K_d = 145 nM) is ideal for estimating resting Ca^{2+} levels but not necessarily optimal for discerning peak amplitudes of cytosolic Ca^{2+} (Hyrc et al., 1997; Stout and Reynolds, 1999), we used the lower affinity Ca^{2+} indicator MagFura-2 (K_d = 25 μM) to confirm the lack of difference in peak NMDAR-evoked Ca^{2+} increases. In response to a 5 min application of 500 μM NMDA, peak F_{334}/F_{380} ratios using MagFura-2 (Figure 14B) for WT vs. YAC128 MSNs were 0.54 ± 0.16 vs. 0.37 ± 0.10, respectively (P>0.05 by paired t-test), ruling out the possibility that indicator dye saturation artifactually equalized the Ca^{2+} responses. We concluded that neither changes in resting Ca^{2+} levels nor enhancement of peak cytosolic Ca^{2+} responses, as seen in YAC46 and YAC72 MSNs (Zeron et al., 2004), explained the enhanced NMDA-induced apoptosis characteristic of YAC128 MSNs.

4.3 Altered Cytosolic Ca^{2+} Clearance Following NMDA Stimulation in YAC128 MSNs

As illustrated in representative experiments (Figure 13), the recovery of cytosolic Ca^{2+} toward baseline levels following washout of NMDA appeared slower in YAC128 MSNs. To investigate this further a subset of experiments, in which Ca^{2+} changes were monitored over longer periods, were performed and cytosolic Ca^{2+} recovery was quantified as a percentage of the peak NMDA-induced change remaining over time following washout of NMDA. These experiments found a significantly slower rate of recovery of Ca^{2+} towards pre-stimulus (500 μM NMDA) levels in YAC128 vs. WT MSNs as early as 15 min (repeated measures ANOVA followed by Bonferroni post-test,

*P<0.05 at 15 min, *P<0.05 at 20 min, **P<0.01 at 25 min) following NMDA washout (Figure 15). These data demonstrated a prolonged elevation of cytosolic Ca^{2+} in YAC128 MSNs that may be toxic in and of itself and/or reflect pathological changes in neuronal function, such as the failure of calcium extrusion processes or sequestration into intracellular stores within organelles.

4.4 Effect of Route of Ca^{2+} Entry on Recovery from an Induced Cytosolic Ca^{2+} Load in YAC128 MSNs

Having identified an unexpected genotypic difference in the return of Ca^{2+} towards pre-stimulus levels, we wondered whether the impaired cytosolic Ca^{2+} recovery reflected a general defect in Ca^{2+} handling in YAC128 MSNs, or if it was specific for NMDAR-mediated Ca^{2+} accumulation. To stimulate an alternate pathway of calcium influx from the extracellular compartment without activating NMDARs, I used 50 mM KCl in combination with the L-type Ca^{2+} channel modulator FPL 64176 (5 μM; FPL), a combination that optimizes depolarization-induced Ca^{2+} influx (Hardingham et al., 1999; Shehadeh et al, 2006) via voltage-gated Ca^{2+} channels (VGCCs). I then compared the cytosolic Ca^{2+} responses to those induced by 100 μM NMDA (representative responses to both stimuli shown in Figure 16A). Quantified in Figure 16B, the maximal peak Ca^{2+} response was similar for these two different stimuli (area under the curve analysis, calculating integrated Ca^{2+} responses during stimulus application, also confirmed no significant differences for genotype or treatment at 1 and 5 min; data not shown), and there was no significant difference in peak cytosolic Ca^{2+} for either stimulus between genotypes (two-way ANOVA; no effect of treatment or genotype). Using the same

method to quantify cytosolic Ca^{2+} clearance as in section 4.3, we found that recovery from a Ca^{2+} load induced by a 5 min application of 100 μM NMDA was significantly slower in YAC128 compared with WT MSNs (two-way ANOVA followed by Bonferroni post-test, $*P<0.05$ at 5 min, $**P<0.01$ at 10 min, $***P<0.01$ at 15 min). These results are similar to those found using 500 μM NMDA as the incident stimulus (Section 4.3, Figure 15). In stark contrast, recovery from a Ca^{2+} load induced by membrane depolarization and VGCC activation with KCl and FPL was relatively rapid, nearly complete by 15 min post-stimulus washout (~10% above pre-stimulus levels), and proceeded at equivalent rates in both genotypes (two way ANOVA; no effect of genotype) (Figure 17). Thus, we concluded that the defect in recovering from an imposed Ca^{2+} load was relatively selective for Ca^{2+} influx that occurred via NMDAR activation, and specific to YAC128 MSNs.

4.5 Summary

Contrary to our hypothesis, we found that YAC128 MSNs did not have a significantly higher basal cytosolic Ca^{2+} level, nor did they respond to NMDAR stimulation with higher peak cytosolic Ca^{2+} than observed in WT MSNs. However, we found an interesting dichotomy in the ability of YAC128 MSNs to recover from an imposed cytosolic Ca^{2+} load. Whereas WT and YAC128 MSNs recovered from depolarization-mediated Ca^{2+} influx at similar rates, YAC128 MSNs were slower than WT MSNs to recover from Ca^{2+} influx via NMDAR activation. Hence it appears that YAC128 MSNs are impaired in their ability to regulate cytosolic Ca^{2+}, particularly after

intense NMDAR activity, which may increase their vulnerability to excitotoxic damage in the context of HD.

Chapter 5

Mitochondrial Dysfunction in YAC128 MSNs

Previous work from our lab documents that mitochondrial membrane depolarization downstream of strong NMDAR stimulation in both YAC46 and YAC72 cultured MSNs is significantly greater than in cultured WT MSNs (Zeron et al., 2004). This enhanced depolarization of mitochondria in mhtt-expressing MSNs correlated with enhanced Ca^{2+} entry resulting from NMDAR activation, which was characterized in parallel experiments. Several studies have demonstrated that NMDAR-mediated excitotoxicity is likely dependent on mitochondrial calcium uptake and overload (Castilho et al., 1998; Stout et al., 1998), and that the loss of mitochondrial membrane potential induced by mitochondrial uptake of free Ca^{2+} from the cytosol is one indicator of the risk for subsequent apoptotic death (Ankarcrona et al., 1995; Ankarcrona et al., 1996; Schinder et al., 1996).

In this series of experiments, our goal was to understand how mitochondria in YAC128 MSNs behaved in response to an NMDA-induced cytosolic Ca^{2+} load (as documented in Chapter 4), and whether any differences existed between the responses of these mitochondria and those in WT MSNs which could explain the enhanced apoptosis of YAC128 MSNs as previously described. In order to accomplish this we combined the monitoring of both parameters, namely cytosolic Ca^{2+} and mitochondrial membrane potential ($\Delta\Psi_m$) in an attempt to understand how the two factors interrelate and affect each other, and whether a loss of mitochondrial function similar to that seen in less

extreme polyQ expansions could occur in the absence of a correspondingly larger Ca^{2+} load.

5.1 Equivalent Cytosolic Ca^{2+} Loads Induce Significantly Different Changes in $\Delta\Psi_m$ in YAC128 Compared with WT MSNs

The initial step was to establish our parameters for imaging both Ca^{2+} and $\Delta\Psi_m$ together using two dyes – Fura-2 and rhod-123 – simultaneously. Figure 18 shows two typical experiments monitoring cytosolic Ca^{2+} and $\Delta\Psi_m$ at the same time in the same cells in WT (top panel) and YAC128 (bottom panel) MSNs. This method allowed one particular advantage over monitoring each parameter in sister experiments, specifically the ability to directly assess the temporal relationship between changes in cytosolic Ca^{2+} and loss of $\Delta\Psi_m$. We predicted that following NMDAR activity, an increase in cytosolic Ca^{2+} would precede a change in $\Delta\Psi_m$, as suggested by the literature. Indeed, we found that the increase in cytosolic Ca^{2+} indicated by an increase in Fura-2 ratio preceded any change in rhod-123 fluorescence (mean lag time between initial changes in Fura-2 and rhod-123 signals: 4.39 ± 0.98 s for WT, 5.89 ± 1.2 s for YAC128 MSN, $P>0.05$ by paired t-test; n= 8 paired experiments per genotype; total of 131 and 147 neurons for WT and YAC128, respectively, from 4 different culture batches); one example is illustrated in the inset in Figure 18. These data are consistent with an increase in cytosolic Ca^{2+} triggering uptake of free Ca^{2+} by mitochondria and, consequently, a reduction in $\Delta\Psi_m$.

We expected under our dual-imaging conditions that our previous findings, that WT and YAC128 MSNs have similar basal and NMDA-induced peak Ca^{2+} levels, would still hold true. As expected, there was no difference between WT and YAC128 MSNs

($P>0.05$ by paired t-test) with regard to resting Ca^{2+} or peak Ca^{2+} in response to a 5 min application of 500 μM NMDA (Figure 19, top panel). Surprisingly, however, the simultaneously monitored changes in $\Delta\Psi_m$ were markedly different with a greater loss of $\Delta\Psi_m$ in YAC128 MSNs as indicated by an approximately 3-fold greater increase in rhod-123 fluorescence compared with WT MSNs (Figure 19, bottom panel; $^*P<0.05$ by paired t-test).

5.2 Comparison of Resting $\Delta\Psi_m$

There are several possible reasons for the larger NMDA-induced loss of $\Delta\Psi_m$ in YAC128 MSNs. This finding could reflect altered resting mitochondrial function and/or enhanced mitochondrial access to the NMDAR-induced Ca^{2+} influx leading to increased uptake and depolarization. We attempted to address the first possibility by comparing the relative resting $\Delta\Psi_m$ in WT and YAC128 MSNs, as this would provide an indication as to the potential for resting mitochondria of either genotype to act as a Ca^{2+} buffering reservoir. We utilized 5 μM CCCP (a mitochondrial protonophore which dissipates $\Delta\Psi_m$; Toescu and Verkhratsky, 2000) to depolarize the mitochondria of MSNs loaded with both Fura-FF and rhod-123 (resulting in the release of accumulated rhod-123 to the cytosol). By comparing the maximum fluorescence responses, we determined that resting mitochondria in YAC128 MSNs had an average polarization state similar as those in WT MSNs ($P>0.05$ by paired t-test; Figure 20A). In some experiments neurons were co-loaded with the Ca^{2+} indicator Fura-FF, allowing us to visualize the release of free Ca^{2+} from the mitochondria during CCCP-induced mitochondrial depolarization. As illustrated in Figure 20B very little free Ca^{2+} was released from resting mitochondria.

5.3 Assessing the Ability of YAC128 MSNs to Act as a Ca^{2+} Sink During NMDAR Activity

To address the possibility that mitochondria in YAC128 MSNs had privileged access to the Ca^{2+} influx pathway activated by NMDA application, we used previously established methods (Brocard et al., 2001) to compare the efficiency of mitochondrial Ca^{2+} uptake between WT and YAC128 MSNs. Illustrated in Figure 21A, we measured the area under the curve (AUC) of Ca^{2+} responses during a 1-min exposure to 500 μM NMDA (N) followed 2 min later by a 1-min application of CCCP (C; to release free Ca^{2+} accumulated by mitochondria) to calculate the C/N ratio (as described in the Methods). We found similar C/N ratios (Figure 21B, $P>0.05$, unpaired t-test), indicating that mitochondria in WT and YAC128 MSNs are equally capable of initially buffering Ca^{2+} entering via NMDARs.

We also noted similar, rapid rates of recovery of cytosolic Ca^{2+} towards baseline following NMDA application for WT and YAC128 MSNs (see Figure 21A as an example) that were not significantly different (Figure 22; $P>0.05$ by unpaired t-test), suggesting that the Ca^{2+} handling defect documented in Chapter 4 (and again demonstrated in Figure 18) is only observed after prolonged NMDAR activity. Based on these experiments, we conclude that mitochondria rapidly and efficiently buffer the Ca^{2+} influx through NMDARs in both WT and YAC128 MSNs, implying that an enhanced mitochondrial Ca^{2+} uptake cannot explain the enhanced depolarization of mitochondria in YAC128 MSNs.

5.4 Potential mPT Involvement in Mitochondrial Depolarization in YAC128 MSNs

Another possible explanation for the dramatically enhanced mitochondrial depolarization found in YAC128 MSNs during 5-min NMDA applications is that the mPT might be acutely activated in this paradigm. We therefore decided to test the effect of mPT inhibition on changes in $\Delta\Psi_m$, maximal peak Ca^{2+} and the subsequent recovery of cytosolic Ca^{2+} towards baseline. Note that for MSNs used in these experiments, the inhibitors of the mPT were present 1 hour prior to NMDA exposure and during the entire experiment, in all solutions used. Cyclosporin A (CsA), which binds the mPT modulator cyclophilin D, had no effect ($P>0.05$ by paired t-test) on NMDA-induced peak cytosolic Ca^{2+} in WT MSNs but was found to significantly ($*P<0.05$ by unpaired t-test) reduce peak Ca^{2+} in YAC128 MSNs (Figure 23A). There was also a trend toward CsA reducing simultaneously monitored NMDA-induced mitochondrial depolarization in YAC128 (but not WT) MSNs, although this effect was not significant (Figure 23B; $P>0.05$ by unpaired t-test). Since CsA is known to inhibit protein phosphatase 2B (calcineurin) in addition to exerting an inhibitory effect on mPT formation, we elected to test another mPT inhibitor, bongkrekic acid (BkA) which binds the ANT, an integral mPT component protein. BkA (5 μM) was found to significantly reduce both peak Ca^{2+} (Figure 24A; $*P<0.05$, unpaired t-test) and mitochondrial depolarization (Figure 24B; $*P<0.05$, unpaired t-test) in YAC128 MSNs, thus having similar effects to CsA. Interestingly, neither parameter was affected by BkA treatment ($P>0.05$, unpaired t-test) in WT MSNs (Figures 24A and 24B).

These results suggest that mPT activation occurs within 5 min of NMDAR activity in YAC128 MSNs, contributing to both peak Ca^{2+} and mitochondrial

depolarization. Neither of the mPT inhibitors had an effect on the rate of Ca^{2+} recovery over a 15 minute period following NMDA application (data not shown).

5.5 Summary

We found that mitochondria in YAC128 MSNs have a similar relative resting membrane potential as those in WT MSNs. This allows mitochondria in YAC128 MSNs to efficiently buffer cytosolic Ca^{2+} elevations that result from transient (60 s) NMDAR stimulation. However, when NMDARs are activated for a longer time period, in this case 5 min, mitochondria in YAC128 MSNs depolarize to a greater extent than those in WT MSNs. We found that the greater relative depolarization of mitochondria in YAC128 MSNs is due, at least in part, to activation of the mPT, and this event contributes to the peak cytosolic Ca^{2+} elevation. Interestingly mPT inhibitors had no effect on NMDA-induced changes in peak cytosolic Ca^{2+} or $\Delta\Psi_m$ in WT MSNs, indicating that mPT formation is not acutely induced. Based on the results presented here we conclude that a greater tendency for mPT activation, a common step in induction of apoptosis, is responsible for enhanced apoptosis in YAC128 MSNs following NMDAR activation.

Chapter 6

General Discussion

6.1 Synopsis of Findings

In this thesis I have examined, for the first time, the relationship between the length of the polyQ repeat in mhtt and NMDAR currents in MSNs *in vitro*. I found that NMDAR current density was significantly enhanced in YAC72 MSNs compared to WT, YAC18, and YAC46, and that there was a trend toward larger NMDAR current density with increasing polyQ length for YAC18, YAC46 and YAC72 MSNs. Furthermore, this increase was selective for NMDARs as kainate-evoked current densities were equivalent between WT and YAC72 MSNs. This finding is consistent with previous work from our lab showing NMDAR currents enhanced by the expression of mhtt in HEK cells (Chen et al., 1999b) and acutely dissociated MSNs from YAC72 mice (Zeron et al., 2002). The increasing NMDAR current correlated with polyQ length for YAC18, YAC46 and YAC72 MSNs is consistent with the idea that increased NMDAR currents can act as an initiating event, producing elevated cytosolic Ca^{2+}, mitochondrial membrane depolarization, mPT and caspase activation to enhance apoptosis in cultured MSNs expressing mhtt (Zeron et al., 2002; Zeron et al., 2004; Shehadeh et al., 2006), and increasing sensitivity to excitotoxic neuronal death *in vivo* (Zeron et al., 2002). The lack of NMDAR current augmentation in YAC128 MSNs will be discussed in the next section.

In this thesis I also showed that the NMDAR current enhancement in YAC72 compared with WT MSNs was dependent upon neuronal subtype, as it was not observed

in CPNs derived from the same mice. Previous findings published by our laboratory showed that NMDAR-mediated apoptosis was not enhanced in cultured CGNs from YAC HD mice (Zeron et al. 2002), consistent with the idea that mhtt increases NMDAR currents and/or cell death signaling in a neuronal type-specific fashion, a finding also confirmed in R6/2 mice (Cepeda et al., 2001b; Andre et al., 2006). As CGNs, under the culture conditions used, did not express NR2B at the time of experimentation (Zeron et al., 2002), it is tempting to suggest that the lack of increased apoptosis in mhtt-expressing CGNs was due to the absence of the NR2B subunit. The demonstration that NR1/NR2B NMDAR currents are selectively enhanced by mhtt (Chen et al., 1999b) supports this hypothesis. Additionally, CPNs did not show mhtt-enhanced NMDAR current and also expressed a significantly lower proportion of NR1/NR2B-type NMDARs than MSNs. On the other hand, ~45-55% of NMDAR current recorded from CPNs was mediated by NR1/NR2B, suggesting that the expression of the NR2B subunit may be required, but is not sufficient, for the mhtt-mediated enhancement of NMDAR activity. Furthermore, I found that neither the proportion of NMDAR current in MSNs sensitive to IFN nor NMDAR desensitization varied significantly with the expression of mhtt containing different polyQ lengths, indicating that a mhtt-mediated shift in NMDAR subunit expression was unlikely.

Since YAC72 MSNs exhibited an increased NMDAR current density without any differences in neuronal capacitance, I attempted to discern the mechanism underlying the increase. It was initially observed that YAC72 MSNs express a greater proportion of their pool of NR1 at the cell surface, relative to WT and YAC18 MSNs (which had similar NR1 surface:internal ratios), while the total amounts of NR1 were similar across

genotypes (Fan et al., 2007). Biotinylation experiments subsequently confirmed that YAC72 MSNs express higher levels of both NR1 and NR2B at the plasma membrane than WT MSNs, but GluR1 expression at the surface was similar for both genotypes (Fan et al., 2007). Previous work from our laboratory established that single-channel properties of NMDARs are not altered by mhtt (Chen et al., 1999b), it follows that this redistribution of NMDARs to the plasma membrane explains the enhancement of peak current density in YAC72 MSNs. Subsequently, seeking an explanation for the altered NMDAR distribution in YAC72 MSNs, our laboratory demonstrated elevated rates for both forward trafficking to the plasma membrane as well as removal and degradation of NMDARs from the surface (Fan et al., 2007); the former is consistent with the finding reported here of a faster rate of NMDAR insertion to the plasma membrane, as assessed by electrophysiological experiments. The net difference in rates favours an accumulation of NMDARs at the plasma membrane, thus explaining the redistribution of NMDARs in YAC72 compared with WT MSNs. Importantly, this enhanced trafficking effect was not noted for GluR1, indicating a change that would selectively affect NMDARs (Fan et al., 2007).

For the first time, I recorded NMDAR currents in YAC128 MSNs, and surprisingly found current densities that were not significantly increased compared to WT or YAC18 MSNs, despite an increased sensitivity to NMDA-induced apoptosis with a maximum ceiling equivalent to YAC72 MSNs (Graham et al., 2006b; Shehadeh et al., 2006). I compared a number of factors with respect to cytosolic Ca^{2+} handling and how changes in $\Delta\Psi_m$ are impacted downstream of NMDAR activation. To summarize, I found that while YAC128 MSNs have a resting level of cytosolic Ca^{2+} similar to WT

MSNs and reach a similar peak cytosolic Ca^{2+} after prolonged (5 min) NMDA application, recovery of Ca^{2+} towards baseline following washout of NMDA is significantly impaired in YAC128 MSNs. This genotypic difference in Ca^{2+} recovery appears to be dependent on the route of Ca^{2+} entry, as the rate of recovery from VGCC-mediated Ca^{2+} entry was similar in both WT and YAC128 MSNs. I also found mitochondria in YAC128 MSNs depolarized to a greater extent than those in WT MSNs, downstream of prolonged NMDA application. Inhibitors of mPT formation were able to reduce both peak Ca^{2+} and the extent of mitochondrial depolarization in YAC128 MSNs but had no effect in WT MSNs, implying that activation of the mPT accounts for some of the differences in these factors between genotypes. Hence mhtt appears to impair mitochondrial responses in YAC128 MSNs downstream of NMDAR activation, resulting in the initiation of mPT formation. This sequence of events can account for the previously reported enhanced neuronal apoptosis in YAC128 MSNs (Tang et al., 2005; Graham et al., 2006b; Shehadeh et al., 2006).

6.2 Dissociation Between NMDAR-Mediated Current and Downstream Changes in Cytosolic Ca^{2+} and $\Delta\Psi_m$ in YAC128 MSNs

I have shown that NMDAR peak current density increases with the length of the htt polyQ repeat in MSNs obtained from YAC18, YAC46, and YAC72 mice, and yet YAC128 MSNs exhibit current densities similar to WT and YAC18. Thus, the observed correlation between htt polyQ length and NMDAR current density in MSNs does not extend to more extreme repeat sizes in the YAC transgenic mouse model.

The increased NMDAR current density correlates well with increased NMDAR surface expression in YAC72 MSNs compared with WT or YAC18 MSNs in culture (Fan et al., 2007). Preliminary data from our lab also indicates that the distribution of NMDARs between surface and internal pools is similar for YAC128, WT and YAC18 MSNs (L. Zhang and L.A. Raymond, unpublished results), which would be consistent with similar current densities between these genotypes. It is possible that mechanisms underlying altered NMDAR trafficking in YAC72 MSNs (Fan et al., 2007) are also active in YAC128 MSNs but that additional mechanisms, arising from the further expansion of the polyQ region that result in the down-regulation of NMDAR surface expression, are recruited in YAC128 MSNs. These pathways could include aberrant activation of proteases, or protein phosphatases and kinases, particularly if stimulated by prolonged elevation of Ca^{2+} levels following sustained NMDAR activity. For example, increased activation of casein kinase 2, which is a calcium-activated protein kinase that phosphorylates NR2B, reduces NMDAR surface expression in hippocampal neurons (Chung et al., 2004). Another candidate for NMDAR downregulation is Ca^{2+}-activated calpain activity, which can cause cleavage of the C-terminus of surface NR2B subunits (Guttmann et al., 2002; Simpkins et al., 2003; Dong et al., 2006) and promote NMDAR internalization (Scott et al., 2004).

In further contrast to our previously published observations in MSN cultures from YAC46 and YAC72 mice (Zeron et al., 2004) but consistent with the results of the NMDAR peak current density experiments, there was no significant difference in NMDA-induced maximal peak cytosolic Ca^{2+} between WT and YAC128 MSNs. This lack of difference in NMDA-induced peak Ca^{2+} was consistently observed using three

different fluorescent Ca^{2+} indicators (Fura-2, Fura-FF and MagFura-2) with differing K_d values, and with two concentrations (100 and 500 μM) of NMDA. Our results in WT and YAC128 MSNs using the combination of KCl/FPL to induce Ca^{2+} influx suggest that VGCCs behave similarly in both genotypes with regards to their contribution to peak Ca^{2+}, and the similar recovery of cytosolic Ca^{2+} following depolarization argues against differential regulation of VGCC function by mhtt in YAC128 MSNs.

Since YAC128 MSNs exhibited a dramatically enhanced loss of $\Delta\Psi_m$ downstream of NMDAR activation, indicative of mitochondrial Ca^{2+} uptake and overload (Castilho et al., 1998; Stout et al., 1998; Pivovarova et al., 2004), and the extent of loss of $\Delta\Psi_m$ induced by Ca^{2+} uptake is one indicator of the risk for subsequent excitotoxic or apoptotic death (White and Reynolds, 1996; Schinder et al., 1996), our results help explain the heightened sensitivity of YAC128 MSNs to NMDA-induced apoptosis.

6.3 Acute NMDA-Evoked mPT Activation in YAC128 MSNs

My results indicate that both mPT inhibitors CsA and BkA, which interact with different components of the mPT, significantly reduced peak Ca^{2+} induced by a 5 min application of 500 μM NMDA in YAC128 MSNs. The change in $\Delta\Psi_m$ was also attenuated, whereas the rate of recovery of the Ca^{2+} response towards pre-stimulus (resting) levels was not significantly altered by either inhibitor. Another study using cultured WT rat MSNs observed activation of the mPT during a prolonged (>20 min) exposure to 1 mM NMDA (Alano et al., 2002). It was therefore surprising to us that the mPT is activated as a consequence of a 5 min application of 500 μM NMDA in YAC128 MSNs, which suggests that very early induction of the apoptotic pathway may occur.

There was no indication of mPT activity during or following a 5 min application of 500 μM NMDA in my experiments with WT MSNs. Others have also reported mPT activation in paradigms of glutamate excitotoxicity in cultured forebrain neurons (White and Reynolds, 1996) and in hippocampal neurons (Schinder et al., 1996; Vergun et al., 1999). The acute NMDA-induced mPT activation observed in YAC128 MSNs occurred in response to similar levels of cytosolic Ca^{2+} as in WT MSNs. Others have reported significant protection against glutamate-induced cell death using putative mPT inhibitors in YAC128 MSNs from a higher mhtt-expressing line (line 53) of YAC transgenic mice (Tang et al., 2005), further supporting our hypothesis that mPT induction contributes to the enhanced NMDA-induced apoptosis in YAC128 MSNs.

Interestingly, the relative changes in cytosolic Ca^{2+} and $\Delta\Psi_m$ in YAC128 MSNs following prolonged NMDAR stimulation contrast with data obtained in YAC72 MSNs, where NMDAR current, cytosolic Ca^{2+} levels and mitochondrial membrane depolarization induced by NMDA application are all increased compared with WT MSNs and correlate with enhanced mPT activation and apoptosis (Zeron et al., 2002; Zeron et al., 2004). In this regard, it is important to note that once NMDAR-mediated cytosolic Ca^{2+} levels in YAC72 MSNs are reduced to those observed in WT MSNs, the amount of NMDA-induced apoptosis is also reduced accordingly, becoming equivalent to levels seen in WT (Zeron et al., 2004; Shehadeh et al., 2006). Taken together, these results suggest that the mechanism by which mhtt enhances NMDAR-mediated apoptosis is different, depending on the length of the CAG repeat (Figure 25).

Previous studies conducted on isolated mitochondria from human lymphoblasts demonstrated that mitochondria from HD patients depolarized more readily than those

from controls when incubated with Ca^{2+} (Panov et al., 2002; Panov et al., 2005), and that this depolarization caused the release of Ca^{2+} from the mitochondria, an event which could be delayed by inhibition of the mPT (Panov et al., 2002). Importantly, the authors observed that mitochondria from juvenile-onset HD patients were even more sensitive to stepwise additions of Ca^{2+} than those from adult-onset patients. These data are consistent with the idea that CAG repeat length can modulate the mechanisms underlying MSN sensitivity to apoptosis. I have demonstrated that mitochondria in YAC128 MSNs can efficiently buffer Ca^{2+} during a 60s application of 500 μM NMDA, and that a longer duration of NMDA application results in mPT activation. A leak of free Ca^{2+} from compromised mitochondria in YAC128 MSNs may contribute to the difference in intracellular Ca^{2+} recovery rates following 5 min NMDAR activation, although other mitochondrial Ca^{2+} transport mechanisms including a mitochondrial Na^{+}/Ca^{2+} exchanger (White and Reynolds, 1997; Gunter et al., 2000) or the mitochondrial Ca^{2+} uniporter (Kirichok et al., 2004) could also play a role in this difference. Further experiments would be required to determine the possible relative contributions of these different mechanisms to mitochondrial failure to regulate cytosolic Ca^{2+}.

Extrapolating these observations together with my data to the human condition, raises the possibility that HD patients with more extreme CAG repeat expansions may be best served by targeting therapies at the level of the mitochondria, for example to better resist mPT induction.

A recent study by Oliveira et al., (2006) found mhtt-induced impairment of cytosolic Ca^{2+} and $\Delta\Psi_m$ responses to a 10 min application of 100 μM NMDA in YAC128 MSNs. However, this study was aimed at delineating events which occur during

neuronal dysfunction, and thus were achieved under conditions of glycolytic inhibition and ATP depletion. In contrast, my results were obtained in YAC128 MSNs in their normal metabolic state, in order to elucidate events that could lead specifically to apoptosis, as characterized by our lab (Shehadeh et al., 2006). This difference in methodology makes a direct comparison of results difficult to interpret. However, their findings also support the idea of a deficit in mitochondrial function that is present, as in our experiments, from an early age during development and that underlies neuronal dysfunction preceding death in HD (Oliveira et al., 2006).

6.4 Mhtt-Induced Impairment of Ca^{2+} Homeostasis in YAC128 MSNs

Consistent with a previous report (Tang et al., 2005), we found similar resting Ca^{2+} levels in WT and YAC128 MSNs. As steady-state resting Ca^{2+} is determined primarily by the balance between Ca^{2+} entry and efflux/sequestration mechanisms (Xiong et al., 2002), these processes are likely to be normally functional during resting (i.e. unstressed) conditions within YAC128 MSNs, at least at the early time-point of our assessment. Further evidence of this comes from our results showing that cytosolic calcium recovery in YAC128 MSNs occurs normally (i.e. shows a rate of recovery similar to WT MSNs) following a brief (60s) stimulation of NMDARs, or even prolonged (5 min) stimulation of VGCCs using KCl with FPL (the L-type Ca^{2+}channel modulator). These data suggest that VGCC activation is also similar between WT and YAC128 MSNs, and that differences in intracellular handling of Ca^{2+}, such as mitochondrial buffering, only become apparent during prolonged (5-min) NMDAR-induced stress, a finding supported by previous research (White and Reynolds, 1995). This requirement of

a stressful stimulus to uncover underlying functional deficits in mitochondria is not surprising, given findings that active glycolysis in the cytosol can mask mhtt-induced mitochondrial deficiencies in Ca^{2+} handling in ST*Hdh*Q^{111} cells that become apparent when glycolysis is inhibited (Oliveira et al., 2006).

While the experiments presented here have largely focused on mitochondrial regulation of cytosolic Ca^{2+}, mPT inhibition had no effect on the rate of Ca^{2+} recovery towards baseline following an NMDA-induced Ca^{2+} load. This observation suggests that other intracellular Ca^{2+} stores and extrusion/sequestration or buffering mechanisms may contribute to impaired calcium homeostasis. Indeed, an interaction between mhtt, htt-associated protein 1A (HAP-1A) and the IP_3 receptor (IP_3R) has been shown, resulting in increased sensitivity of the IP_3 receptor to IP_3 (Tang et al., 2003). In turn, this abnormal interaction appears to enhance the toxicity of glutamate-mediated IP_3R activation in YAC128 MSNs, facilitating Ca^{2+} release from the ER in YAC128 MSNs in response to the selective mGluR1/5 agonist 3, 5 - DHPG (Tang et al., 2005). This mechanism was not likely to be activated in our paradigm using NMDA, although Tang et al. (2005) also reported enhanced sensitivity of YAC128 MSNs to NMDAR-mediated apoptosis. Consistent with our results demonstrating impaired Ca^{2+} recovery following NMDAR activation in YAC128 MSNs, repetitive glutamate stimulation produced a gradual elevation in cytosolic Ca^{2+} in YAC128 MSNs, but not WT or YAC18 MSNs over a similar timeframe (Tang et al., 2005).

One interesting possibility that could contribute to impaired extrusion of cytosolic Ca^{2+} is dysfunction of the Na^+/Ca^{2+} exchanger isoform 3 (NCX3). A recent report (Bano et al., 2005) demonstrated that NCX3 is cleaved by calpains in striatal tissue following

focal ischemia and in cerebellar granule neurons under excitotoxic conditions. Overexpression of calpastatin, an endogenous inhibitor of calpains, in CGNs prevented secondary elevations in cytosolic Ca^{2+} following glutamate application and protected neurons from glutamate-mediated excitotoxicity (Bano et al., 2005). Others have reported that plasmalemmal Na^{+}/Ca^{2+} exchange activity plays a role in buffering glutamate-mediated Ca^{2+} increases in forebrain neurons (White and Reynolds, 1995). If activation of μ- or m-calpains in YAC128 MSNs following NMDAR activity is enhanced (Nicotera et al., 1986), another important homeostatic Ca^{2+} clearance route would be impaired. If this increased calpain activity is Ca^{2+}-dependent (Gafni and Ellerby, 2000; Gafni et al., 2004), then it could result in a feed-forward mechanism that slowly amplifies to a maximum over time, resulting in the gradual development of more severe Ca^{2+}-handling deficits.

Another interesting explanation for impaired Ca^{2+} clearance in YAC128 MSNs following prolonged NMDA application is a possible difference in cytosolic Ca^{2+} buffering factors, for example differential expression of Ca^{2+} buffering proteins such as calbindin (CaBP), or other cytosolic buffering factors in YAC128 compared to WT MSNS. CaBP overexpression did not alter peak Ca^{2+} downstream of NMDAR activation but did prolong the recovery of Ca^{2+} towards baseline values (Rintoul et al., 2001), reminiscent of our observations in YAC128 MSNs.

Evidence from human HD patient brains indicates increasing CaBP expression, with increases in expression in MSN dendrites and spines associated with more advanced (grades 3 and 4) cases (Huang et al., 1995). Following intrastriatal injection of quinolinic acid, surviving MSNs expressed increased levels of CaBP; the upregulated expression

was found to be dependent upon NMDAR activity, suggesting that this expression change was a excitotoxicity-driven attempt to buffer elevated Ca^{2+} levels (Huang et al., 1995). Similar observations have been made in the striatum of R6/2 mice. A pattern of increased CaBP expression was observed in the dorsolateral striatum, an area normally associated with low CaBP expression; this increase was viewed as an attempt to buffer Ca^{2+} downstream of an excitotoxic process (Sun et al., 2005), and occurred at an age associated with resistance to excitotoxicity in R6/2 mice (Hansson et al., 2001). However, our data in YAC128 MSNs do not support the idea of enhanced NMDAR activity driving a compensatory upregulation in CaBP expression. CaBP overexpression was also found to reduce mitochondrial depolarization in response to ionophore-mediated Ca^{2+} elevations, and enhance the 24h survival rate following NMDA incubation (Rintoul et al., 2001), findings which are inconsistent with our observations of increased apoptosis in YAC128 MSNs 24h following NMDA exposure (Graham et al., 2006b; Shehadeh et al., 2006;) and enhanced mitochondrial depolarization in YAC128 MSNs following NMDAR activity.

There is however an interesting similarity between results obtained in my study and a previous study using artificial Ca^{2+} buffers in an excitotoxicity paradigm in hippocampal neurons. In that study, following glutamate exposure, the presence of buffers did not have an impact on peak cytosolic Ca^{2+} but significantly slowed the recovery of Ca^{2+} towards baseline levels and enhanced, rather than reduced, neuronal death (Abdel-Hamid and Baimbridge, 1997). These are similar observations to what we report here in YAC128 MSNs. The authors argued that the effect of artificial Ca^{2+}-buffering actually enhanced overall Ca^{2+} entry into the neurons, possibly by inhibiting

normal Ca^{2+}-dependent feedback mechanisms on NMDAR function (Abdel-Hamid & Baimbridge, 1997), and that excitotoxicity better correlates with total Ca^{2+} influx rather than peak free cytosolic Ca^{2+} (Michaels and Rothman, 1990; Hartley et al., 1993; Abdel-Hamid and Baimbridge, 1997).

This last point is an issue of controversy, as other work has suggested that the Ca^{2+} influx pathway (Peng and Greenamyre, 1998; Sattler et al., 1998;) is the most important factor determining neuronal excitotoxicity, while a different set of studies showed that peak Ca^{2+} is in fact predictive of excitotoxicity under the right conditions (Cheng et al., 1999; Stout and Reynolds, 1999). The findings regarding YAC128 MSNs presented here, along with data on NMDA-induced apoptosis in the same cells (Graham et al., 2006b; Shehadeh et al., 2006) indicate that peak Ca^{2+} was not predictive of excitotoxicity even when low-affinity Ca^{2+} indicators were used. It could be that the presence of mhtt, which affects mitochondrial function and Ca^{2+} handling as mentioned earlier, alters the predictive value of Ca^{2+} changes on excitotoxic outcomes. Also, there is no evidence presented here to support the idea that total Ca^{2+} influx is greater in YAC128 MSNs, or that the Ca^{2+} buffering potential of the cytosol in YAC128 MSNs is in any way different from WT. As suggested earlier (Section 6.2), it may be that mitochondrial depolarization and Ca^{2+} uptake are the best predictors for neuronal viability in HD models. Further experiments will be required to address these questions. Overall, these observations suggest that a strategy of using Ca^{2+} buffers as a therapeutic intervention to spare MSNs in HD would be difficult at best.

The finding that YAC128 MSNs exhibit significantly longer delays in recovery of cytosolic Ca^{2+} following NMDA challenge than WT MSNs may be important with regard

to downstream toxic consequences, particularly those mediated by Ca^{2+}-activated pathways, as in calpain activation. Indeed, in excitotoxicity-resistant R6/2 mice, it is speculated that elevated resting Ca^{2+} levels in MSNs may be a stress-induced alteration which could cause neuronal dysfunction underlying behavioural deficits preceding neuronal death (Hansson et al., 2001). A similar phenomenon, stemming from a cumulative dysfunction downstream of NMDAR activity, may manifest itself over time in YAC128 mice, which start showing behavioural changes prior to any apparent neuronal loss (Slow et al., 2003). The changes in YAC128 MSN function that we have characterized here are present from early development, and thus are consistent with a progressively developing condition arising from cumulative insult.

6.5 Selective Vulnerability of MSNs in HD

There are a number of observations that could provide an explanation for the selective vulnerability of MSNs to neurodegeneration in HD. A natural starting place would be the distribution of htt; however, studies of htt distribution in rat striatal and cortical neurons showed no correlation between neuronal subtypes that express htt and those that preferentially degenerate in HD (Fusco et al., 1999). In fact, mRNA evidence suggests that several regions of the brain in humans, including hippocampus, cerebellum, and cerebral cortex, exhibit higher levels of htt than the striatum (Landwehrmeyer et al., 1995b). These observations suggest that the expression pattern of htt does not explain selective neurodegeneration.

Mitochondria isolated from rat striatal tissue were found to depolarize to a greater extent, have reduced ATP:ADP ratios, and be more susceptible to permeability

transition than those isolated from cortical tissue, when challenged with Ca^{2+}. This inherent difference in brain mitochondria was attributed to an increased expression of the mPT component cyclophilin D in striatal mitochondria, suggesting that striatal mitochondria are more prone to mPT activation than mitochondria from other brain regions (Brustovetsky et al., 2003). My findings of enhanced mitochondrial depolarization in the absence of increased NMDAR current in YAC128 MSNs, and the effects of mPT inhibitors on peak Ca^{2+} and mitochondrial depolarization support the idea of a mhtt-mediated enhancement of mPT formation. However, in this study I have not addressed the issue of what molecular mechanisms underlie the enhanced sensitivity to Ca^{2+}-induced mPT formation (e.g., whether cyclophilin D expression is altered in mitochondria from YAC128 versus WT MSNs) nor whether enhanced mPT activation occurs selectively in mhtt-expressing MSNs versus CPNs. Further experiments would be required to investigate these questions.

Another strong possible candidate as a factor explaining enhanced MSN vulnerability in HD would be the expression pattern of NMDARs and in particular the specific NMDAR subunits expressed within neuronal subtypes which may underlie selective neurodegeneration of MSNs. Whereas MSNs express predominantly NR1-1A, NR2A and NR2B (Landwehrmeyer et al., 1995a; Kuppenbender et al., 1999; Chapman et al., 2003), striatal interneurons express reduced levels of NR2B and preferentially express NR2D (Landwehrmeyer et al., 1995a). NMDA-evoked currents were much larger in MSNs vs. larger interneurons, as were EPSCs, whereas kainate-evoked currents showed the opposite pattern (Cepeda et al., 2001a). Notably, MSNs swelled in response to exogenous NMDA application, whereas striatal interneurons responded with very little

change, indicating that MSNs are at a greater risk, even in the absence of mhtt, for excitotoxic damage (Cepeda et al., 2001a). Perhaps the context of impaired mitochondrial function in MSNs provides the background conditions required for the NR2B-selective hypothesis (see Section 1.2.4.2) to be realized, i.e. the combination of NR2B-containing NMDARs on a cellular background with mitochondria more likely to transition to mPT formation is a key factor in MSN vulnerability in HD. Our findings of selective enhancement of NMDAR (but not AMPA/kainate receptor) currents in MSNs (and not CPNs) support this concept, but further experiments with respect to mitochondrial function would be required to determine whether this hypothesis is valid.

6.6 Limitations of This Study and Suggested Further Experiments

The main goals of this study were to examine the relationship between polyQ length and modulation of NMDAR function, and explain the mechanism(s) underlying enhanced NMDA-induced apoptosis in YAC128 MSNs. The opportunity to look back with hindsight allows the subsequent identification of limitations on interpretation of results, either because of a deficit in experimental design or execution, or because further experimentation is required to answer new questions which arise from our findings and the recent findings of others.

Our finding of an enhanced rate of NMDAR insertion into the plasma membrane over a span of minutes (Chapter 3) in YAC72 MSNs relative to WT MSNs may be attributable to the effect of mhtt on overall rates of NMDAR trafficking towards the plasma membrane (Fan et al., 2007). However, considering that YAC72 MSNs express a greater total amount of htt, mutant or otherwise, than WT MSNs raises the possibility that

the difference in insertion rates was due to an effect related to the total amount of htt (including mhtt) rather than the polyQ expansion in mhtt. Although the finding that surface:internal NR1 ratios are equivalent in WT and YAC18 MSNs argues against this possibility, the inclusion of data from YAC18 MSNs on insertion rate to the plasma membrane (as determined electrophysiologically) would provide a more definitive answer to this question. The lack of such a finding would not disprove the hypothesis being true in MSNs, but rather indicate a striatal-specific trafficking mechanism that may in turn help to explain striatal vulnerability in HD. Furthermore, if the enhanced rates of NMDAR trafficking are due to the expanded polyQ region in YAC72 MSNs, then a similar alteration in trafficking would be expected in YAC128 MSNs. A confirmation of increased NMDAR forward trafficking in YAC128 MSNs would necessitate the existence of an opposing mechanism in order to maintain a steady-state distribution of NMDARs similar to that seen in WT MSNs. Hence it would be useful to conduct these experiments in genotypes other than what I have assessed thus far.

All of the experiments in this thesis monitoring Ca^{2+} dynamics and $\Delta\Psi_m$ changes involved a comparison between WT and YAC128 MSNs. This choice of comparison is subject to the same criticism as above in that our control expresses less total htt, endogenous and mhtt combined, than the experimental group, a possible confounding factor. Our choice of WT as the control was driven by observations that YAC18 mice, and cultured MSNs derived from them, show a resistance to noxious stimuli including excitotoxins, Ca^{2+} ionophores, and even general apoptotic inducers (Leavitt et al., 2006; Shehadeh et al., 2006;). This resistance is ascribed to a possible neuroprotective role of normal htt (Leavitt et al., 2001; Leavitt et al., 2006). In our mind, the use of a control

that is inherently resistant to excitotoxicity, the induction of which we are attempting to characterize in order to differentiate alterations caused by mhtt expression, would not be an appropriate representation of normal events. However, having obtained data from the 'normal' situation (WT MSNs) it would be of great interest to see if the neuroprotection afforded by htt overexpression is due to neuroprotective modulation of Ca^{2+} handling and $\Delta\Psi_m$ maintenance. This would be of further interest when compared in parallel with MSNs from YAC128 mice expressing a caspase-6 resistant (C6R) form of mhtt. These mice do not develop HD and appear to have a WT phenotype, and MSN cultures derived from these mice show no enhanced apoptosis or neurotoxicity in response to excitotoxins (Graham et al., 2006b). A particularly interesting comparison of Ca^{2+} handling and mitochondrial function would be between YAC18, C6R-YAC128, and YAC128 to see if neuroprotection in the first two models correlates with reduced sensitivity of mitochondria to Ca^{2+}-induced mPT formation. If so, it would support the ideas that mhtt retains at least some normal function of htt (arguing against the loss of function hypothesis) and that cleavage of mhtt is an initiating toxic event.

As the correlative relationship between htt polyQ length and NMDAR current density in MSNs is intact up to YAC72 but does not extend beyond to YAC128 MSNs, the idea that altered NMDAR function is solely responsible for the selective vulnerability of MSNs must be questioned. Our results suggest that mhtt containing a polyQ expansion greater than a certain threshold number may modulate neurotoxicity in a different manner than shorter pathogenic polyQ expansions. If the impairment of mitochondrial function in YAC128 MSNs is also apparent in other neuronal populations,

it would support the argument that different lengths of pathogenic polyQ expansions in htt are toxic by different mechanisms.

Lastly, the work presented here has identified an abnormality in YAC128 MSN responses to NMDA that can explain enhanced excitotoxicity in these cells; however, the reason for the particular sensitivity of mitochondria in YAC128 MSNs still needs to be elucidated. One possibility may be that the physical localization of mitochondria within YAC128 MSNs makes them more vulnerable to sudden Ca^{2+} changes, for example if a disproportionate number of mitochondria are near extrasynaptic NMDARs, the activation of which are associated with neuronal death (Hardingham et al., 2002; Liu et al., 2004). Another related possibility is that movement of mitochondria, shown to be impaired by mutant htt (Chang et al., 2006), is restricted in YAC128 MSNs such that they are unable to respond appropriately to localized energy (or other functional) demands within the cell. Combined with the greater predisposition of striatal mitochondria towards mPT formation (Brustovetsky et al., 2003), such circumstances could not only explain enhanced sensitivity to NMDAR activation in YAC128 MSNs (Shehadeh et al., 2006) but also possibly explain the enhanced vulnerability of MSNs in HD.

6.7 Conclusions

Our findings using primary MSN cultures from YAC mice transgenic for human htt suggest a critical role for NMDARs in initiating MSN dysfunction and death in HD. Our research suggests that NMDAR activity can be selectively enhanced in a neuronal type-specific manner, through a mechanism that increases the expression of NMDARs on the plasma membrane (Fan et al., 2007). This redistribution results in an increased

sensitivity to NMDAR-mediated excitotoxicity. Our findings also support a mhtt-mediated mechanism whereby sustained NMDAR activation reveals an inability to regulate cytosolic Ca^{2+} in MSNs, in the absence of increased NMDAR peak current. Diverging from YAC models with shorter polyQ expansions, the enhanced NMDA-induced apoptosis in YAC128 MSNs appears largely determined by increased susceptibility to Ca^{2+}-induced mitochondrial depolarization, acute mitochondrial dysfunction, and mPT activation. These observations may help to refine the choice of therapeutic strategies to test in YAC HD mouse models with different CAG sizes. Importantly, signalling pathways activated by strong NMDAR stimulation converge on the mitochondria in all YAC HD models, indicating that intervention downstream of NMDAR activity, such as bolstering mitochondrial function and/or mPT inhibition, may represent viable targets for ameliorating excitotoxicity-driven apoptosis in HD.

Table 1. A Summary of Relevant Full-Length and N-Terminal Fragment HD Models

	R6/1, R6/2	YAC46, YAC72, YAC128	N171	CAG80	CAG94	*Hdh*Q92, *Hdh*Q111	tgHD100
References	Mangiarini et al. (1996)	Hodgson et al. (1999), Slow et al. (2003)	Schilling et al. (1999)	Shelbourne et al. (1999)	Levine et al. (1999)	Wheeler et al. (2000)	Laforet et al. (2001)
Promoter	Human	Human	Prion	Murine	Murine	Murine	Rat NSE
Transcript	Exon 1	All 67 exons	cDNA for N-terminal 171aa	CAG knock-in	CAG knock-in	CAG knock-in	cDNA for N-terminal 3 kb
# CAG repeats	120, 150	46, 72, 128	82	80	94	92, 111	100
Striatal NMDAR protein expression	NR1 unchanged or increased, NR2A/NR2B decreased	NR1/NR2B unchanged in YAC46 or YAC72	NR2A transiently decreased	N.R.	N.R.	N.R.	N.R.
Electrophysiological properties	Altered	Altered	N.R.	N.R.	Altered	Altered	Altered
Hippocampal and/or striatal LTP/LTD	Altered	Altered	N.R.	Altered	N.R.	N.R.	N.R.
Striatal NMDAR-current	Increased	Increased	N.R.	N.R.	N.R.	N.R.	Increased
Striatal NMDAR-Ca^{2+} or cell swelling response	Increased	Increased	N.R.	N.R.	Increased	N.R.	Increased
Striatal NMDAR-mitochondrial membrane depolarization	N.R.	Increased	N.R.	N.R.	N.R.	N.R.	N.R.
Cellular energy metabolism	N.R.	N.R.	N.R.	N.R.	N.R.	Impaired	N.R.
Striatal NMDAR toxicity	No change early, resistant late	Increased; remains susceptible	Resistant late	N.R.	N.R.	N.R.	Not different from wt

N.R. = not reported
NSE = neuron specific enolase

Table taken directly from (Fan and Raymond, 2007)

FIGURES

Figure 1. Representative whole-cell current response of a voltage-clamped (V_H = -60 mV) WT MSN to a 4 s application of 1 mM NMDA. The peak current amplitude (I_{peak}) is measured as indicated, and the 200 ms region which is averaged to derive the value for steady-state current (I_{ss}) is identified near the end of the NMDA application period.

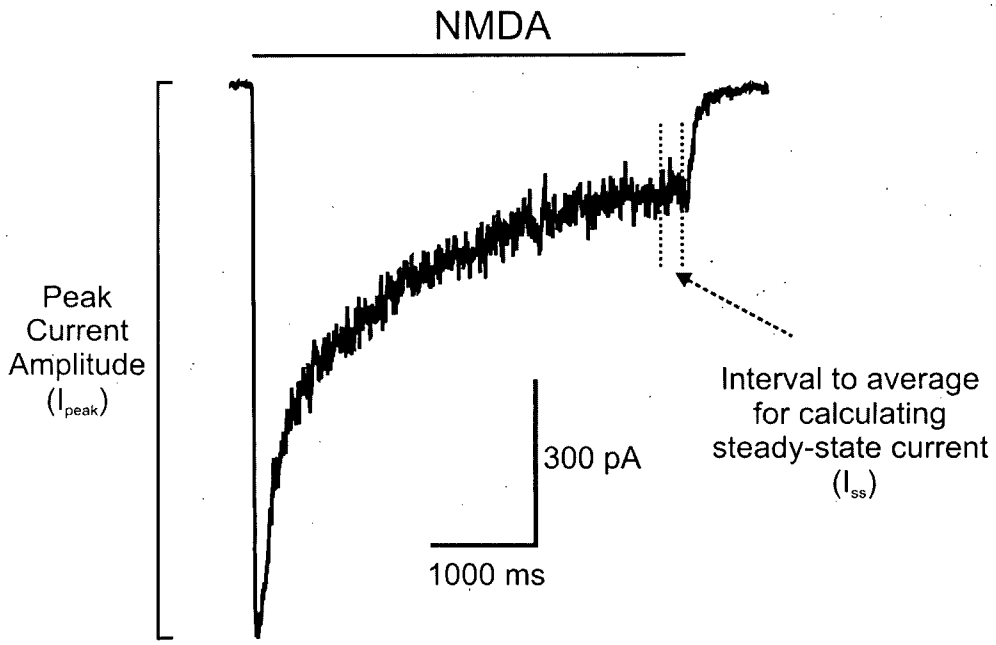
NMDA
Peak
Current
Amplitude
(I_{peak})
300 pA
1000 ms
Interval to average
for calculating
steady-state current
(I_{ss})

Figure 2. Peak NMDAR current density varies with htt polyQ length in cultured MSNs. Whole-cell patch clamp recording was performed on cultured MSNs at 9-10 d.i.v. stimulated with 1 mM NMDA. Bars represent mean peak current density (peak current normalized to cell capacitance) ± SEM. n = 42 (WT), 13 (YAC18), 11 (YAC46), 16 (YAC72) or 20 (YAC128) cells total. Significant difference between genotypes by one-way ANOVA, effect of genotype $F(4,97) = 5.113$, $P<0.001$; * $P< 0.05$, ** $P< 0.01$ by Bonferroni post-test.

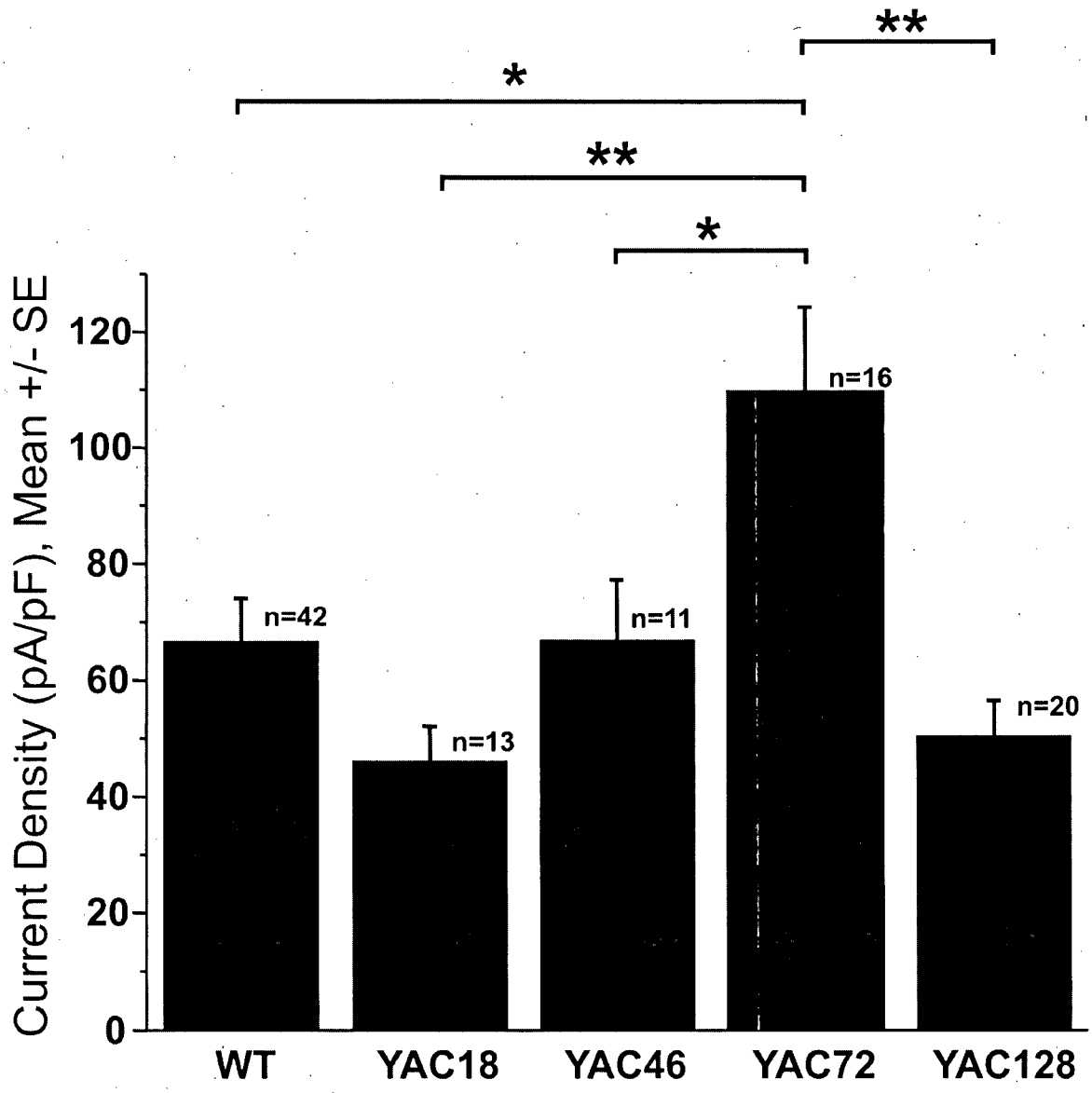
**
*
**
*
Current Density (pA/pF), Mean +/- SE
120
100
80
60
40
20
0
n=42
n=13
n=11
n=16
n=20
WT
YAC18
YAC46
YAC72
YAC128

Figure 3. PolyQ length does not affect kainate receptor current density. **A)** Representative whole-cell current response of a voltage-clamped (V_H = -60 mV) MSN to a 4 s application of 1 mM kainate. **B)** Mean peak current densities of WT and YAC72 MSNs in response to exogenous application of 1 mM kainate as in A). Whole-cell patch clamp recordings were performed on cultured MSNs at 9-10 d.i.v. as described in Methods. n=11 (WT) or 10 (YAC72) cells total. Bars represent mean peak current density (peak current normalized to cell capacitance) ± SEM. No significant difference between genotypes by unpaired t-test.

A

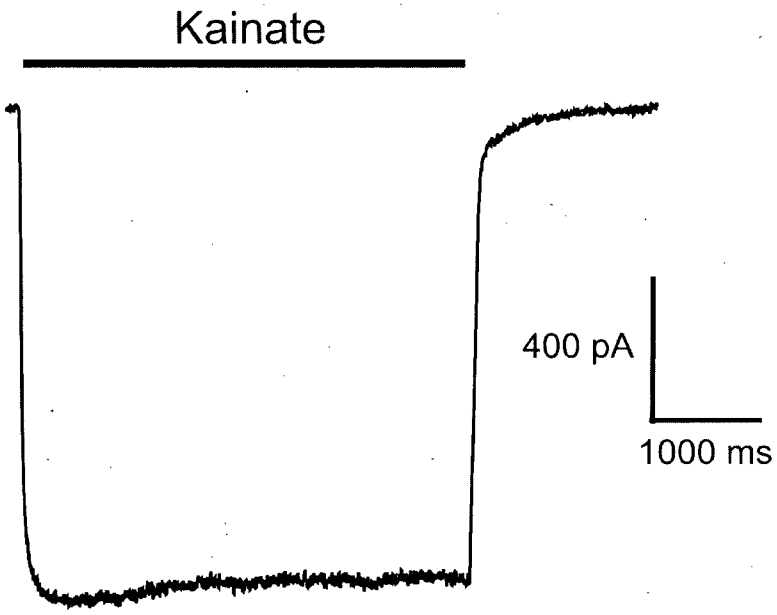
Kainate
400 pA
1000 ms

B

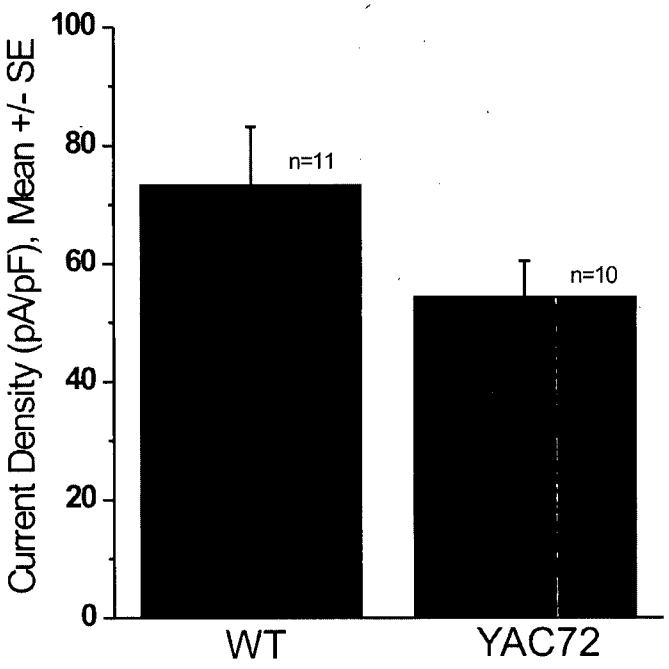
Current Density (pA/pF), Mean +/- SE
100
80
60
40
20
0
n=11
n=10
WT
YAC72

Figure 4. Peak NMDAR current density is not influenced by htt polyQ length in cultured CPNs. Whole-cell current density was measured under voltage clamp (V_H = -60 mV) in cultured CPNs (4-7 d.i.v.) from WT, YAC18, YAC72 and YAC128 mice, stimulated with 1 mM NMDA. n=20 (WT), 11 (YAC18), 19 (YAC72) or 17 (YAC128) cells total. Bars represent mean peak current density (peak current normalized to cell capacitance) ± SEM. No significant difference between genotypes by one-way ANOVA.

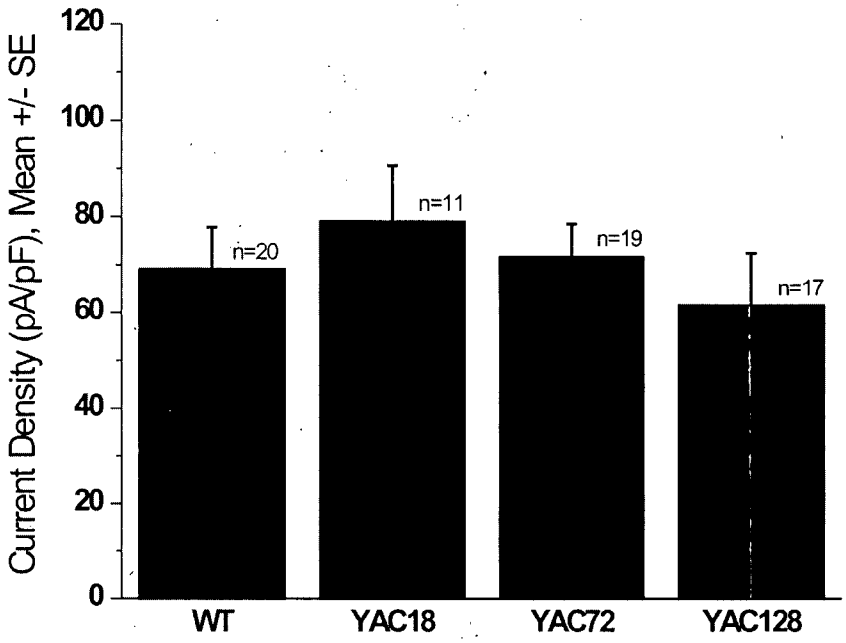
Current Density (pA/pF), Mean +/- SE
120
100
80
60
40
20
0
n=20
n=11
n=19
n=17
WT
YAC18
YAC72
YAC128

Figure 5. Desensitization of whole-cell NMDAR current in MSNs is not governed in a polyQ length-dependent fashion. Steady-state (I_{ss}) to peak (I_{peak}) current was calculated and expressed as a percentage as described in Methods, from MSNs responding to exogenous application of 1 mM NMDA while held under voltage clamp (V_H = -60 mV). Bars represent mean peak current density (peak current normalized to cell capacitance) ± SEM. n=42 (WT), 13 (YAC18), 11 (YAC46), 16 (YAC72) or 20 (YAC128) cells total. Significant difference between genotypes by one-way ANOVA, $F(4,96) = 4.935$, $P<0.01$; *$P< 0.05$ YAC18 vs. WT, **$P<0.01$ YAC18 vs. YAC46 or YAC18 vs. YAC128 by Bonferroni post-test.

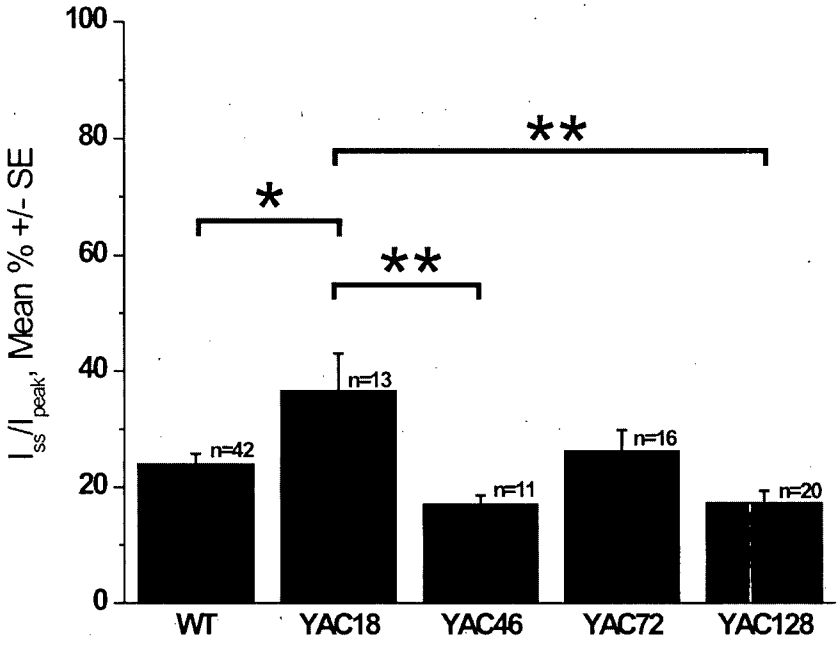
100
80
60
40
20
0
I_{ss}/I_{peak}, Mean % +/- SE
*
**
**
n=42
n=13
n=11
n=16
n=20
WT
YAC18
YAC46
YAC72
YAC128

Figure 6. Desensitization of whole-cell NMDAR current in CPNs is not altered by polyQ length. Steady-state (I_{ss}) to Peak (I_{peak}) current was calculated and expressed as a percentage as described in Methods, from CPNs responding to exogenous application of 1 mM NMDA while held under voltage clamp (V_H = -60 mV). Bars represent mean peak current density (peak current normalized to cell capacitance) ± SEM. n=20 (WT), 11 (YAC18), 19 (YAC72) or 16 (YAC128) cells total. No significant difference between genotypes by one-way ANOVA.

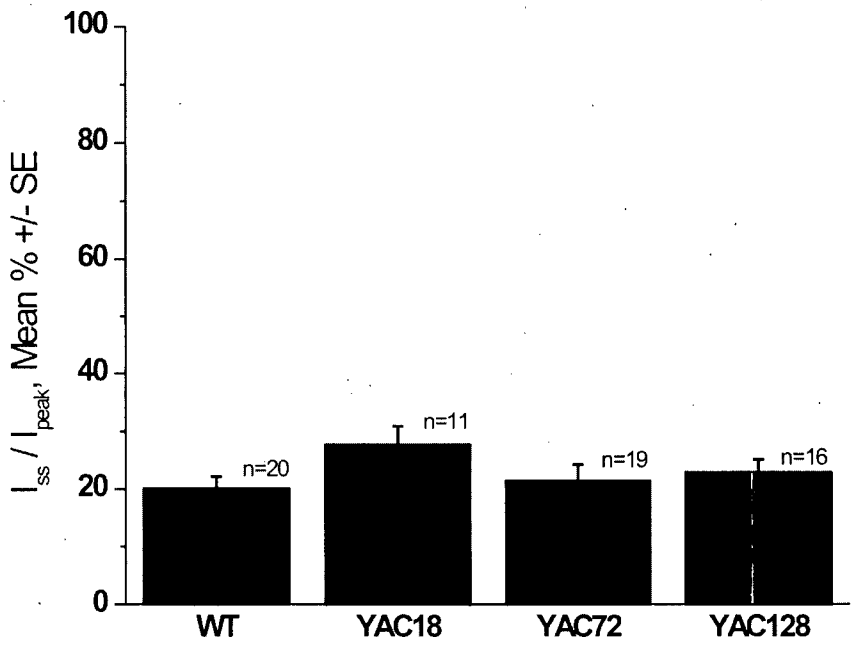
100
80
60
40
20
0
I_{ss} / I_{peak}, Mean % +/- SE
n=20
n=11
n=19
n=16
WT
YAC18
YAC72
YAC128

Figure 7. IFN blocks NR1/NR2B-containing NMDARs. **A)** Representative whole-cell current responses of a voltage-clamped (V_H = -60 mV) YAC72 MSN to a 4 s application of 1 mM NMDA, in the absence (black trace) and subsequent presence (grey trace) of 3 μM IFN. The difference between the two responses represents the fraction of current conducted by NR1/NR2B-containing NMDARs. Note that co-application of IFN with NMDA blocks the majority of NMDAR current. **B)** Representative whole-cell current responses of a voltage-clamped (V_H = -60 mV) WT CGN to a 4 s application of 1 mM NMDA, in the absence (black trace) and subsequent presence (grey trace) of 3 μM IFN. In contrast to the effect of IFN in MSNs, note that co-application of IFN with NMDA in CGNs had no effect on NMDAR I_{peak} or I_{ss}, indicating its selectivity for NR1/NR2B-containing NMDARs.

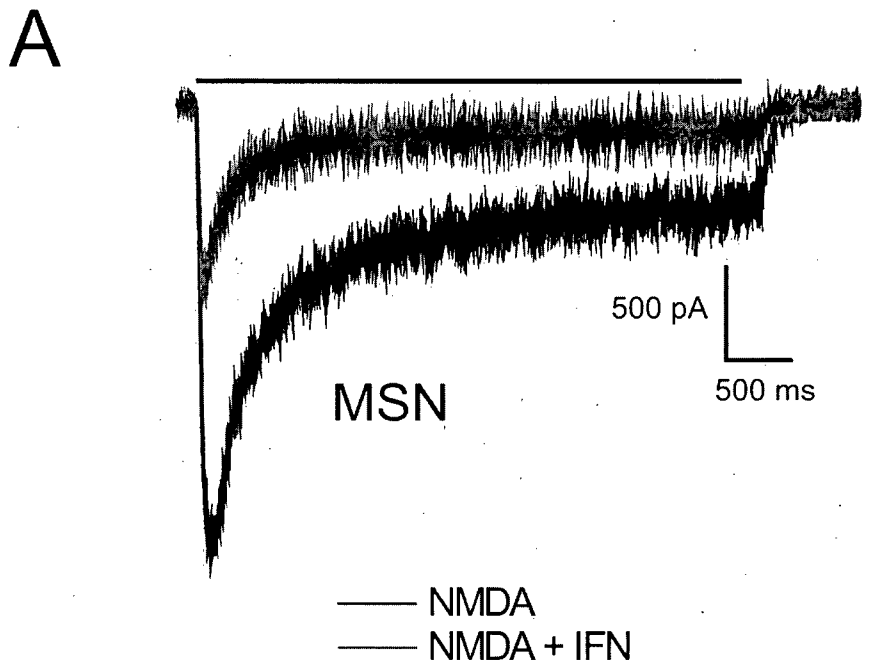
A
500 pA
500 ms
MSN
NMDA
NMDA + IFN

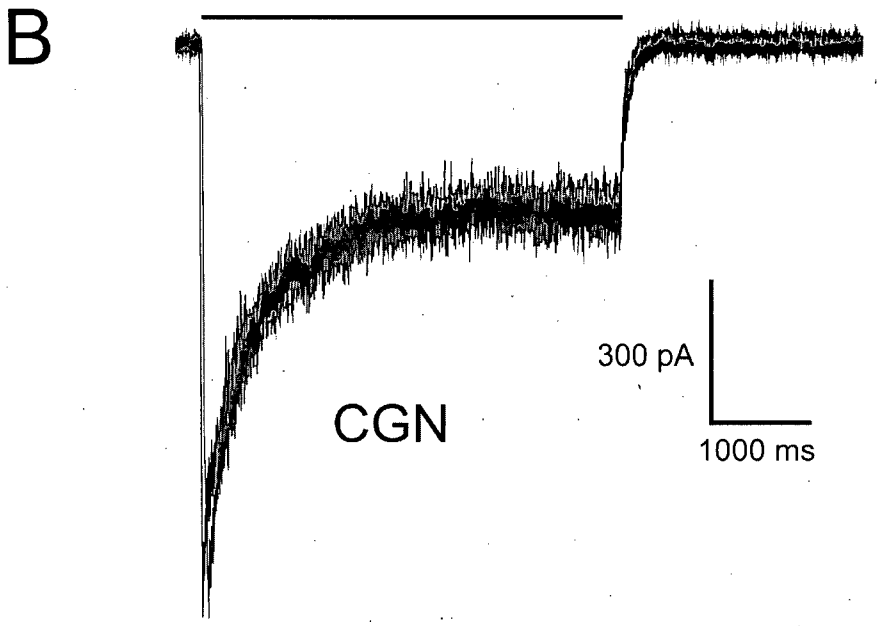
B
300 pA
1000 ms
CGN

Figure 8. Neither overexpression of htt or expression of mhtt affects the proportion of NMDARs containing NR1/NR2B in cultured MSNs. The percentage of current mediated by NR1/NR2B-containing NMDARs (those blocked by IFN) was calculated as described in Methods, from cells responding to exogenous application of 1 mM NMDA (± 3 μM IFN) while held under voltage clamp (V_H = -60 mV). Bars represent mean peak current density (peak current normalized to cell capacitance) ± SEM. n=18 (WT), 5 (YAC18), 5 (YAC46), 5 (YAC72) or 10 (YAC128) cells total. No significant difference between genotypes by one-way ANOVA.

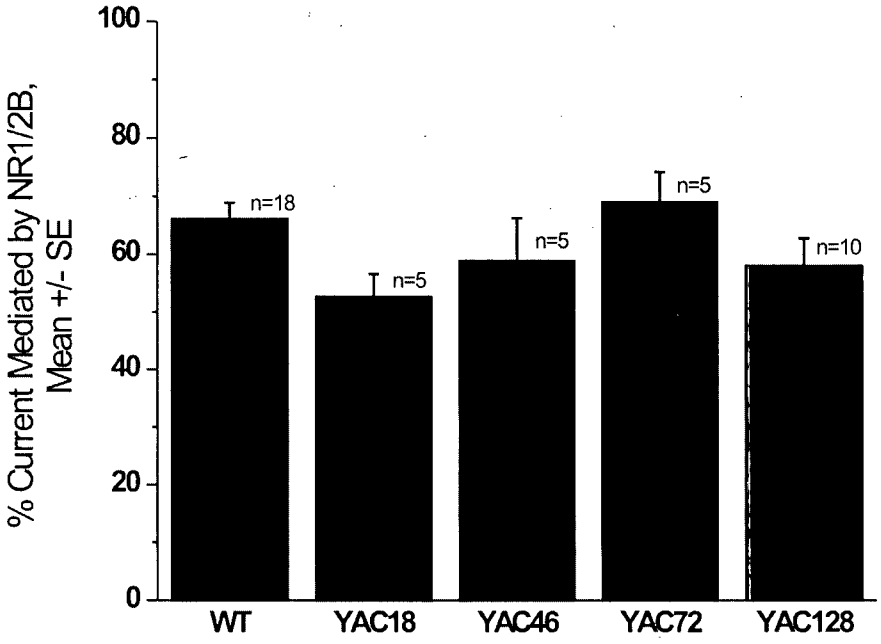
% Current Mediated by NR1/2B, Mean +/- SE
100
80
60
40
20
0
n=18
n=5
n=5
n=5
n=10
WT
YAC18
YAC46
YAC72
YAC128

Figure 9. Neither overexpression of htt or expression of mhtt affects the proportion of NMDARs containing NR1/NR2B in cultured CPNs. The percentage of current mediated by NR1/NR2B-containing NMDARs (those blocked by IFN) was calculated as described in Methods, from cells responding to exogenous application of 1 mM NMDA (± 3 μM IFN) while held under voltage clamp (V_H = -60 mV). Bars represent mean peak current density (peak current normalized to cell capacitance) ± SEM. n=9 (WT), 6 (YAC18), 10 (YAC72) or 7 (YAC128) cells total. No significant difference between genotypes by one-way ANOVA.

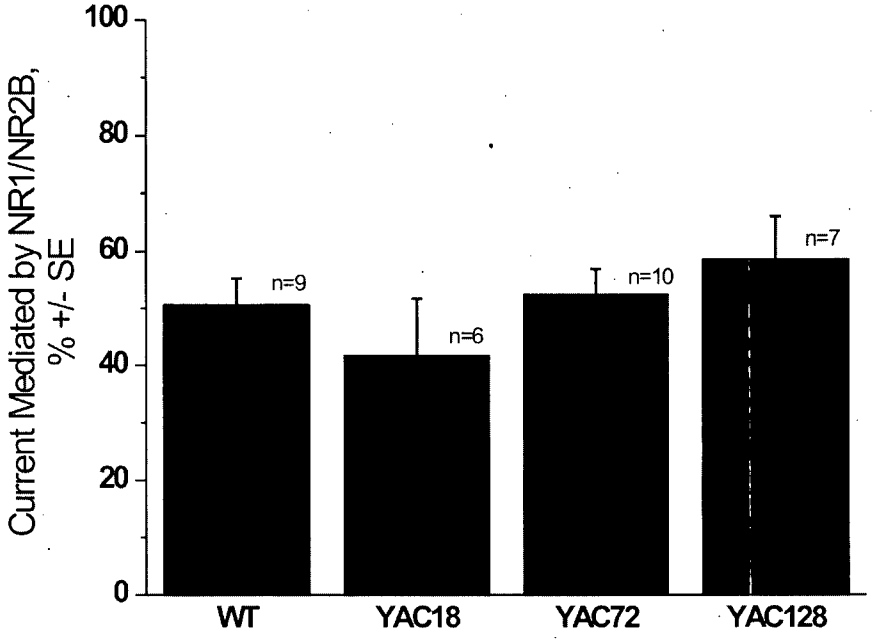
Current Mediated by NR1/NR2B, % +/- SE
100
80
60
40
20
0
n=9
n=6
n=10
n=7
WT
YAC18
YAC72
YAC128

Figure 10. Electrophysiological silencing of surface NMDARs allows for detection of naïve NMDAR insertion to the plasma membrane. **A)** Example of method used for electrophysiological silencing of cell surface NMDARs in an MSN using whole-cell patch clamp. Note clear NMDAR I_{peak} and desensitization of current during Pre-Block (pre-MK-801) phase, and decay of current towards zero during the Post-Block (Post-MK-801) phase. Initial stimulation used 1 mM NMDA (Pre-Block), followed by blockade of surface NMDARs by co-application of 1 mM NMDA and 5 μM MK-801 (Post-Block). Application of NMDA + MK-801 continued for approximately 4 s beyond what is depicted in figure. This paradigm was repeated to ensure full block of all surface NMDARs. **B)** Example of NMDAR current recovery following block by MK-801. A representative series of recordings from a YAC72 MSN showing NMDA-evoked current recovery following electrophysiological silencing of surface NMDARs; each current trace represents average of 3 consecutive responses (every 5 min) to 500 ms pulses of 1 mM NMDA.

A

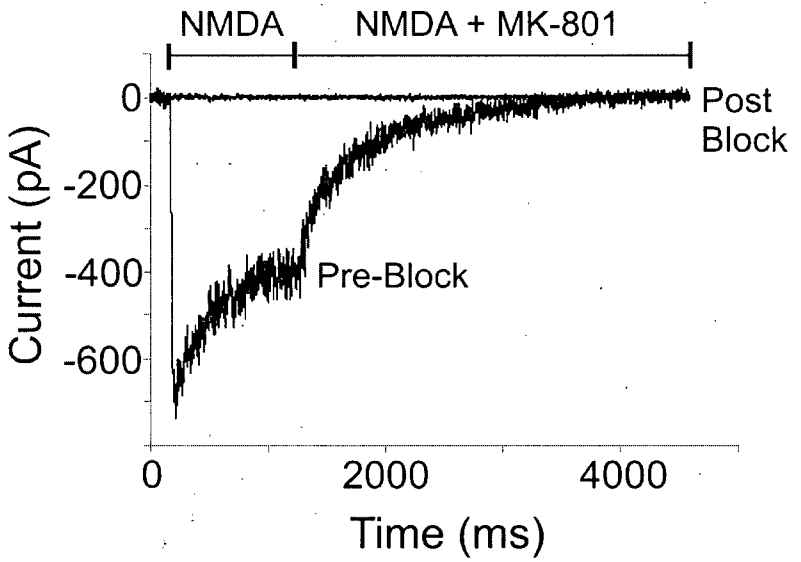
NMDA
NMDA + MK-801
0
-200
-400
-600
Current (pA)
Post
Block
Pre-Block
0
2000
4000
Time (ms)

B

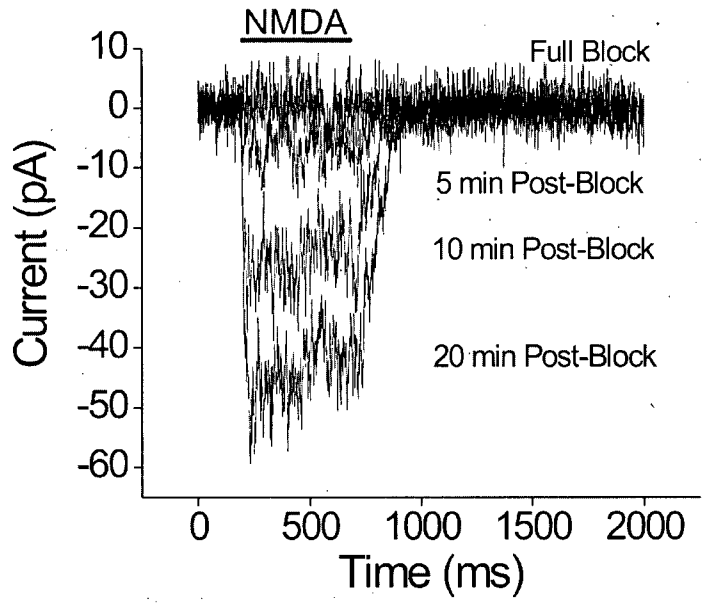
NMDA
10
0
-10
-20
-30
-40
-50
-60
Current (pA)
Full Block
5 min Post-Block
10 min Post-Block
20 min Post-Block
0
500
1000
1500
2000
Time (ms)

Figure 11. The rate of whole-cell current recovery in YAC72 MSNs following MK-801 binding is significantly faster than in WT MSNs. Plot of recovery of NMDA-evoked I_{AUC} (integrated current, normalized to C_m) over time shows that NMDAR current recovery is significantly faster in YAC72 vs. WT MSNs by 10 min post-block. Each data point represents mean ± SEM from n = 15, 10, 6 (WT) and 8, 6, 5 (YAC72) cells for 5, 10 and 15 min time points, respectively, post-block by MK-801. Significant difference in recovery of current, WT vs. YAC72 by two-way ANOVA; effect of genotype $F(1,44) = 18.39$, $P<0.001$; effect of time $F(2,44) = 11.00$, $P<0.001$; $*P< 0.05$, $**P< 0.01$ by Bonferroni post-test.

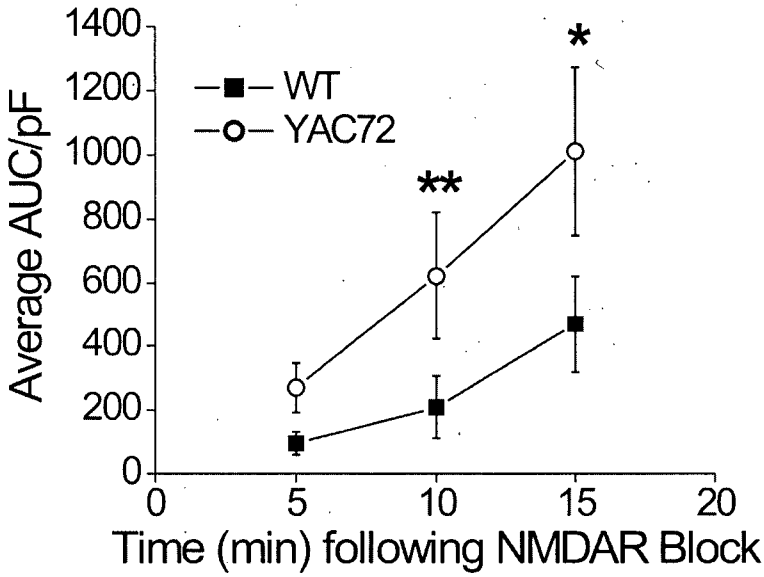
1400
1200
1000
800
600
400
200
0
Average AUC/pF
WT
YAC72
**
*
0
5
10
15
20
Time (min) following NMDAR Block

Figure 12. Example of cytosolic Ca^{2+} imaging experiment using the fluorescent Ca^{2+} indicator Fura-2. During the initial monitoring phase, the resting Ca^{2+} level is determined. A rise in cytosolic Ca^{2+} imaging is produced by a 5 min application of 500 μM NMDA, and the NMDA-induced Ca^{2+} peak is calculated accordingly. This example also shows a subsequent rise in cytosolic Ca^{2+} following the application of 2 μM 4Br-A23187, a calcium ionophore, demonstrating that our responses were not saturated by NMDA-induced Ca^{2+} influx. The response shown is a mean of 13 MSNs, and in this example is not baseline-subtracted.

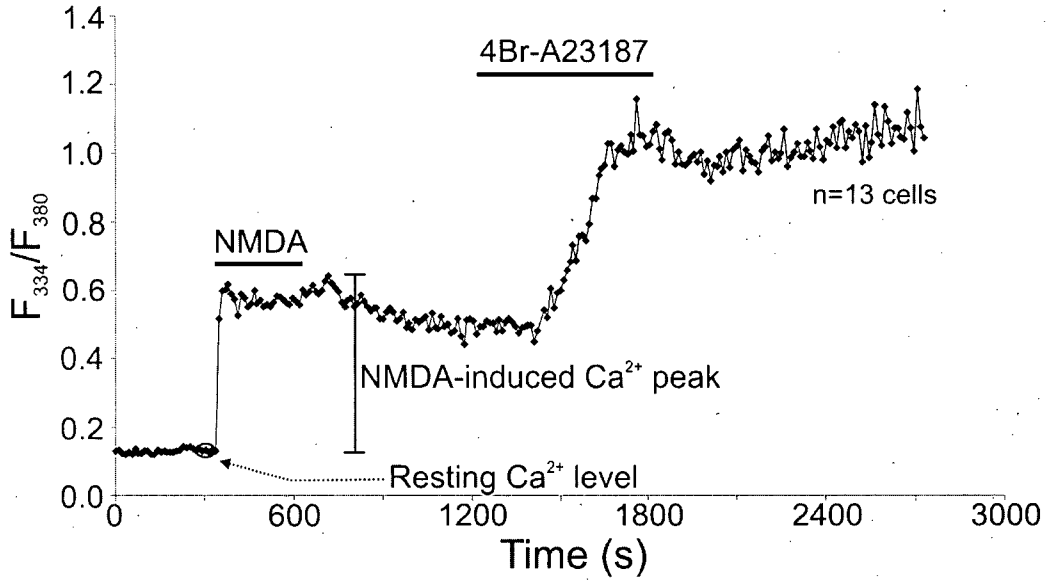
4Br-A23187
NMDA
n=13 cells
NMDA-induced Ca2+ peak
Resting Ca2+ level
F334/F380
Time (s)
1.4
1.2
1.0
0.8
0.6
0.4
0.2
0.0
0
600
1200
1800
2400
3000

Figure 13. Representative cytosolic Ca^{2+} responses of WT and YAC128 MSNs to 500 μM NMDA. Intracellular Ca^{2+} was monitored using Fura-2. Responses shown are mean responses of one experiment each from WT (solid line, n=27 cells) and YAC128 (dashed line, n=21 cells) MSNs prior to, during, and following a 5 min application of 500 μM NMDA as indicated.

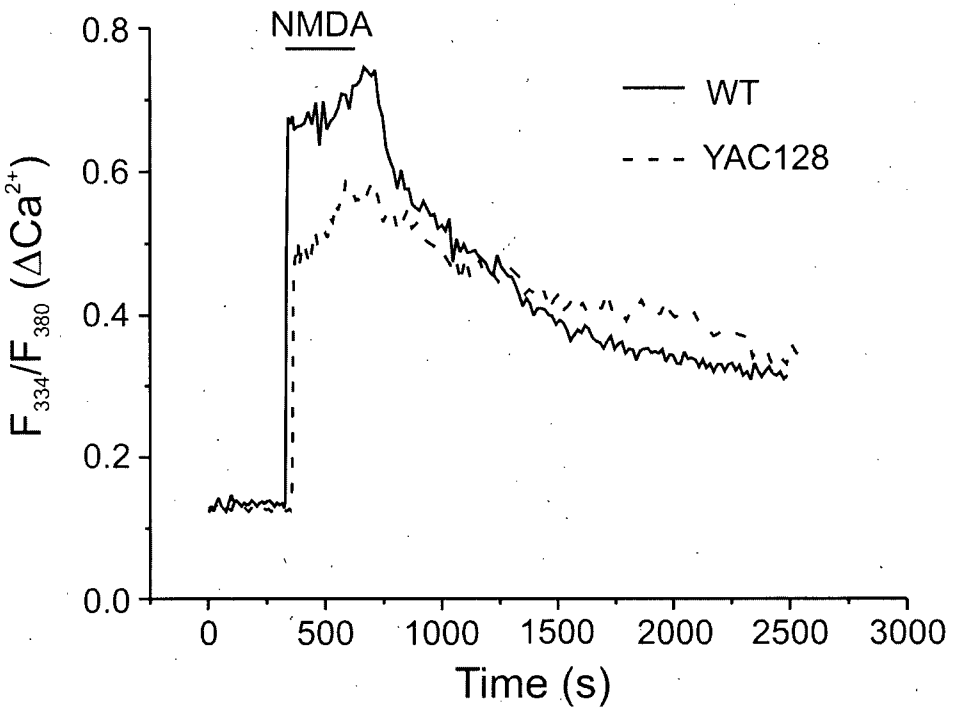
NMDA
WT
YAC128
0.8
0.6
0.4
0.2
0.0
F_{334}/F_{380} (ΔCa^{2+})
0
500
1000
1500
2000
2500
3000
Time (s)

Figure 14. WT and YAC128 MSNs have similar cytosolic Ca^{2+} responses to NMDA. **A)** Basal (n=10 experiments per genotype, total of 168 and 163 neurons for WT and YAC128, respectively, from 6 different batches of cultured neurons) and peak cytosolic Ca^{2+} responses to 100 μM NMDA (n=4 experiments per genotype, total of 73 and 68 neurons for WT and YAC128, respectively, from 2 different culture batches) or 500 μM NMDA (n=10 experiments per genotype, total of 168 and 163 neurons for WT and YAC128, respectively, from 6 different culture batches) in WT (black bars) or YAC128 (open bars) MSNs. Not significant between genotypes by paired t-test for basal cytosolic Ca^{2+}, or responses to 100 or 500 μM NMDA. Data expressed as mean ± SEM. **B)** Peak cytosolic Ca^{2+} responses of WT (black bar) and YAC128 (open bar) MSNs to 500 μM NMDA using the low affinity Ca^{2+} indicator MagFura-2. n=4 experiments per genotype, 74 and 80 neurons total for WT and YAC128, respectively, from 2 different culture batches. No significant difference between genotypes by paired t-test.

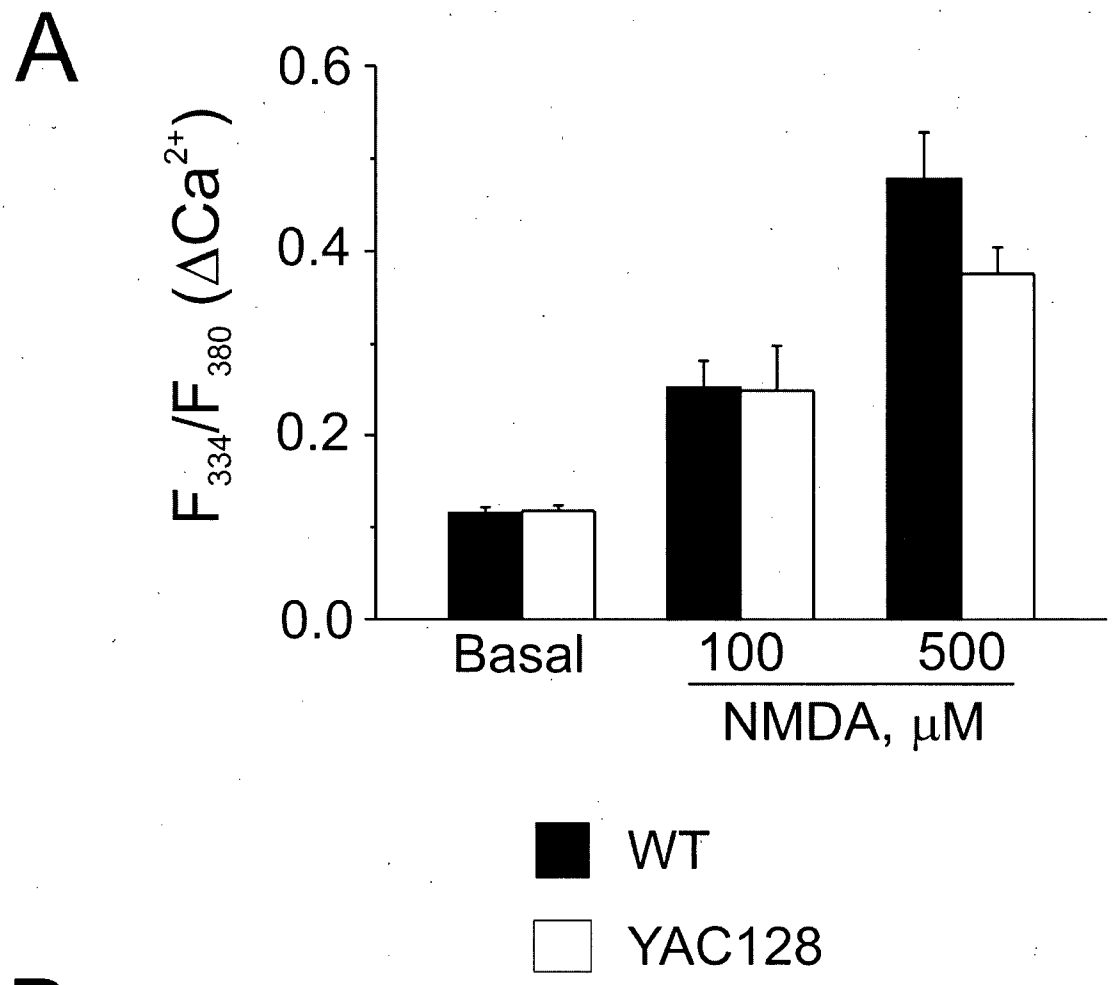

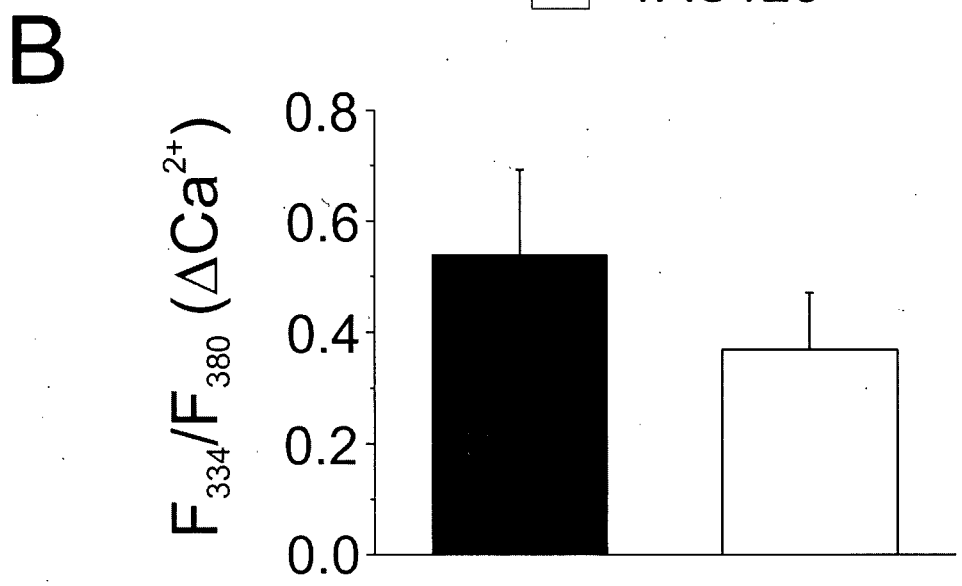

MagFura-2 data, 4 exp'ts per genotype, 80 cells for Y128 and 74 cells for WT. Data from Dec-05 XL spreadsheet

Figure 15. Recovery from an NMDA-induced Ca^{2+} load in WT and YAC128 MSNs. Recovery of cytosolic Ca^{2+} (imaged using Fura-2) towards basal levels following the application of 500 μM NMDA in WT (black squares, n=5 experiments, total of 91 neurons from 3 different culture batches) or YAC128 (open circles, n=5 experiments, total of 90 neurons, from 3 different culture batches) MSNs. Repeated measures ANOVA, effect of genotype $F(1,20) = 33.78$, $P<0.0001$; effect of time $F(4,20) = 4.04$, $*P<0.05$; $*P<0.05$ at 15 min, $*P<0.05$ at 20 min, $**P<0.01$ at 25 min by Bonferroni post-test.

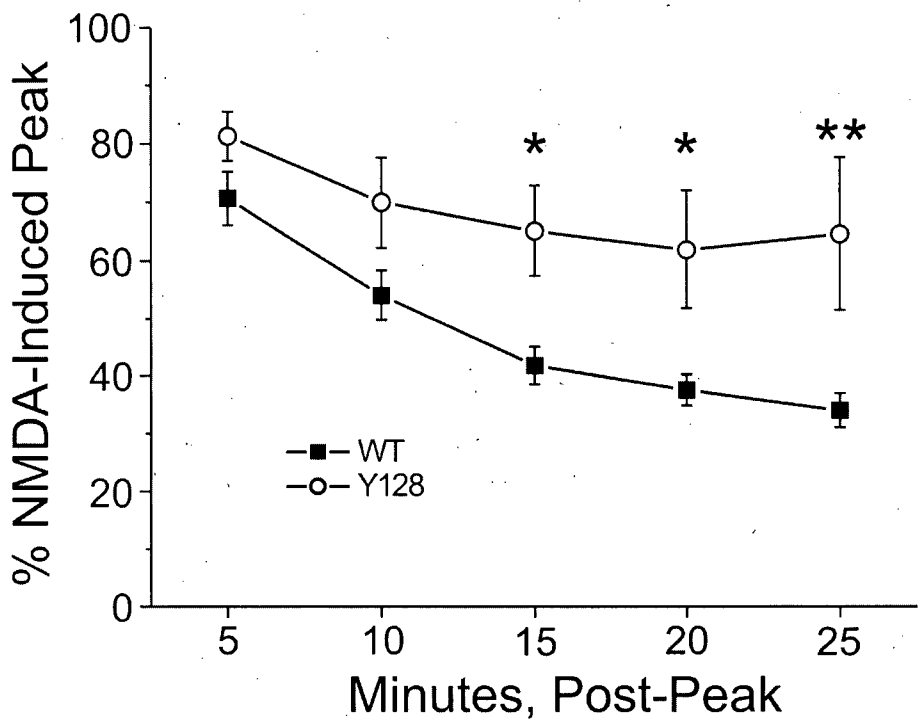
100
80
60
40
20
0
% NMDA-Induced Peak
*
*
**
WT
Y128
5
10
15
20
25
Minutes, Post-Peak

Figure 16. Contrasting responses of WT and YAC128 MSNs to different stimuli that increase cytosolic Ca^{2+} to similar peak levels. **A)** Representative mean responses of WT MSNs to 100 μM NMDA (solid line, n=14 cells) or 50 mM KCl + 5 μM FPL64176 (dotted line, n=23 cells) as indicated. Note that the peak amplitude of the cytosolic Ca^{2+} response to either stimulus is similar. Each trace is representative of a single experiment. **B)** Peak cytosolic Ca^{2+} responses to 100 μM NMDA (n=6 experiments for WT, n=5 for YAC128; total of 108 and 86 neurons for WT and YAC128, respectively, from 3 different culture batches) or 50 mM KCl + 5 μM FPL64176 (n=6 experiments per genotype, total of 107 and 106 neurons for WT and YAC128, respectively, from 3 different culture batches) in WT (black bars) or YAC128 (open bars) MSNs. No significant difference by two-way ANOVA; no effect of treatment $F(1,19) = 1.99$, $P>0.05$ or genotype ($F(1,19)= 0.01$, $P>0.05$. Data expressed as mean ± SEM. Intracellular Ca^{2+} was monitored using Fura-FF in these experiments.

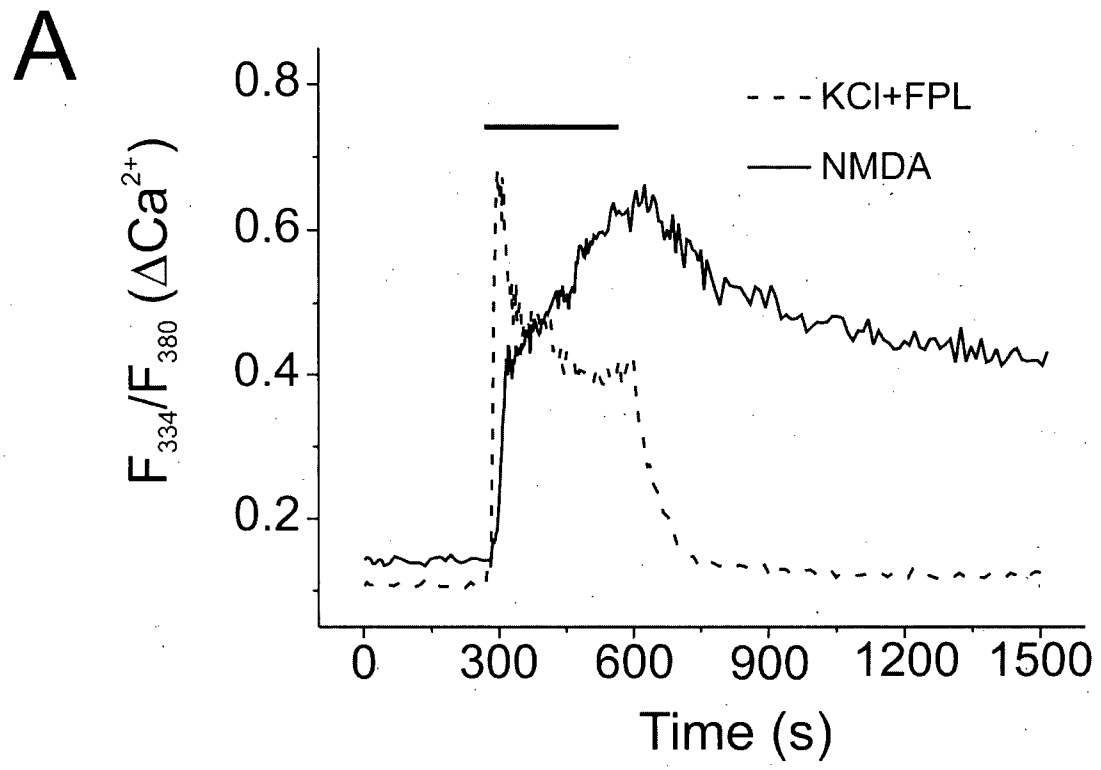
A
0.8
0.6
0.4
0.2
F_{334}/F_{380} (ΔCa^{2+})
KCl+FPL
NMDA
0
300
600
900
1200
1500
Time (s)

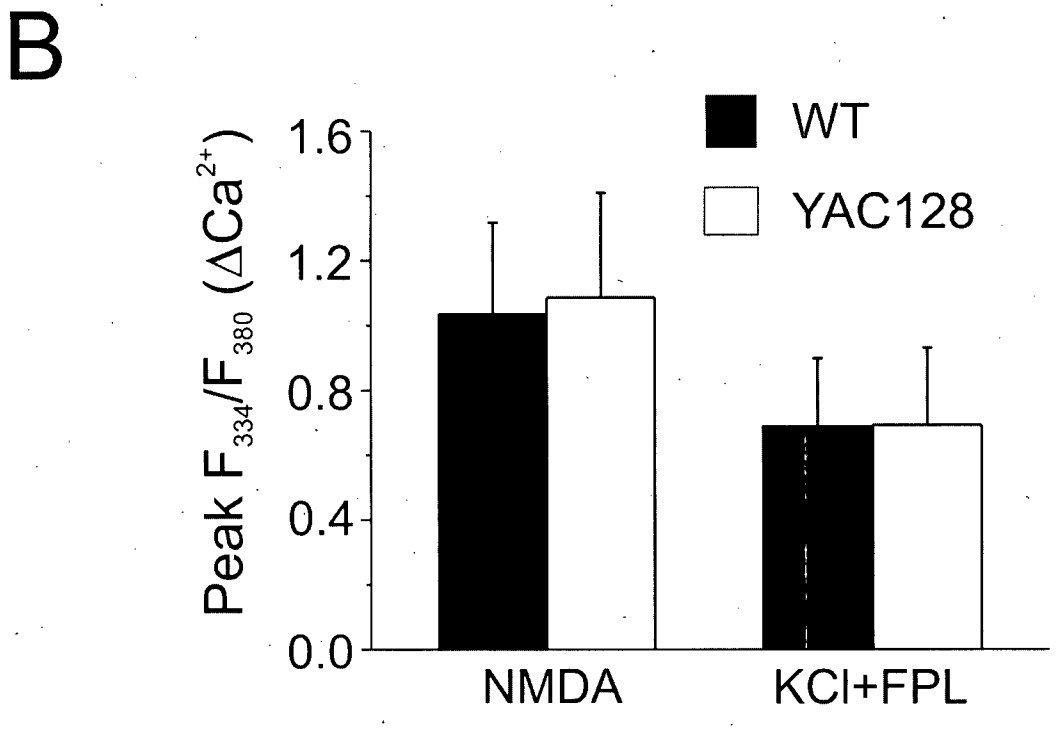
B
1.6
1.2
0.8
0.4
0.0
Peak F_{334}/F_{380} (ΔCa^{2+})
WT
YAC128
NMDA
KCl+FPL

Figure 17. The impairment in recovery of YAC128 MSNs from a cytosolic Ca^{2+} load is selective for NMDA-induced Ca^{2+} loads. Recovery of cytosolic Ca^{2+} towards pre-stimulus levels following application of 100 μM NMDA (WT: black squares; YAC128: open circles; n=5 experiments per genotype, total of 97 and 86 neurons for WT and YAC128, respectively, from 5 different culture batches) or 50 mM KCl + 5 μM FPL64176 (WT: black triangles; YAC128: open triangles; n=6 experiments per genotype, total of 107 and 106 neurons for WT and YAC128, respectively, from 3 different culture batches). Significant difference in recovery of cytosolic Ca^{2+}, WT vs. YAC128 (100 μM NMDA): two-way ANOVA; effect of genotype $F(1,21) = 36.76$, $P<0.0001$; $^{*}P<0.05$, $^{**}P<0.01$, $^{***}P<0.01$ by Bonferroni post-test; effect of time $F(2,21) = 2.23$, $P>0.05$. Significant difference in recovery of cytosolic Ca^{2+}, YAC128 (NMDA vs. KCl + FPL64176): two-way ANOVA; effect of treatment $F(1,24) = 136.34$, $P<0.0001$; effect of time $F(2,24) = 14.98$, $P<0.0001$; effect of interaction $F(2,24) = 8.94$, $P<0.01$; $^{\#}P<0.05$, $^{\#\#\#}P<0.001$ by Bonferroni post-test. Significant difference in recovery of cytosolic Ca^{2+}, WT (NMDA vs. KCl + FPL64176): two-way ANOVA; effect of treatment $F(1,27) = 31.46$, $P<0.0001$; effect of time $F(2,27) = 10.64$, $P<0.001$; $^{@@@}P<0.001$ by Bonferroni post-test. No significant difference in recovery of cytosolic Ca^{2+}, WT vs. YAC128 (50 mM KCl + 5 μM FPL64176): two way ANOVA; effect of genotype $F(1,39) = 0.20$, $P>0.05$; effect of time $F(3,39) = 30.94$, $P<0.0001$.

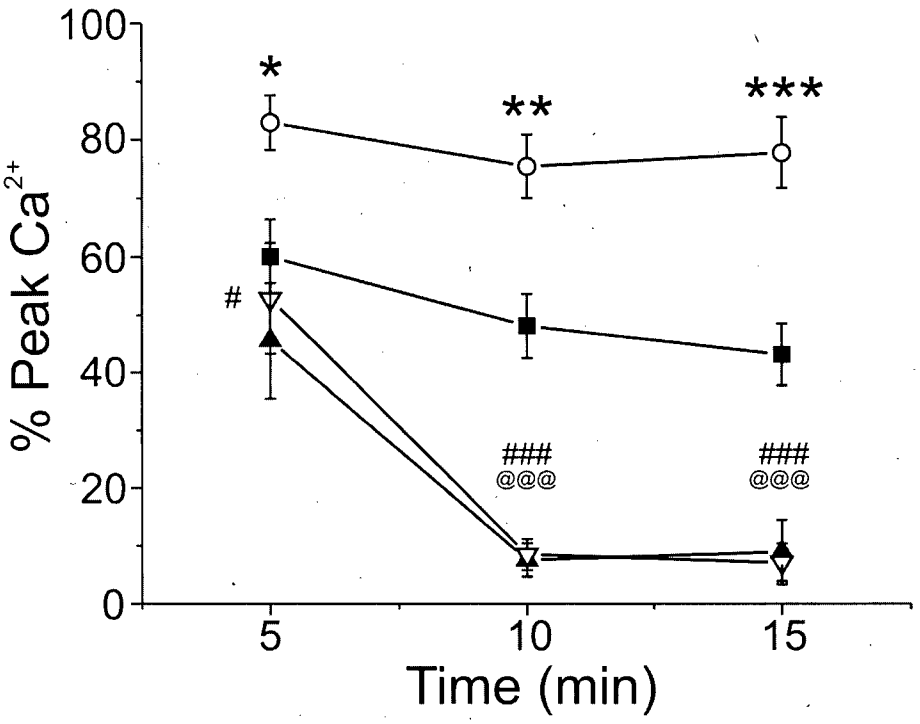
100
80
60
40
20
0
% Peak Ca2+
*
**
***
#
###
@@@
###
@@@
5
10
15
Time (min)

Figure 18. Simultaneous monitoring of NMDA-induced changes in cytosolic Ca^{2+} and $\Delta\Psi_m$ in WT and YAC128 MSNs. **A)** Representative mean cytosolic Ca^{2+} (solid line, Fura-2) and mitochondrial $\Delta\Psi_m$ (dashed line, rhodamine-123) responses of WT (top, n=20 cells) and YAC128 (bottom, n=15 cells) MSNs prior to, during, and following 5 min application of 500 μM NMDA as indicated. Note the relatively rapid recovery of Ca^{2+} in WT MSNs, compared to that seen in YAC128 MSNs, as well as the relative changes in $\Delta\Psi_m$ in each genotype. Expanded region of YAC128 timescale (bottom) illustrates the temporal order of changes in Ca^{2+} (solid line) preceding changes in $\Delta\Psi_m$ (dashed line) during the initial phase of response to NMDA (arrow indicates start of NMDA application).

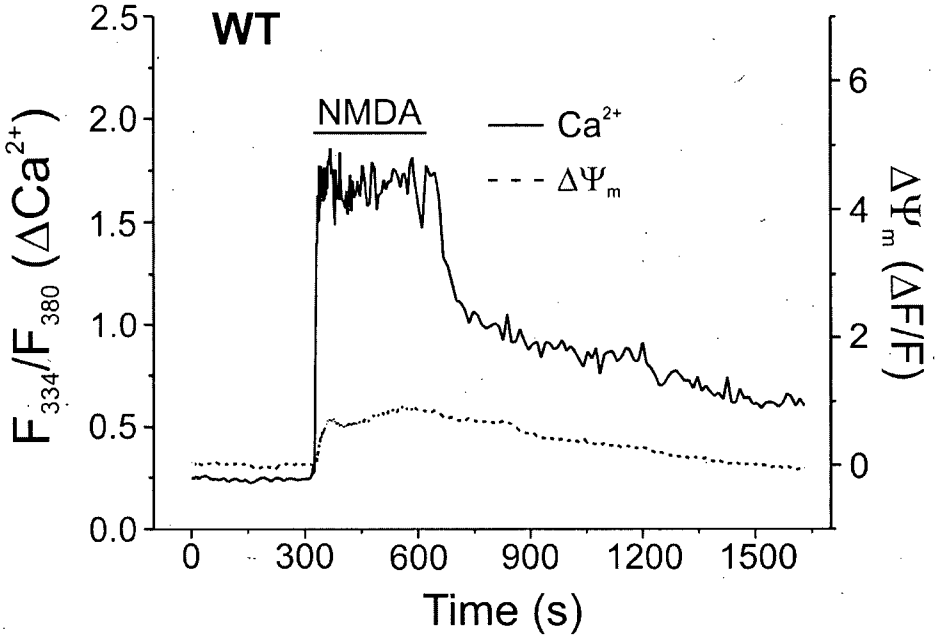
WT
NMDA
Ca2+
ΔΨm
F334/F380 (ΔCa2+)
ΔΨm (ΔF/F)
Time (s)

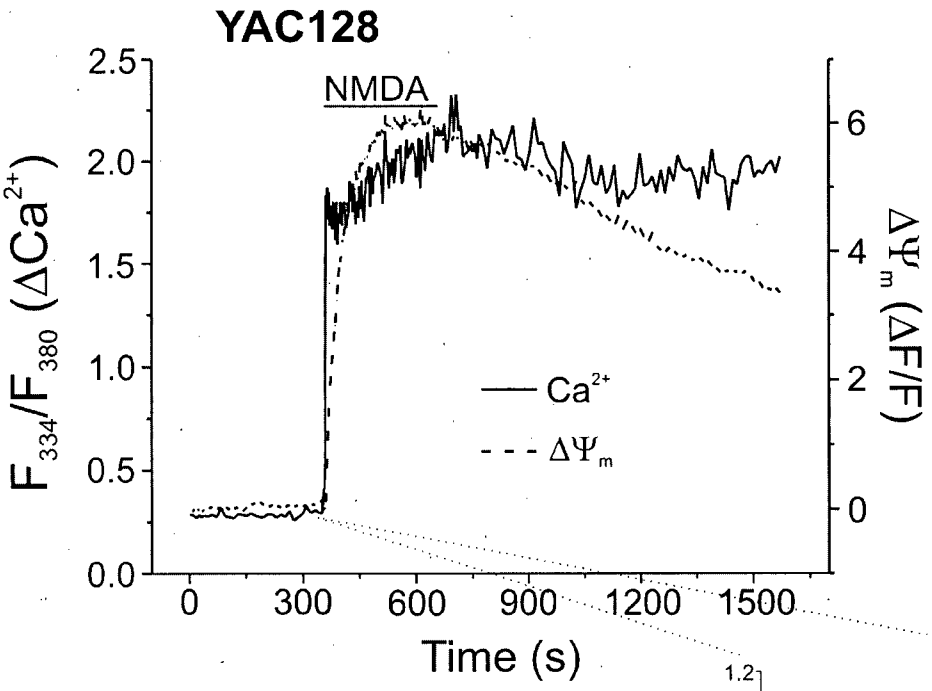
YAC128
NMDA
Ca2+
ΔΨm
F334/F380 (ΔCa2+)
ΔΨm (ΔF/F)
Time (s)

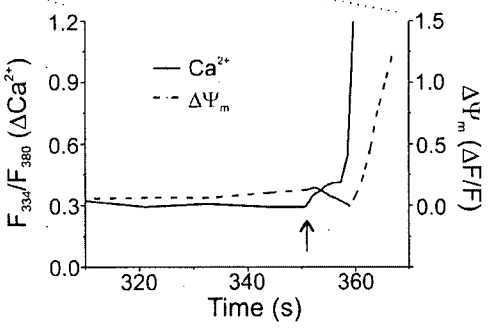
Ca2+
ΔΨm
F334/F380 (ΔCa2+)
ΔΨm (ΔF/F)
Time (s)

Figure 19. YAC128 MSNs undergo a more dramatic loss of $\Delta\Psi_m$ as a consequence of NMDA challenge than WT MSNs, despite similar cytosolic Ca^{2+} loads. **Top panel:** basal and peak cytosolic Ca^{2+} responses (measured using Fura-2) to 500 μM NMDA in WT (black bars) or YAC128 (open bars) MSNs. No significant difference between genotypes by paired t-test; data expressed as mean ± SEM. **Bottom panel:** Concurrent changes in $\Delta\Psi_m$ ($\Delta F/F$) in WT (black bar) or YAC128 (open bar) MSNs, n= 8 paired experiments per genotype; total of 131 and 147 neurons for WT and YAC128, respectively, from 4 different culture batches. Significant difference between genotypes $^*P<0.05$ by paired t-test; data expressed as mean ± SEM.

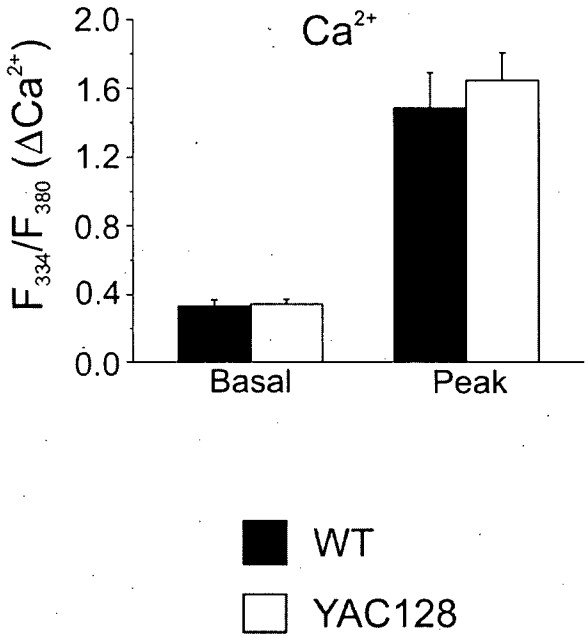
Ca2+
F334/F380 (ΔCa2+)
2.0
1.6
1.2
0.8
0.4
0.0
Basal
Peak
WT
YAC128

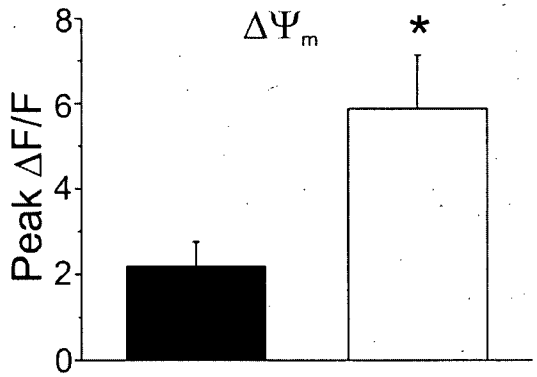
ΔΨm
*
Peak ΔF/F
8
6
4
2
0

Figure 20. Characteristics of resting mitochondria in WT and YAC128 MSNs. **A)** Determination of resting mitochondrial polarization ($\Delta\Psi_m$) status (i.e. prior to any stimulation). Mitochondria in previously unstimulated WT and Y128 MSNs were maximally depolarized by the addition of 5 μM CCCP (see Methods), and the mean fluorescent signal for each genotype was quantified. n=6 paired experiments per genotype; total of 121 and 113 neurons for WT (black bar) and YAC128 (open bar), respectively, from 3 different culture batches. No significant difference between genotypes by paired t-test; data expressed as mean ± SEM. **B)** Depolarization of resting mitochondria by 5 μM CCCP in previously unstimulated YAC128 MSNs results in the release of very little free Ca^{2+} from the mitochondria into the cytosol. Mean cytosolic Ca^{2+} (solid line, Fura-FF) and $\Delta\Psi_m$ (dashed line, rhodamine-123) responses of 13 MSNs.

A

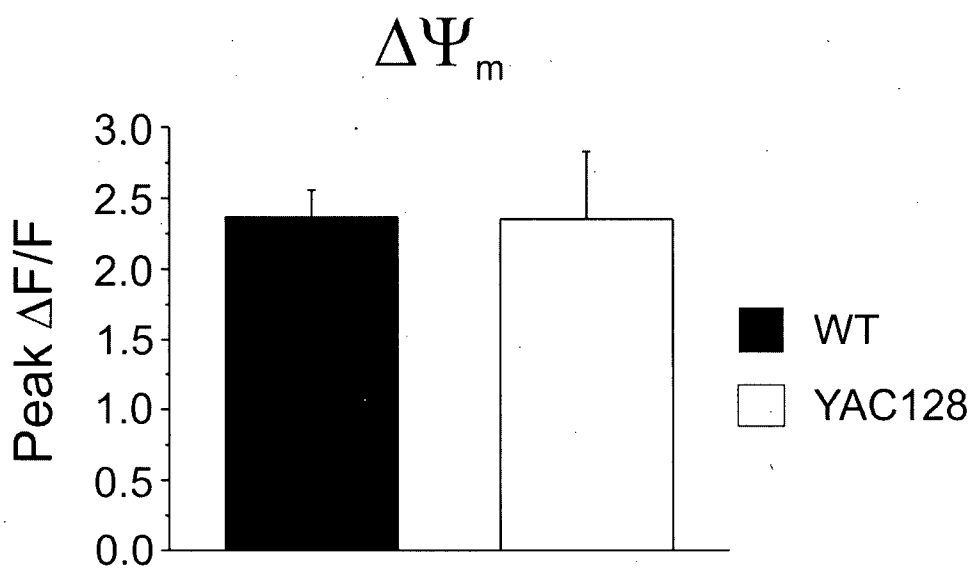
ΔΨm
Peak ΔF/F
3.0
2.5
2.0
1.5
1.0
0.5
0.0
WT
YAC128

B

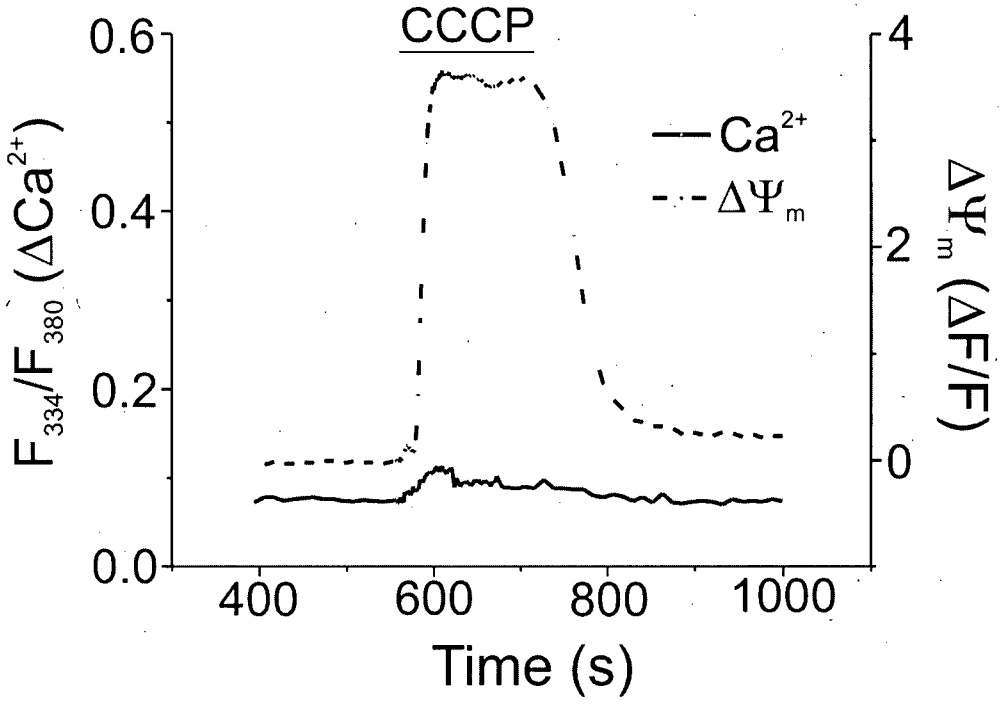
CCCP
0.6
0.4
0.2
0.0
F334/F380 (ΔCa2+)
Ca2+
ΔΨm
4
2
0
ΔΨm (ΔF/F)
400
600
800
1000
Time (s)

Figure 21. Mitochondria in both WT and YAC128 MSNs have a similar capability to buffer transient cytosolic Ca^{2+} increases produced by short application of NMDA. **A)** A representative example of a mitochondrial Ca^{2+} uptake experiment, showing the mean cytosolic Ca^{2+} responses (± SEM) of 13 WT MSNs, to a 60 s application of 500 μM NMDA followed 2 min later by a 60 s application of 5 μM CCCP (in Ca^{2+}-free buffer). Fura-FF was used as the Ca^{2+} indicator for these experiments. The hatched areas, corresponding to the stimulus duration, were used in AUC calculations to determine C/N ratios as described in the Methods. **B)** C/N ratios for WT (black bar, n=8 experiments) and YAC128 (open bar, n=6 experiments) MSNs (total of 92 and 105 neurons for WT and YAC128, respectively, from 3 – 4 different culture batches). No significant difference by unpaired t-test; data expressed as mean ± SEM.

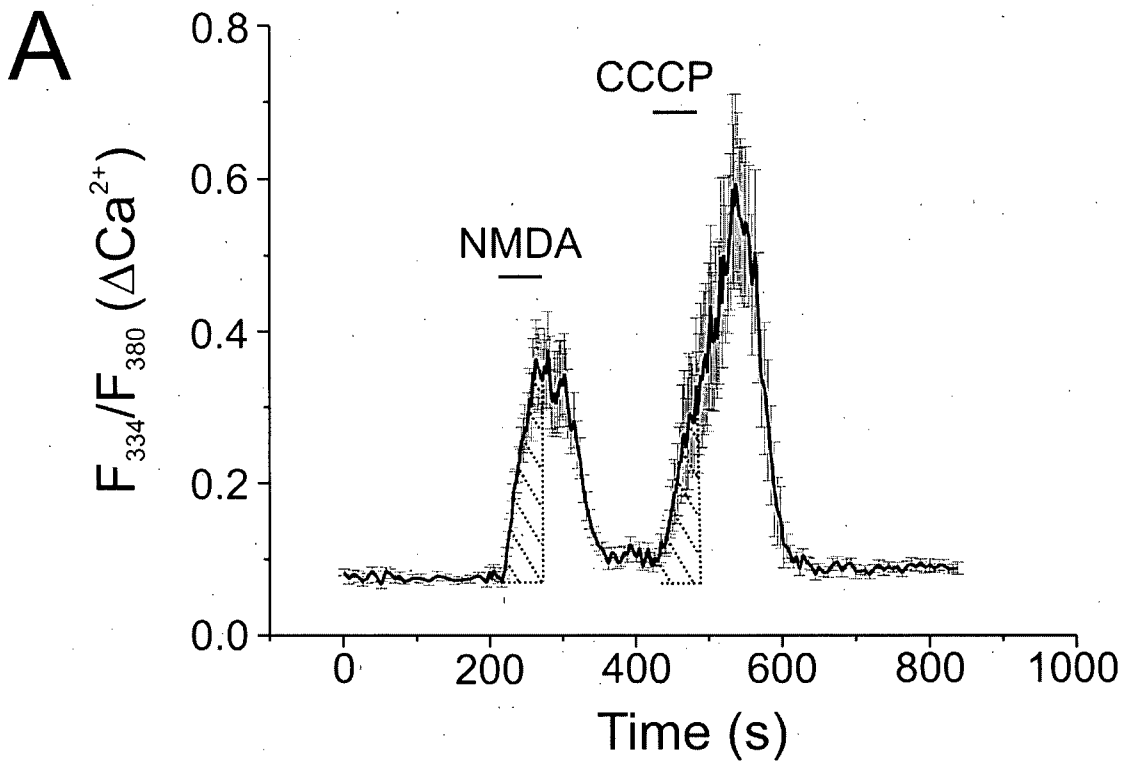
A
0.8
0.6
0.4
0.2
0.0
F_{334}/F_{380} (ΔCa^{2+})
CCCP
NMDA
0
200
400
600
800
1000
Time (s)

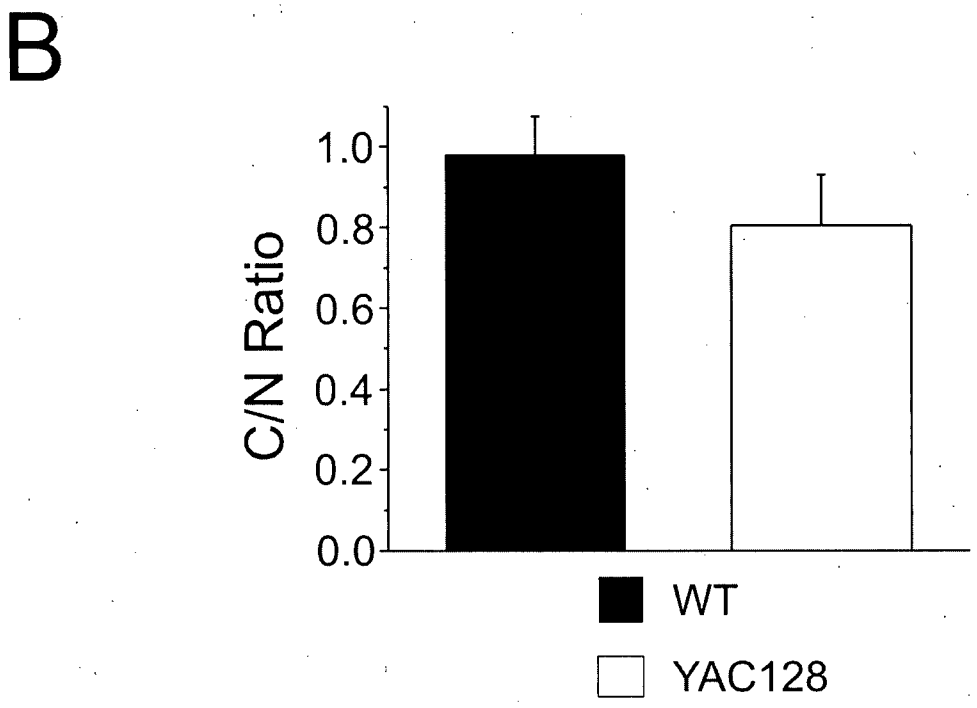
B
1.0
0.8
0.6
0.4
0.2
0.0
C/N Ratio
WT
YAC128

Figure 22. Recovery of YAC128 MSNs from a cytosolic Ca^{2+} load produced by a short application of NMDA is similar in timecourse to that of WT MSNs. The recovery of WT and YAC128 MSNs from peak Ca^{2+} towards prestimulus levels following a 60 s application of 500 μM NMDA (as performed to calculate the C/N ratios) was quantified by calculating the mean time of recovery to 50% and 25% of the peak. n=8 experiments and 92 cells total for WT; n=6 experiments and 105 cells total for YAC128. No significant difference between genotypes by unpaired t-test.

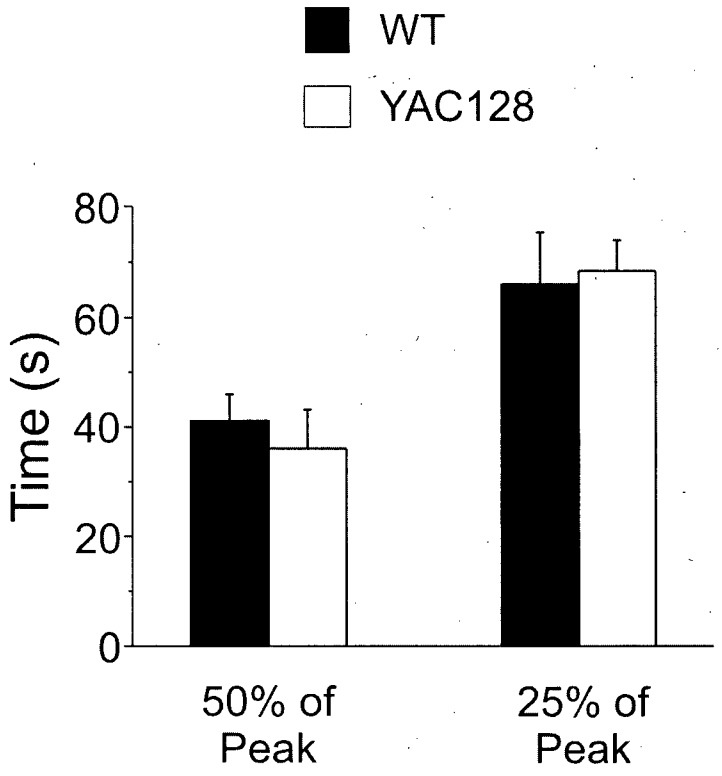
WT
YAC128
80
60
40
20
0
Time (s)
50% of Peak
25% of Peak

Figure 23. The effect of the mPT inhibitor CsA on simultaneously measured peak cytosolic Ca^{2+} and $\Delta\Psi_m$ in WT and YAC128 MSNs. **A)** Peak cytosolic Ca^{2+} in WT MSNs (black bars; with 10 μM CsA: n= 6 experiments, 81 neurons total; without 10 μM CsA: n=6 experiments, 109 neurons total; from 3-4 different culture batches) and YAC128 MSNs (open bars; with 10 μM CsA: n=5 experiments, 106 neurons total; without 10 μM CsA: n=7 experiments, 88 neurons total; from 3 – 4 different culture batches) following a 5 min application of 500 μM NMDA, with or without 10 μM CsA present in all solutions as indicated. $^*P<0.05$ by unpaired t-test comparing treatments within genotype; data expressed as mean ± SEM. Intracellular calcium was monitored using Fura-FF in these experiments. **B)** Simultaneously observed changes in $\Delta\Psi_m$ (ΔF/F). No significant difference by unpaired t-test within genotypes; data expressed as mean ± SEM.

A

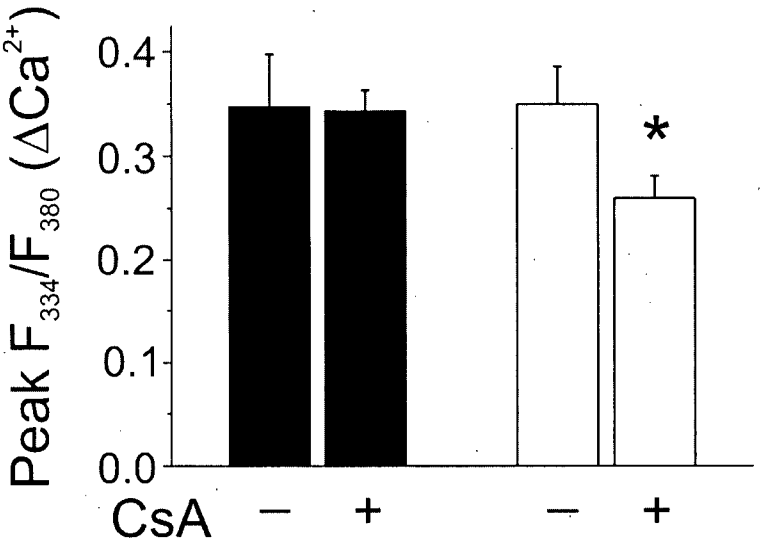
Peak F_{334}/F_{380} (ΔCa^{2+})
0.4
0.3
0.2
0.1
0.0
*
CsA
–
+
–
+

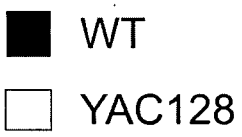
WT
YAC128

B

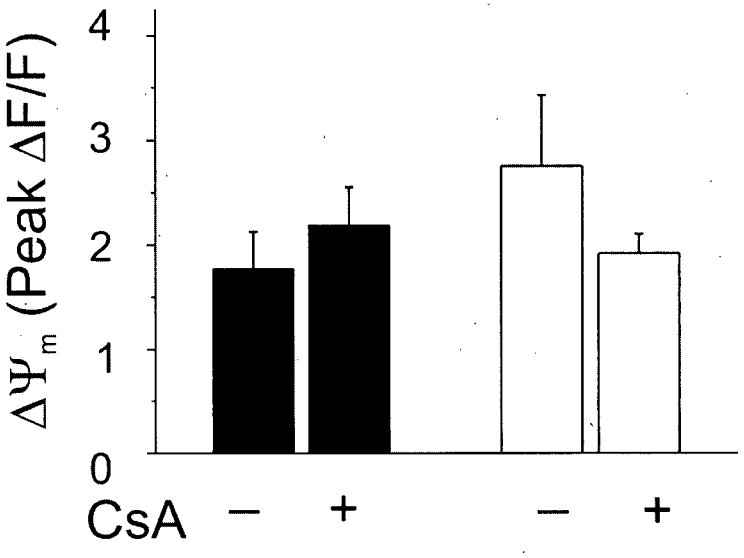
$\Delta\Psi_m$ (Peak $\Delta F/F$)
4
3
2
1
0
CsA
–
+
–
+

Figure 24. The effect of the mPT inhibitor BkA on simultaneously measured peak cytosolic Ca^{2+} and $\Delta\Psi_m$ in WT and YAC128 MSNs. **A)** Peak cytosolic Ca^{2+} in WT MSNs (black bars; with BkA: n=9 experiments, 135 cells total; without BkA: n=10 experiments, 129 cells total; from 5 different culture batches) and YAC128 MSNs (open bars; with 5 μM BkA: n=10 experiments, 145 cells total; without 5 μM BkA: n=9 experiments, 148 cells total; from 5 different culture batches) following a 5 min application of 500 μM NMDA, with or without 5 μM BkA present in all solutions as indicated. No significant difference by unpaired t-test within genotypes; data expressed as mean ± SEM. **B)** Simultaneously observed changes in $\Delta\Psi_m$ ($\Delta F/F$). $^*P<0.05$ by unpaired t-test comparing treatments within genotype; data expressed as mean ± SEM.

A

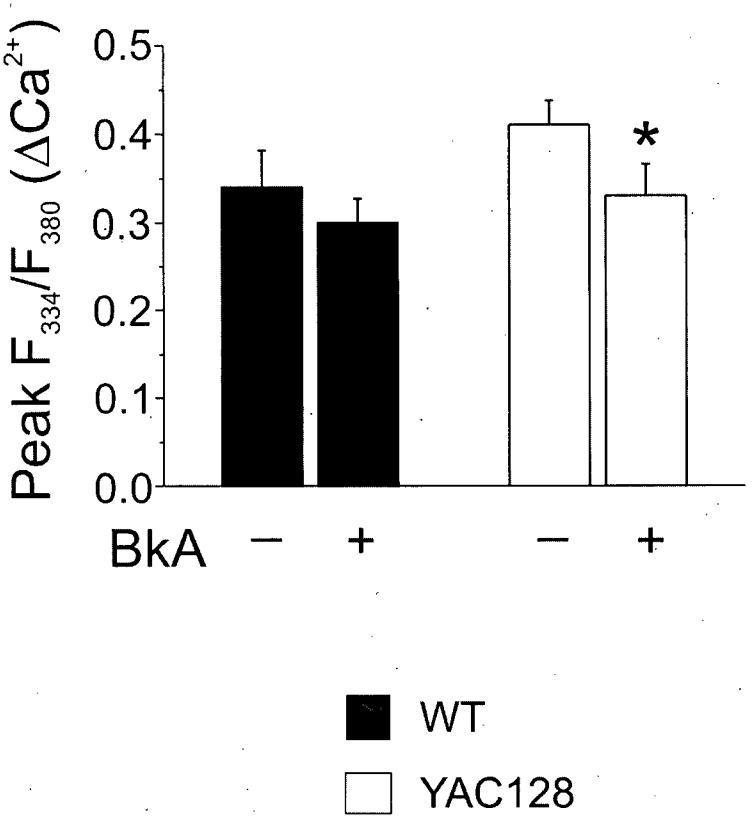
Peak F_{334}/F_{380} (ΔCa^{2+})
0.5
0.4
0.3
0.2
0.1
0.0
*
BkA
–
+
–
+
WT
YAC128

B

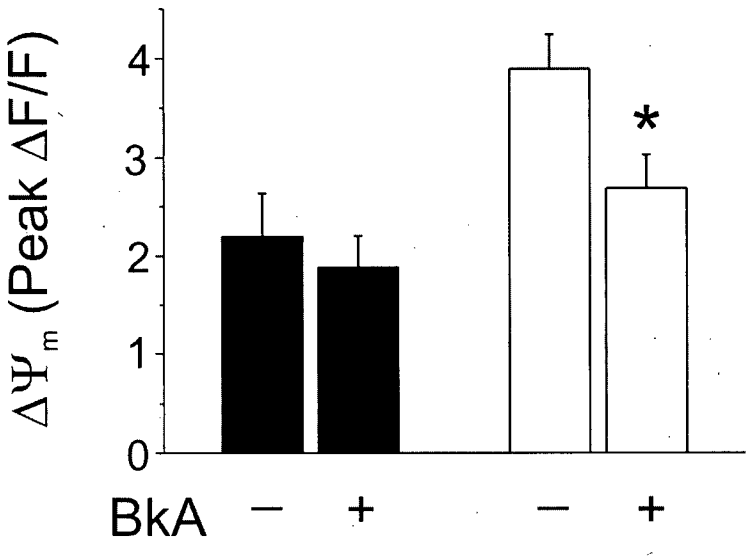
$\Delta\Psi_m$ (Peak ΔF/F)
4
3
2
1
0
*
BkA
–
+
–
+

Figure 25. A general overview of the main excitotoxic events in the YAC HD mouse models of varying htt polyQ length. Previous research established that enhanced NMDAR activation (step 1) leads to elevated peak cytosolic Ca^{2+} (step 2) and subsequent mitochondrial depolarization (step 3). Consequently, activation of caspases (step 4) and apoptosis (step 5) in YAC46 and YAC72 MSNs occurs. In the YAC128 mouse model, steps 1 and 2 do not appear to play a role in the enhancement of apoptosis for YAC128 versus WT MSNs, as the work presented here indicates that neither the NMDAR peak current nor the resultant peak in cytosolic Ca^{2+} is any different from that seen in WT MSNs. The key excitotoxic step augmented in YAC128 MSNs appears to occur at the level of the mitochondria (step 3, mitochondrial depolarization), and yet is still dependent on NMDAR activation. The release of free Ca^{2+} from the mitochondria back into the cytosol (step 3a, recently taken up downstream of NMDAR activation) follows mitochondrial depolarization. Thus, the increased sensitivity to NMDA-induced toxicity occurs at a later point in the sequence of events leading to apoptotic death in YAC128 compared with YAC72 MSNs. The delayed recovery from NMDA-induced Ca^{2+} loads in YAC128 MSNs may also serve to enhance calpain activity levels following bouts of intense NMDAR activity.

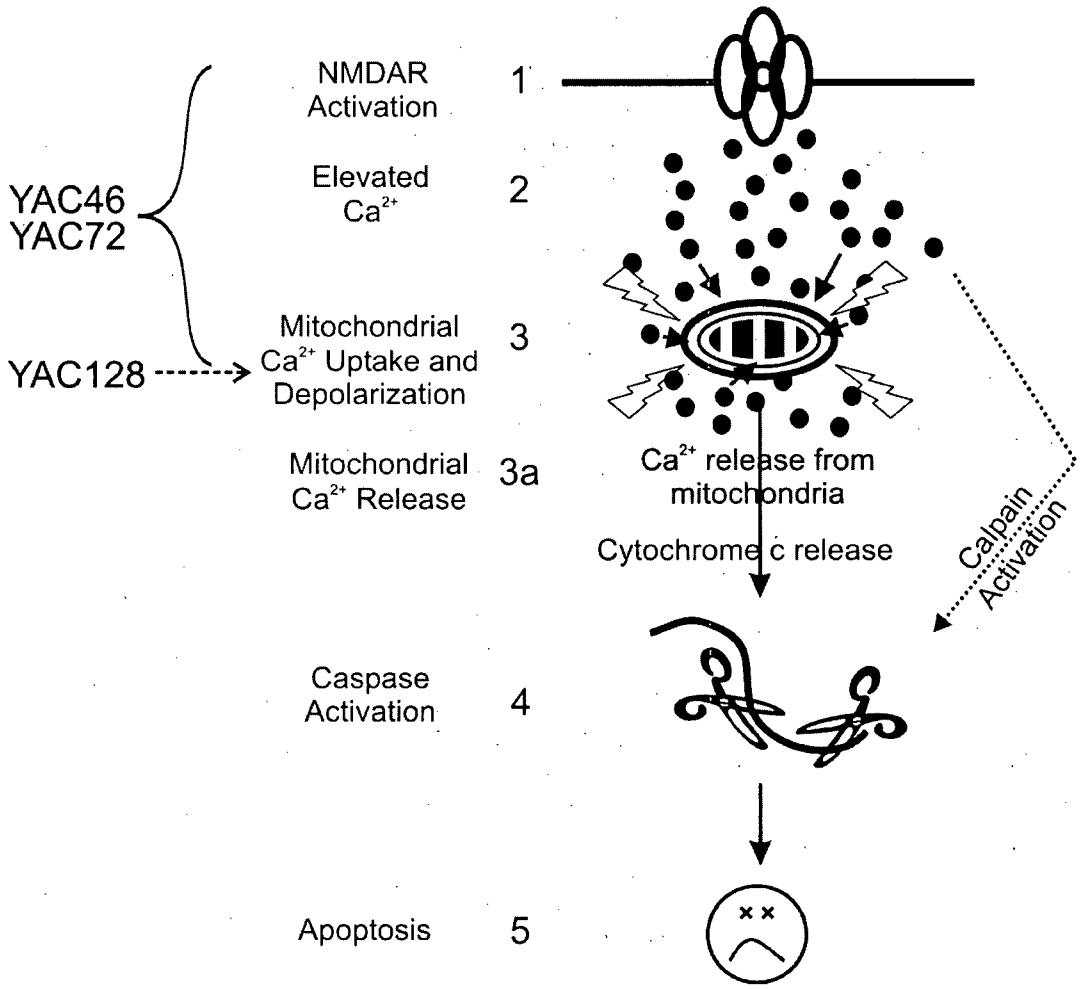
NMDAR Activation
1
Elevated Ca^{2+}
2
YAC46
YAC72
YAC128
Mitochondrial Ca^{2+} Uptake and Depolarization
3
Mitochondrial Ca^{2+} Release
3a
Ca^{2+} release from mitochondria
Cytochrome c release
Calpain Activation
Caspase Activation
4
Apoptosis
5

REFERENCES

Abdel-Hamid KM, Baimbridge KG (1997) The effects of artificial calcium buffers on calcium responses and glutamate-mediated excitotoxicity in cultured hippocampal neurons. Neuroscience 81:673-687.

Akazawa C, Shigemoto R, Bessho Y, Nakanishi S, Mizuno N (1994) Differential expression of five N-methyl-D-aspartate receptor subunit mRNAs in the cerebellum of developing and adult rats. J Comp Neurol 347:150-160.

Alano CC, Beutner G, Dirksen RT, Gross RA, Sheu SS (2002) Mitochondrial permeability transition and calcium dynamics in striatal neurons upon intense NMDA receptor activation. J Neurochem 80:531-538.

Albin RL, Reiner A, Anderson KD, Penney JB, Young AB (1990a) Striatal and nigral neuron subpopulations in rigid Huntington's disease: implications for the functional anatomy of chorea and rigidity-akinesia. Ann Neurol 27:357-365.

Albin RL, Young AB, Penney JB, Handelin B, Balfour R, Anderson KD, Markel DS, Tourtellotte WW, Reiner A (1990b) Abnormalities of striatal projection neurons and N-methyl-D-aspartate receptors in presymptomatic Huntington's disease. N Engl J Med 322:1293-1298.

Andre VM, Cepeda C, Venegas A, Gomez Y, Levine MS (2006) Altered cortical glutamate receptor function in the R6/2 model of Huntington's disease. J Neurophysiol 95:2108-2119.

Andrew SE, Goldberg YP, Kremer B, Telenius H, Theilmann J, Adam S, Starr E, Squitieri F, Lin B, Kalchman MA, et al. (1993) The relationship between trinucleotide (CAG) repeat length and clinical features of Huntington's disease. Nat Genet 4:398-403.

Anegawa NJ, Lynch DR, Verdoorn TA, Pritchett DB (1995) Transfection of N-methyl-D-aspartate receptors in a nonneuronal cell line leads to cell death. J Neurochem 64:2004-2012.

Anegawa NJ, Guttmann RP, Grant ER, Anand R, Lindstrom J, Lynch DR (2000) N-Methyl-D-aspartate receptor mediated toxicity in nonneuronal cell lines: characterization using fluorescent measures of cell viability and reactive oxygen species production. Brain Res Mol Brain Res 77:163-175.

Ankarcrona M, Dypbukt JM, Orrenius S, Nicotera P (1996) Calcineurin and mitochondrial function in glutamate-induced neuronal cell death. FEBS Lett 394:321-324.

Ankarcrona M, Dypbukt JM, Bonfoco E, Zhivotovsky B, Orrenius S, Lipton SA, Nicotera P (1995) Glutamate-induced neuronal death: a succession of necrosis or apoptosis depending on mitochondrial function. Neuron 15:961-973.

Anson LC, Schoepfer R, Colquhoun D, Wyllie DJ (2000) Single-channel analysis of an NMDA receptor possessing a mutation in the region of the glutamate binding site. J Physiol 527 Pt 2:225-237.

Anson LC, Chen PE, Wyllie DJ, Colquhoun D, Schoepfer R (1998) Identification of amino acid residues of the NR2A subunit that control glutamate potency in recombinant NR1/NR2A NMDA receptors. J Neurosci 18:581-589.

Aronin N, Chase K, Young C, Sapp E, Schwarz C, Matta N, Kornreich R, Landwehrmeyer B, Bird E, Beal MF, et al. (1995) CAG expansion affects the expression of mutant Huntingtin in the Huntington's disease brain. Neuron 15:1193-1201.

Banke TG, Traynelis SF (2003) Activation of NR1/NR2B NMDA receptors. Nat Neurosci 6:144-152.

Bano D, Young KW, Guerin CJ, Lefeuvre R, Rothwell NJ, Naldini L, Rizzuto R, Carafoli E, Nicotera P (2005) Cleavage of the plasma membrane Na+/Ca2+ exchanger in excitotoxicity. Cell 120:275-285.

Barria A, Malinow R (2002) Subunit-specific NMDA receptor trafficking to synapses. Neuron 35:345-353.

Beal MF (1995) Aging, energy, and oxidative stress in neurodegenerative diseases. Ann Neurol 38:357-366.

Beal MF, Ferrante RJ, Swartz KJ, Kowall NW (1991) Chronic quinolinic acid lesions in rats closely resemble Huntington's disease. J Neurosci 11:1649-1659.

Beal MF, Kowall NW, Ellison DW, Mazurek MF, Swartz KJ, Martin JB (1986) Replication of the neurochemical characteristics of Huntington's disease by quinolinic acid. Nature 321:168-171.

Beal MF, Brouillet E, Jenkins B, Henshaw R, Rosen B, Hyman BT (1993a) Age-dependent striatal excitotoxic lesions produced by the endogenous mitochondrial inhibitor malonate. J Neurochem 61:1147-1150.

Beal MF, Brouillet E, Jenkins BG, Ferrante RJ, Kowall NW, Miller JM, Storey E, Srivastava R, Rosen BR, Hyman BT (1993b) Neurochemical and histologic characterization of striatal excitotoxic lesions produced by the mitochondrial toxin 3-nitropropionic acid. J Neurosci 13:4181-4192.

Bence NF, Sampat RM, Kopito RR (2001) Impairment of the ubiquitin-proteasome system by protein aggregation. Science 292:1552-1555.

Benchoua A, Trioulier Y, Zala D, Gaillard MC, Lefort N, Dufour N, Saudou F, Elalouf JM, Hirsch E, Hantraye P, Deglon N, Brouillet E (2006) Involvement of mitochondrial complex II defects in neuronal death produced by N-terminus fragment of mutated huntingtin. Mol Biol Cell 17:1652-1663.

Bernardi P, Broekemeier KM, Pfeiffer DR (1994) Recent progress on regulation of the mitochondrial permeability transition pore; a cyclosporin-sensitive pore in the inner mitochondrial membrane. J Bioenerg Biomembr 26:509-517.

Bizat N, Hermel JM, Boyer F, Jacquard C, Creminon C, Ouary S, Escartin C, Hantraye P, Kajewski S, Brouillet E (2003) Calpain is a major cell death effector in selective striatal degeneration induced in vivo by 3-nitropropionate: implications for Huntington's disease. J Neurosci 23:5020-5030.

Boeckman FA, Aizenman E (1996) Pharmacological properties of acquired excitotoxicity in Chinese hamster ovary cells transfected with N-methyl-D-aspartate receptor subunits. J Pharmacol Exp Ther 279:515-523.

Bogdanov MB, Ferrante RJ, Kuemmerle S, Klivenyi P, Beal MF (1998) Increased vulnerability to 3-nitropropionic acid in an animal model of Huntington's disease. J Neurochem 71:2642-2644.

Brandt J, Bylsma FW, Gross R, Stine OC, Ranen N, Ross CA (1996) Trinucleotide repeat length and clinical progression in Huntington's disease. Neurology 46:527-531.

Brennan WA, Jr., Bird ED, Aprille JR (1985) Regional mitochondrial respiratory activity in Huntington's disease brain. J Neurochem 44:1948-1950.

Brinkman RR, Mezei MM, Theilmann J, Almqvist E, Hayden MR (1997) The likelihood of being affected with Huntington disease by a particular age, for a specific CAG size. Am J Hum Genet 60:1202-1210.

Brocard JB, Tassetto M, Reynolds IJ (2001) Quantitative evaluation of mitochondrial calcium content in rat cortical neurones following a glutamate stimulus. J Physiol 531:793-805.

Brouillet E, Hantraye P, Ferrante RJ, Dolan R, Leroy-Willig A, Kowall NW, Beal MF (1995) Chronic mitochondrial energy impairment produces selective striatal degeneration and abnormal choreiform movements in primates. Proc Natl Acad Sci U S A 92:7105-7109.

Brouillet E, Jenkins BG, Hyman BT, Ferrante RJ, Kowall NW, Srivastava R, Roy DS, Rosen BR, Beal MF (1993) Age-dependent vulnerability of the striatum to the mitochondrial toxin 3-nitropropionic acid. J Neurochem 60:356-359.

Browne SE, Bowling AC, MacGarvey U, Baik MJ, Berger SC, Muqit MM, Bird ED, Beal MF (1997) Oxidative damage and metabolic dysfunction in Huntington's disease: selective vulnerability of the basal ganglia. Ann Neurol 41:646-653.

Brustovetsky N, Brustovetsky T, Jemmerson R, Dubinsky JM (2002) Calcium-induced cytochrome c release from CNS mitochondria is associated with the permeability transition and rupture of the outer membrane. J Neurochem 80:207-218.

Brustovetsky N, Brustovetsky T, Purl KJ, Capano M, Crompton M, Dubinsky JM (2003) Increased susceptibility of striatal mitochondria to calcium-induced permeability transition. J Neurosci 23:4858-4867.

Buller AL, Larson HC, Schneider BE, Beaton JA, Morrisett RA, Monaghan DT (1994) The molecular basis of NMDA receptor subtypes: native receptor diversity is predicted by subunit composition. J Neurosci 14:5471-5484.

Burnashev N, Zhou Z, Neher E, Sakmann B (1995) Fractional calcium currents through recombinant GluR channels of the NMDA, AMPA and kainate receptor subtypes. J Physiol 485 (Pt 2):403-418.

Castilho RF, Hansson O, Ward MW, Budd SL, Nicholls DG (1998) Mitochondrial control of acute glutamate excitotoxicity in cultured cerebellar granule cells. J Neurosci 18:10277-10286.

Cattaneo E, Rigamonti D, Goffredo D, Zuccato C, Squitieri F, Sipione S (2001) Loss of normal huntingtin function: new developments in Huntington's disease research. Trends Neurosci 24:182-188.

Cepeda C, Itri JN, Flores-Hernandez J, Hurst RS, Calvert CR, Levine MS (2001a) Differential sensitivity of medium- and large-sized striatal neurons to NMDA but not kainate receptor activation in the rat. Eur J Neurosci 14:1577-1589.

Cepeda C, Ariano MA, Calvert CR, Flores-Hernandez J, Chandler SH, Leavitt BR, Hayden MR, Levine MS (2001b) NMDA receptor function in mouse models of Huntington disease. J Neurosci Res 66:525-539.

Cepeda C, Hurst RS, Calvert CR, Hernandez-Echeagaray E, Nguyen OK, Jocoy E, Christian LJ, Ariano MA, Levine MS (2003) Transient and progressive electrophysiological alterations in the corticostriatal pathway in a mouse model of Huntington's disease. J Neurosci 23:961-969.

Cha JH, Frey AS, Alsdorf SA, Kerner JA, Kosinski CM, Mangiarini L, Penney JB, Jr., Davies SW, Bates GP, Young AB (1999) Altered neurotransmitter receptor expression in transgenic mouse models of Huntington's disease. Philos Trans R Soc Lond B Biol Sci 354:981-989.

Chan EY, Luthi-Carter R, Strand A, Solano SM, Hanson SA, DeJohn MM, Kooperberg C, Chase KO, DiFiglia M, Young AB, Leavitt BR, Cha JH, Aronin N, Hayden MR, Olson JM (2002) Increased huntingtin protein length reduces the number of polyglutamine-induced gene expression changes in mouse models of Huntington's disease. Hum Mol Genet 11:1939-1951.

Chang DT, Rintoul GL, Pandipati S, Reynolds IJ (2006) Mutant huntingtin aggregates impair mitochondrial movement and trafficking in cortical neurons. Neurobiol Dis 22:388-400.

Chapman DE, Keefe KA, Wilcox KS (2003) Evidence for functionally distinct synaptic NMDA receptors in ventromedial versus dorsolateral striatum. J Neurophysiol 89:69-80.

Chen N, Luo T, Raymond LA (1999a) Subtype-dependence of NMDA receptor channel open probability. J Neurosci 19:6844-6854.

Chen N, Ren J, Raymond LA, Murphy TH (2001a) Changes in agonist concentration dependence that are a function of duration of exposure suggest N-methyl-D-aspartate receptor nonsaturation during synaptic stimulation. Mol Pharmacol 59:212-219.

Chen N, Luo T, Wellington C, Metzler M, McCutcheon K, Hayden MR, Raymond LA (1999b) Subtype-specific enhancement of NMDA receptor currents by mutant huntingtin. J Neurochem 72:1890-1898.

Chen S, Ferrone FA, Wetzel R (2002) Huntington's disease age-of-onset linked to polyglutamine aggregation nucleation. Proc Natl Acad Sci U S A 99:11884-11889.

Chen S, Berthelier V, Yang W, Wetzel R (2001b) Polyglutamine aggregation behavior in vitro supports a recruitment mechanism of cytotoxicity. J Mol Biol 311:173-182.

Cheng C, Fass DM, Reynolds IJ (1999) Emergence of excitotoxicity in cultured forebrain neurons coincides with larger glutamate-stimulated [Ca(2+)](i) increases and NMDA receptor mRNA levels. Brain Res 849:97-108.

Choo YS, Johnson GV, MacDonald M, Detloff PJ, Lesort M (2004) Mutant huntingtin directly increases susceptibility of mitochondria to the calcium-induced permeability transition and cytochrome c release. Hum Mol Genet 13:1407-1420.

Christie JM, Jane DE, Monaghan DT (2000) Native N-methyl-D-aspartate receptors containing NR2A and NR2B subunits have pharmacologically distinct competitive antagonist binding sites. J Pharmacol Exp Ther 292:1169-1174.

Chung HJ, Huang YH, Lau LF, Huganir RL (2004) Regulation of the NMDA receptor complex and trafficking by activity-dependent phosphorylation of the NR2B subunit PDZ ligand. J Neurosci 24:10248-10259.

Cik M, Chazot PL, Stephenson FA (1994) Expression of NMDAR1-1a (N598Q)/NMDAR2A receptors results in decreased cell mortality. Eur J Pharmacol 266:R1-3.

Clements JD, Westbrook GL (1991) Activation kinetics reveal the number of glutamate and glycine binding sites on the N-methyl-D-aspartate receptor. Neuron 7:605-613.

Cooper JK, Schilling G, Peters MF, Herring WJ, Sharp AH, Kaminsky Z, Masone J, Khan FA, Delanoy M, Borchelt DR, Dawson VL, Dawson TM, Ross CA (1998) Truncated N-terminal fragments of huntingtin with expanded glutamine repeats form nuclear and cytoplasmic aggregates in cell culture. Hum Mol Genet 7:783-790.

Cowan CM, Raymond LA (2006) Selective neuronal degeneration in Huntington's disease. Curr Top Dev Biol 75:25-71.

Cramer H, Warter JM, Renaud B (1984) Analysis of neurotransmitter metabolites and adenosine 3',5'-monophosphate in the CSF of patients with extrapyramidal motor disorders. Adv Neurol 40:431-435.

Crompton M (1999) The mitochondrial permeability transition pore and its role in cell death. Biochem J 341 (Pt 2):233-249.

Cummings CJ, Reinstein E, Sun Y, Antalffy B, Jiang Y, Ciechanover A, Orr HT, Beaudet AL, Zoghbi HY (1999) Mutation of the E6-AP Ubiquitin Ligase Reduces Nuclear Inclusion Frequency While Accelerating Polyglutamine-Induced Pathology in SCA1 Mice. Neuron 24:879-892.

Cudkowicz M, Kowall NW (1990) Degeneration of pyramidal projection neurons in Huntington's disease cortex. Ann Neurol 27:200-204.

Davies SW, Turmaine M, Cozens BA, Raza AS, Mahal A, Mangiarini L, Bates GP (1999) From neuronal inclusions to neurodegeneration: neuropathological investigation of a transgenic mouse model of Huntington's disease. Philos Trans R Soc Lond B Biol Sci 354:981-989.

Davies SW, Turmaine M, Cozens BA, DiFiglia M, Sharp AH, Ross CA, Scherzinger E, Wanker EE, Mangiarini L, Bates GP (1997) Formation of neuronal intranuclear inclusions underlies the neurological dysfunction in mice transgenic for the HD mutation. Cell 90:537-548.

de la Monte SM, Vonsattel JP, Richardson EP, Jr. (1988) Morphometric demonstration of atrophic changes in the cerebral cortex, white matter, and neostriatum in Huntington's disease. J Neuropathol Exp Neurol 47:516-525.

de Lima AD, Merten MD, Voigt T (1997) Neuritic differentiation and synaptogenesis in serum-free neuronal cultures of the rat cerebral cortex. J Comp Neurol 382:230-246.

del Toro D, Canals JM, Gines S, Kojima M, Egea G, Alberch J (2006) Mutant huntingtin impairs the post-Golgi trafficking of brain-derived neurotrophic factor but not its Val66Met polymorphism. J Neurosci 26:12748-12757.

DiFiglia M (1990) Excitotoxic injury of the neostriatum: a model for Huntington's disease. Trends Neurosci 13:286-289.

DiFiglia M, Sapp E, Chase KO, Davies SW, Bates GP, Vonsattel JP, Aronin N (1997) Aggregation of huntingtin in neuronal intranuclear inclusions and dystrophic neurites in brain. Science 277:1990-1993.

DiFiglia M, Sapp E, Chase K, Schwarz C, Meloni A, Young C, Martin E, Vonsattel JP, Carraway R, Reeves SA, et al. (1995) Huntingtin is a cytoplasmic protein associated with vesicles in human and rat brain neurons. Neuron 14:1075-1081.

Dingledine R, Borges K, Bowie D, Traynelis SF (1999) The glutamate receptor ion channels. Pharmacol Rev 51:7-61.

Dong YN, Wu HY, Hsu FC, Coulter DA, Lynch DR (2006) Developmental and cell-selective variations in N-methyl-D-aspartate receptor degradation by calpain. J Neurochem 99:206-217.

Dragatsis I, Levine MS, Zeitlin S (2000) Inactivation of Hdh in the brain and testis results in progressive neurodegeneration and sterility in mice. Nat Genet 26:300-306.

Dubinsky JM, Levi Y (1998) Calcium-induced activation of the mitochondrial permeability transition in hippocampal neurons. J Neurosci Res 53:728-741.

Duchen MR (2004) Mitochondria in health and disease: perspectives on a new mitochondrial biology. Mol Aspects Med 25:365-451.

Durr A, Hahn-Barma V, Brice A, Pecheux C, Dode C, Feingold J (1999) Homozygosity in Huntington's disease. J Med Genet 36:172-173.

Duyao M, Ambrose C, Myers R, Novelletto A, Persichetti F, Frontali M, Folstein S, Ross C, Franz M, Abbott M, et al. (1993) Trinucleotide repeat length instability and age of onset in Huntington's disease. Nat Genet 4:387-392.

Dyer RB, McMurray CT (2001) Mutant protein in Huntington disease is resistant to proteolysis in affected brain. Nat Genet 29:270-278.

Engelender S, Sharp AH, Colomer V, Tokito MK, Lanahan A, Worley P, Holzbaur EL, Ross CA (1997) Huntingtin-associated protein 1 (HAP1) interacts with the p150Glued subunit of dynactin. Hum Mol Genet 6:2205-2212.

Fan MM, Raymond LA (2007) N-Methyl-d-aspartate (NMDA) receptor function and excitotoxicity in Huntington's disease. Prog Neurobiol 81:272-293.

Fan MM, Fernandes HB, Zhang LY, Hayden MR, Raymond LA (2007) Altered NMDA receptor trafficking in a yeast artificial chromosome transgenic mouse model of Huntington's disease. J Neurosci 27:3768-3779.

Ferrante RJ, Kowall NW, Beal MF, Richardson EP, Jr., Bird ED, Martin JB (1985) Selective sparing of a class of striatal neurons in Huntington's disease. Science 230:561-563.

Ferrante RJ, Kowall NW, Beal MF, Martin JB, Bird ED, Richardson EP, Jr. (1987) Morphologic and histochemical characteristics of a spared subset of striatal neurons in Huntington's disease. J Neuropathol Exp Neurol 46:12-27.

Flint AC, Maisch US, Weishaupt JH, Kriegstein AR, Monyer H (1997) NR2A subunit expression shortens NMDA receptor synaptic currents in developing neocortex. J Neurosci 17:2469-2476.

Fusco FR, Chen Q, Lamoreaux WJ, Figueredo-Cardenas G, Jiao Y, Coffman JA, Surmeier DJ, Honig MG, Carlock LR, Reiner A (1999) Cellular localization of huntingtin in striatal and cortical neurons in rats: lack of correlation with neuronal vulnerability in Huntington's disease. J Neurosci 19:1189-1202.

Gafni J, Ellerby LM (2002) Calpain activation in Huntington's disease. J Neurosci 22:4842-4849.

Gafni J, Hermel E, Young JE, Wellington CL, Hayden MR, Ellerby LM (2004) Inhibition of calpain cleavage of huntingtin reduces toxicity: accumulation of calpain/caspase fragments in the nucleus. J Biol Chem 279:20211-20220.

Gauthier LR, Charrin BC, Borrell-Pages M, Dompierre JP, Rangone H, Cordelieres FP, De Mey J, MacDonald ME, Lessmann V, Humbert S, Saudou F (2004) Huntingtin controls neurotrophic support and survival of neurons by enhancing BDNF vesicular transport along microtubules. Cell 118:127-138.

Ghasemzadeh MB, Sharma S, Surmeier DJ, Eberwine JH, Chesselet MF (1996) Multiplicity of glutamate receptor subunits in single striatal neurons: an RNA amplification study. Mol Pharmacol 49:852-859.

Gines S, Seong IS, Fossale E, Ivanova E, Trettel F, Gusella JF, Wheeler VC, Persichetti F, MacDonald ME (2003) Specific progressive cAMP reduction implicates energy deficit in presymptomatic Huntington's disease knock-in mice. Hum Mol Genet 12:497-508.

Goldberg YP, Nicholson DW, Rasper DM, Kalchman MA, Koide HB, Graham RK, Bromm M, Kazemi-Esfarjani P, Thornberry NA, Vaillancourt JP, Hayden MR (1996) Cleavage of huntingtin by apopain, a proapoptotic cysteine protease, is modulated by the polyglutamine tract. Nat Genet 13:442-449.

Graham RK, Slow EJ, Deng Y, Bissada N, Lu G, Pearson J, Shehadeh J, Leavitt BR, Raymond LA, Hayden MR (2006a) Levels of mutant huntingtin influence the phenotypic severity of Huntington disease in YAC128 mouse models. Neurobiol Dis 21:444-455.

Graham RK, Deng Y, Slow EJ, Haigh B, Bissada N, Lu G, Pearson J, Shehadeh J, Bertram L, Murphy Z, Warby SC, Doty CN, Roy S, Wellington CL, Leavitt BR, Raymond LA, Nicholson DW, Hayden MR (2006b) Cleavage at the caspase-6 site is required for neuronal dysfunction and degeneration due to mutant huntingtin. Cell 125:1179-1191.

Graveland GA, Williams RS, DiFiglia M (1985) Evidence for degenerative and regenerative changes in neostriatal spiny neurons in Huntington's disease. Science 227:770-773.

Green DR, Reed JC (1998) Mitochondria and apoptosis. Science 281:1309-1312.

Greene JG, Porter RH, Eller RV, Greenamyre JT (1993) Inhibition of succinate dehydrogenase by malonic acid produces an "excitotoxic" lesion in rat striatum. J Neurochem 61:1151-1154.

Group HsDCR (1993) A novel gene containing a trinucleotide repeat that is expanded and unstable on Huntington's disease chromosomes. The Huntington's Disease Collaborative Research Group. Cell 72:971-983.

Gu M, Gash MT, Mann VM, Javoy-Agid F, Cooper JM, Schapira AH (1996) Mitochondrial defect in Huntington's disease caudate nucleus. Ann Neurol 39:385-389.

Gunter TE, Buntinas L, Sparagnà G, Eliseev R, Gunter K (2000) Mitochondrial calcium transport: mechanisms and functions. Cell Calcium 28:285-296.

Guttmann RP, Sokol S, Baker DL, Simpkins KL, Dong Y, Lynch DR (2002) Proteolysis of the N-methyl-d-aspartate receptor by calpain in situ. J Pharmacol Exp Ther 302:1023-1030.

Hackam AS, Singaraja R, Wellington CL, Metzler M, McCutcheon K, Zhang T, Kalchman M, Hayden MR (1998) The influence of huntingtin protein size on nuclear localization and cellular toxicity. J Cell Biol 141:1097-1105.

Hansson O, Petersen A, Leist M, Nicotera P, Castilho RF, Brundin P (1999) Transgenic mice expressing a Huntington's disease mutation are resistant to quinolinic acid-induced striatal excitotoxicity. Proc Natl Acad Sci U S A 96:8727-8732.

Hansson O, Guatteo E, Mercuri NB, Bernardi G, Li XJ, Castilho RF, Brundin P (2001) Resistance to NMDA toxicity correlates with appearance of nuclear inclusions, behavioural deficits and changes in calcium homeostasis in mice transgenic for exon 1 of the huntington gene. Eur J Neurosci 14:1492-1504.

Hantraye P, Riche D, Maziere M, Isacson O (1990) A primate model of Huntington's disease: behavioral and anatomical studies of unilateral excitotoxic lesions of the caudate-putamen in the baboon. Exp Neurol 108:91-104.

Hardingham GE, Bading H (2003) The Yin and Yang of NMDA receptor signalling. Trends Neurosci 26:81-89.

Hardingham GE, Fukunaga Y, Bading H (2002) Extrasynaptic NMDARs oppose synaptic NMDARs by triggering CREB shut-off and cell death pathways. Nat Neurosci 5:405-414.

Hardingham GE, Chawla S, Cruzalegui FH, Bading H (1999) Control of recruitment and transcription-activating function of CBP determines gene regulation by NMDA receptors and L-type calcium channels. Neuron 22:789-798.

Harper PS (1996) Huntington's Disease, 2nd Edition. London: W.B. Saunders.

Hartley DM, Kurth MC, Bjerkness L, Weiss JH, Choi DW (1993) Glutamate receptor-induced 45Ca2+ accumulation in cortical cell culture correlates with subsequent neuronal degeneration. J Neurosci 13:1993-2000.

Hayden M (1981) Huntington's Chorea. Berlin: Springer-Verlag.

Hedreen JC, Peyser CE, Folstein SE, Ross CA (1991) Neuronal loss in layers V and VI of cerebral cortex in Huntington's disease. Neurosci Lett 133:257-261.

Hickey MA, Chesselet MF (2003) The use of transgenic and knock-in mice to study Huntington's disease. Cytogenet. Genome Res. 100:276-286.

Hilditch-Maguire P, Trettel F, Passani LA, Auerbach A, Persichetti F, MacDonald ME (2000) Huntingtin: an iron-regulated protein essential for normal nuclear and perinuclear organelles. Hum Mol Genet 9:2789-2797.

Hodges A, Strand AD, Aragaki AK, Kuhn A, Sengstag T, Hughes G, Elliston LA, Hartog C, Goldstein DR, Thu D, Hollingsworth ZR, Collin F, Synek B, Holmans PA, Young AB, Wexler NS, Delorenzi M, Kooperberg C, Augood SJ, Faull RL, Olson JM, Jones L, Luthi-Carter R (2006) Regional and cellular gene expression changes in human Huntington's disease brain. Hum Mol Genet 15:965-977.

Hodgson JG, Agopyan N, Gutekunst CA, Leavitt BR, LePiane F, Singaraja R, Smith DJ, Bissada N, McCutcheon K, Nasir J, Jamot L, Li XJ, Stevens ME, Rosemond E, Roder JC, Phillips AG, Rubin EM, Hersch SM, Hayden MR (1999) A YAC mouse model for Huntington's disease with full-length mutant huntingtin, cytoplasmic toxicity, and selective striatal neurodegeneration. Neuron 23:181-192.

Hollmann M, Heinemann S (1994) Cloned glutamate receptors. Annu Rev Neurosci 17:31-108.

Hollmann M, Boulter J, Maron C, Beasley L, Sullivan J, Pecht G, Heinemann S (1993) Zinc potentiates agonist-induced currents at certain splice variants of the NMDA receptor. Neuron 10:943-954.

Huang Q, Zhou D, Sapp E, Aizawa H, Ge P, Bird ED, Vonsattel JP, DiFiglia M (1995) Quinolinic acid-induced increases in calbindin D28k immunoreactivity in rat striatal neurons in vivo and in vitro mimic the pattern seen in Huntington's disease. Neuroscience 65:397-407.

Huettner JE, Bean BP (1988) Block of N-methyl-D-aspartate-activated current by the anticonvulsant MK-801: selective binding to open channels. Proc Natl Acad Sci U S A 85:1307-1311.

Hyrc K, Handran SD, Rothman SM, Goldberg MP (1997) Ionized intracellular calcium concentration predicts excitotoxic neuronal death: observations with low-affinity fluorescent calcium indicators. J Neurosci 17:6669-6677.

Ishii T, Moriyoshi K, Sugihara H, Sakurada K, Kadotani H, Yokoi M, Akazawa C, Shigemoto R, Mizuno N, Masu M, et al. (1993) Molecular characterization of the family of the N-methyl-D-aspartate receptor subunits. J Biol Chem 268:2836-2843.

Jarabek BR, Yasuda RP, Wolfe BB (2004) Regulation of proteins affecting NMDA receptor-induced excitotoxicity in a Huntington's mouse model. Brain 127:505-516.

Jenkins BG, Koroshetz WJ, Beal MF, Rosen BR (1993) Evidence for impairment of energy metabolism in vivo in Huntington's disease using localized 1H NMR spectroscopy. Neurology 43:2689-2695.

Kalchman MA, Koide HB, McCutcheon K, Graham RK, Nichol K, Nishiyama K, Kazemi-Esfarjani P, Lynn FC, Wellington C, Metzler M, Goldberg YP, Kanazawa I, Gietz RD, Hayden MR (1997) HIP1, a human homologue of S. cerevisiae Sla2p, interacts with membrane-associated huntingtin in the brain. Nat Genet 16:44-53.

Kegel KB, Meloni AR, Yi Y, Kim YJ, Doyle E, Cuiffo BG, Sapp E, Wang Y, Qin ZH, Chen JD, Nevins JR, Aronin N, DiFiglia M (2002) Huntingtin is present in the nucleus, interacts with the transcriptional corepressor C-terminal binding protein, and represses transcription. J Biol Chem 277:7466-7476.

Kim YJ, Yi Y, Sapp E, Wang Y, Cuiffo B, Kegel KB, Qin ZH, Aronin N, DiFiglia M (2001) Caspase 3-cleaved N-terminal fragments of wild-type and mutant huntingtin are present in normal and Huntington's disease brains, associate with membranes, and undergo calpain-dependent proteolysis. Proc Natl Acad Sci U S A 98:12784-12789.

Kirichok Y, Krapivinsky G, Clapham DE (2004) The mitochondrial calcium uniporter is a highly selective ion channel. Nature 427:360-4.

Koroshetz WJ, Jenkins BG, Rosen BR, Beal MF (1997) Energy metabolism defects in Huntington's disease and effects of coenzyme Q10. Ann Neurol 41:160-165.

Kovacs AD, Cebers G, Cebere A, Moreira T, Liljequist S (2001) Cortical and striatal neuronal cultures of the same embryonic origin show intrinsic differences in glutamate receptor expression and vulnerability to excitotoxicity. Exp Neurol 168:47-62.

Kremer B, Goldberg P, Andrew SE, Theilmann J, Telenius H, Zeisler J, Squitieri F, Lin B, Bassett A, Almqvist E, et al. (1994) A worldwide study of the Huntington's disease mutation. The sensitivity and specificity of measuring CAG repeats. N Engl J Med 330:1401-1406.

Kuppenbender KD, Albers DS, Iadarola MJ, Landwehrmeyer GB, Standaert DG (1999) Localization of alternatively spliced NMDAR1 glutamate receptor isoforms in rat striatal neurons. J Comp Neurol 415:204-217.

Kuryatov A, Laube B, Betz H, Kuhse J (1994) Mutational analysis of the glycine-binding site of the NMDA receptor: structural similarity with bacterial amino acid-binding proteins. Neuron 12:1291-1300.

Laforet GA, Sapp E, Chase K, McIntyre C, Boyce FM, Campbell M, Cadigan BA, Warzecki L, Tagle DA, Reddy PH, Cepeda C, Calvert CR, Jokel ES, Klapstein GJ, Ariano MA, Levine MS, DiFiglia M, Aronin N (2001) Changes in cortical and striatal neurons predict behavioral and electrophysiological abnormalities in a transgenic murine model of Huntington's disease. J Neurosci 21:9112-9123.

Lan JY, Skeberdis VA, Jover T, Grooms SY, Lin Y, Araneda RC, Zheng X, Bennett MV, Zukin RS (2001) Protein kinase C modulates NMDA receptor trafficking and gating. Nat Neurosci 4:382-390.

Landwehrmeyer GB, Standaert DG, Testa CM, Penney JB, Jr., Young AB (1995a) NMDA receptor subunit mRNA expression by projection neurons and interneurons in rat striatum. J Neurosci 15:5297-5307.

Landwehrmeyer GB, McNeil SM, Dure LSt, Ge P, Aizawa H, Huang Q, Ambrose CM, Duyao MP, Bird ED, Bonilla E, et al. (1995b) Huntington's disease gene: regional and cellular expression in brain of normal and affected individuals. Ann Neurol 37:218-230.

Laube B, Kuhse J, Betz H (1998) Evidence for a tetrameric structure of recombinant NMDA receptors. J Neurosci 18:2954-2961.

Leavitt BR, Guttman JA, Hodgson JG, Kimel GH, Singaraja R, Vogl AW, Hayden MR (2001) Wild-type huntingtin reduces the cellular toxicity of mutant huntingtin in vivo. Am J Hum Genet 68:313-324.

Leavitt BR, van Raamsdonk JM, Shehadeh J, Fernandes H, Murphy Z, Graham RK, Wellington CL, Raymond LA, Hayden MR (2006) Wild-type huntingtin protects neurons from excitotoxicity. J Neurochem 96:1121-1129.

Lee ST, Chu K, Park JE, Kang L, Ko SY, Jung KH, Kim M (2006) Memantine reduces striatal cell death with decreasing calpain level in 3-nitropropionic model of Huntington's disease. Brain Res 1118:199-207.

Levine MS, Klapstein GJ, Koppel A, Gruen E, Cepeda C, Vargas ME, Jokel ES, Carpenter EM, Zanjani H, Hurst RS, Efstratiadis A, Zeitlin S, Chesselet MF (1999) Enhanced sensitivity to N-methyl-D-aspartate receptor activation in transgenic and knockin mouse models of Huntington's disease. J Neurosci Res 58:515-532.

Li JH, Wang YH, Wolfe BB, Krueger KE, Corsi L, Stocca G, Vicini S (1998) Developmental changes in localization of NMDA receptor subunits in primary cultures of cortical neurons. Eur J Neurosci 10:1704-1715.

Li L, Murphy TH, Hayden MR, Raymond LA (2004) Enhanced striatal NR2B-containing N-methyl-D-aspartate receptor-mediated synaptic currents in a mouse model of Huntington disease. J Neurophysiol 92:2738-2746.

Li L, Fan M, Icton CD, Chen N, Leavitt BR, Hayden MR, Murphy TH, Raymond LA (2003a) Role of NR2B-type NMDA receptors in selective neurodegeneration in Huntington disease. Neurobiol Aging 24:1113-1121.

Li SH, Yu ZX, Li CL, Nguyen HP, Zhou YX, Deng C, Li XJ (2003b) Lack of huntingtin-associated protein-1 causes neuronal death resembling hypothalamic degeneration in Huntington's disease. J Neurosci 23:6956-6964.

Lin CH, Tallaksen-Greene S, Chien WM, Cearley JA, Jackson WS, Crouse AB, Ren S, Li XJ, Albin RL, Detloff PJ (2001) Neurological abnormalities in a knock-in mouse model of Huntington's disease. Hum Mol Genet 10:137-144.

Lin Y, Skeberdis VA, Francesconi A, Bennett MV, Zukin RS (2004) Postsynaptic density protein-95 regulates NMDA channel gating and surface expression. J Neurosci 24:10138-10148.

Liu L, Wong TP, Pozza MF, Lingenhoehl K, Wang Y, Sheng M, Auberson YP, Wang YT (2004) Role of NMDA receptor subtypes in governing the direction of hippocampal synaptic plasticity. Science 304:1021-1024.

Lucas DR, Newhouse JP (1957) The toxic effect of sodium L-glutamate on the inner layers of the retina. Arch. Ophthamol. 58:193-201.

Luthi-Carter R, Strand A, Peters NL, Solano SM, Hollingsworth ZR, Menon AS, Frey AS, Spektor BS, Penney EB, Schilling G, Ross CA, Borchelt DR, Tapscott SJ, Young AB, Cha JH, Olson JM (2000) Decreased expression of striatal signaling genes in a mouse model of Huntington's disease. Hum Mol Genet 9:1259-1271.

MacGibbon GA, Hamilton LC, Crocker SF, Costain WJ, Murphy KM, Robertson HA, Denovan-Wright EM (2002) Immediate-early gene response to methamphetamine, haloperidol, and quinolinic acid is not impaired in Huntington's disease transgenic mice. J Neurosci Res 67:372-378.

Mangiarini L, Sathasivam K, Seller M, Cozens B, Harper A, Hetherington C, Lawton M, Trottier Y, Lehrach H, Davies SW, Bates GP (1996) Exon 1 of the HD gene with an expanded CAG repeat is sufficient to cause a progressive neurological phenotype in transgenic mice. Cell 87:493-506.

Marchetti P, Castedo M, Susin SA, Zamzami N, Hirsch T, Macho A, Haeffner A, Hirsch F, Geuskens M, Kroemer G (1996) Mitochondrial permeability transition is a central coordinating event of apoptosis. J Exp Med 184:1155-1160.

Martindale D, Hackam A, Wieczorek A, Ellerby L, Wellington C, McCutcheon K, Singaraja R, Kazemi-Esfarjani P, Devon R, Kim SU, Bredesen DE, Tufaro F,

Hayden MR (1998) Length of huntingtin and its polyglutamine tract influences localization and frequency of intracellular aggregates. Nat Genet 18:150-154.

Massey PV, Johnson BE, Moult PR, Auberson YP, Brown MW, Molnar E, Collingridge GL, Bashir ZI (2004) Differential roles of NR2A and NR2B-containing NMDA receptors in cortical long-term potentiation and long-term depression. J Neurosci 24:7821-7828.

Mattson MP (2003) Excitotoxic and excitoprotective mechanisms: abundant targets for the prevention and treatment of neurodegenerative disorders. Neuromolecular Med 3:65-94.

Mayer ML, Westbrook GL, Guthrie PB (1984) Voltage-dependent block by Mg2+ of NMDA responses in spinal cord neurones. Nature 309:261-263.

McCampbell A, Taye AA, Whitty L, Penney E, Steffan JS, Fischbeck KH (2001) Histone deacetylase inhibitors reduce polyglutamine toxicity. Proc Natl Acad Sci U S A 98:15179-15184.

McCampbell A, Taylor JP, Taye AA, Robitschek J, Li M, Walcott J, Merry D, Chai Y, Paulson H, Sobue G, Fischbeck KH (2000) CREB-binding protein sequestration by expanded polyglutamine. Hum Mol Genet 9:2197-2202.

McIlhinney RA, Le Bourdelles B, Molnar E, Tricaud N, Streit P, Whiting PJ (1998) Assembly intracellular targeting and cell surface expression of the human N-methyl-D-aspartate receptor subunits NR1a and NR2A in transfected cells. Neuropharmacology 37:1355-1367.

Menalled LB, Sison JD, Dragatsis I, Zeitlin S, Chesselet MF (2003) Time course of early motor and neuropathological anomalies in a knock-in mouse model of Huntington's disease with 140 CAG repeats. J Comp Neurol 465:11-26.

Menalled LB, Sison JD, Wu Y, Olivieri M, Li XJ, Li H, Zeitlin S, Chesselet MF (2002) Early motor dysfunction and striosomal distribution of huntingtin microaggregates in Huntington's disease knock-in mice. J Neurosci 22:8266-8276.

Mende-Mueller LM, Toneff T, Hwang SR, Chesselet MF, Hook VY (2001) Tissue-specific proteolysis of Huntingtin (htt) in human brain: evidence of enhanced levels of N- and C-terminal htt fragments in Huntington's disease striatum. J Neurosci 21:1830-1837.

Metzler M, Legendre-Guillemin V, Gan L, Chopra V, Kwok A, McPherson PS, Hayden MR (2001) HIP1 functions in clathrin-mediated endocytosis through binding to clathrin and adaptor protein 2. J Biol Chem 276:39271-39276.

Metzler M, Li B, Gan L, Georgiou J, Gutekunst CA, Wang Y, Torre E, Devon RS, Oh R, Legendre-Guillemin V, Rich M, Alvarez C, Gertsenstein M, McPherson PS, Nagy A, Wang YT, Roder JC, Raymond LA, Hayden MR (2003) Disruption of the endocytic protein HIP1 results in neurological deficits and decreased AMPA receptor trafficking. Embo J 22:3254-3266.

Michaels RL, Rothman SM (1990) Glutamate neurotoxicity in vitro: antagonist pharmacology and intracellular calcium concentrations. J Neurosci 10:283-292.

Misra C, Brickley SG, Wyllie DJ, Cull-Candy SG (2000) Slow deactivation kinetics of NMDA receptors containing NR1 and NR2D subunits in rat cerebellar Purkinje cells. J Physiol 525 Pt 2:299-305.

Monoi H, Futaki S, Kugimiya S, Minakata H, Yoshihara K (2000) Poly-L-glutamine forms cation channels: relevance to the pathogenesis of the polyglutamine diseases. Biophys J 78:2892-2899.

Monyer H, Burnashev N, Laurie DJ, Sakmann B, Seeburg PH (1994) Developmental and regional expression in the rat brain and functional properties of four NMDA receptors. Neuron 12:529-540.

Monyer H, Sprengel R, Schoepfer R, Herb A, Higuchi M, Lomeli H, Burnashev N, Sakmann B, Seeburg PH (1992) Heteromeric NMDA receptors: molecular and functional distinction of subtypes. Science 256:1217-1221.

Mu Y, Otsuka T, Horton AC, Scott DB, Ehlers MD (2003) Activity-dependent mRNA splicing controls ER export and synaptic delivery of NMDA receptors. Neuron 40:581-594.

Myers RH, Madden JJ, Teague JL, Falek A (1982) Factors related to onset age of Huntington disease. Am J Hum Genet 34:481-488.

Myers RH, Leavitt J, Farrer LA, Jagadeesh J, McFarlane H, Mastromauro CA, Mark RJ, Gusella JF (1989) Homozygote for Huntington disease. Am J Hum Genet 45:615-618.

Nasir J, Floresco SB, O'Kusky JR, Diewert VM, Richman JM, Zeisler J, Borowski A, Marth JD, Phillips AG, Hayden MR (1995) Targeted disruption of the Huntington's disease gene results in embryonic lethality and behavioral and morphological changes in heterozygotes. Cell 81:811-823.

Nicholls DG, Budd SL (1998) Mitochondria and neuronal glutamate excitotoxicity. Biochim Biophys Acta 1366:97-112.

Nicholls DG, Ward MW (2000) Mitochondrial membrane potential and neuronal glutamate excitotoxicity: mortality and millivolts. Trends Neurosci 23:166-174.

Nicotera P, Hartzell P, Baldi C, Svensson SA, Bellomo G, Orrenius S (1986) Cystamine induces toxicity in hepatocytes through the elevation of cytosolic Ca2+ and the stimulation of a nonlysosomal proteolytic system. J Biol Chem 261:14628-14635.

Nowak L, Bregestovski P, Ascher P, Herbet A, Prochiantz A (1984) Magnesium gates glutamate-activated channels in mouse central neurones. Nature 307:462-465.

Nucifora FC, Jr., Sasaki M, Peters MF, Huang H, Cooper JK, Yamada M, Takahashi H, Tsuji S, Troncoso J, Dawson VL, Dawson TM, Ross CA (2001) Interference by huntingtin and atrophin-1 with cbp-mediated transcription leading to cellular toxicity. Science 291:2423-2428.

Oliveira JM, Chen S, Almeida S, Riley R, Goncalves J, Oliveira CR, Hayden MR, Nicholls DG, Ellerby LM, Rego AC (2006) Mitochondrial-dependent Ca2+ handling in Huntington's disease striatal cells: effect of histone deacetylase inhibitors. J Neurosci 26:11174-11186.

Olney JW (1969) Brain lesion, obesity and other disturbances in mice treated with monosodium glutamate. Science 164:719-721.

Orrenius S (2004) Mitochondrial regulation of apoptotic cell death. Toxicol Lett 149:19-23.

Palfi S, Ferrante RJ, Brouillet E, Beal MF, Dolan R, Guyot MC, Peschanski M, Hantraye P (1996) Chronic 3-nitropropionic acid treatment in baboons replicates the cognitive and motor deficits of Huntington's disease. J Neurosci 16:3019-3025.

Panov AV, Lund S, Greenamyre JT (2005) Ca2+-induced permeability transition in human lymphoblastoid cell mitochondria from normal and Huntington's disease individuals. Mol Cell Biochem 269:143-152.

Panov AV, Gutekunst CA, Leavitt BR, Hayden MR, Burke JR, Strittmatter WJ, Greenamyre JT (2002) Early mitochondrial calcium defects in Huntington's disease are a direct effect of polyglutamines. Nat Neurosci 5:731-736.

Paulsen JS, Zhao H, Stout JC, Brinkman RR, Guttman M, Ross CA, Como P, Manning C, Hayden MR, Shoulson I (2001) Clinical markers of early disease in persons near onset of Huntington's disease. Neurology 57:658-662.

Peng TI, Greenamyre JT (1998) Privileged access to mitochondria of calcium influx through N-methyl-D-aspartate receptors. Mol Pharmacol 53:974-980.

Perutz M (1994) Polar zippers: their role in human disease. Protein Sci 3:1629-1637.

Petit PX, Susin SA, Zamzami N, Mignotte B, Kroemer G (1996) Mitochondria and programmed cell death: back to the future. FEBS Lett 396:7-13.

Pivovarova NB, Nguyen HV, Winters CA, Brantner CA, Smith CL, Andrews SB (2004) Excitotoxic calcium overload in a subpopulation of mitochondria triggers delayed death in hippocampal neurons. J Neurosci 24:5611-5622.

Rameau GA, Akaneya Y, Chiu L, Ziff EB (2000) Role of NMDA receptor functional domains in excitatory cell death. Neuropharmacology 39:2255-2266.

Raymond LA, Moshaver A, Tingley WG, Huganir RL (1996) Glutamate receptor ion channel properties predict vulnerability to cytotoxicity in a transfected nonneuronal cell line. Mol Cell Neurosci 7:102-115.

Reddy PH, Williams M, Charles V, Garrett L, Pike-Buchanan L, Whetsell WO, Jr., Miller G, Tagle DA (1998) Behavioural abnormalities and selective neuronal loss in HD transgenic mice expressing mutated full-length HD cDNA. Nat Genet 20:198-202.

Regalado MP, Villarroel A, Lerma J (2001) Intersubunit cooperativity in the NMDA receptor. Neuron 32:1085-1096.

Richfield EK, Maguire-Zeiss KA, Vonkeman HE, Voorn P (1995) Preferential loss of preproenkephalin versus preprotachykinin neurons from the striatum of Huntington's disease patients. Ann Neurol 38:852-861.

Rigamonti D, Bauer JH, De-Fraja C, Conti L, Sipione S, Sciorati C, Clementi E, Hackam A, Hayden MR, Li Y, Cooper JK, Ross CA, Govoni S, Vincenz C, Cattaneo E (2000) Wild-type huntingtin protects from apoptosis upstream of caspase-3. J Neurosci 20:3705-3713.

Rigby M, Le Bourdelles B, Heavens RP, Kelly S, Smith D, Butler A, Hammans R, Hills R, Xuereb JH, Hill RG, Whiting PJ, Sirinathsinghji DJ (1996) The messenger RNAs for the N-methyl-D-aspartate receptor subunits show region-specific expression of different subunit composition in the human brain. Neuroscience 73:429-447.

Rintoul GL, Raymond LA, Baimbridge KG (2001) Calcium buffering and protection from excitotoxic cell death by exogenous calbindin-D28k in HEK 293 cells. Cell Calcium 29:277-287.

Rockabrand E, Slepko N, Pantalone A, Nukala VN, Kazantsev A, Marsh JL, Sullivan PG, Steffan JS, Sensi SL, Thompson LM (2006) The 1st 17 amino acids of Huntingtin modulate its sub-cellular localization, aggregation and effects on calcium homeostasis. Hum Mol Genet.

Ross CA (2002) Polyglutamine pathogenesis: emergence of unifying mechanisms for Huntington's disease and related disorders. Neuron 35:819-822.

Rubinsztein DC, Leggo J, Coles R, Almqvist E, Biancalana V, Cassiman JJ, Chotai K, Connarty M, Crauford D, Curtis A, Curtis D, Davidson MJ, Differ AM, Dode C, Dodge A, Frontali M, Ranen NG, Stine OC, Sherr M, Abbott MH, Franz ML, Graham CA, Harper PS, Hedreen JC, Hayden MR, et al. (1996) Phenotypic characterization of individuals with 30-40 CAG repeats in the Huntington disease (HD) gene reveals HD cases with 36 repeats and apparently normal elderly individuals with 36-39 repeats. Am J Hum Genet 59:16-22.

Sanberg PR, Calderon SF, Giordano M, Tew JM, Norman AB (1989) The quinolinic acid model of Huntington's disease: locomotor abnormalities. Exp Neurol. 105:45-53.

Sapp E, Penney J, Young A, Aronin N, Vonsattel JP, DiFiglia M (1999) Axonal transport of N-terminal huntingtin suggests early pathology of corticostriatal projections in Huntington disease. J Neuropathol Exp Neurol. 58:165-73.

Sather W, Dieudonne S, MacDonald JF, Ascher P (1992) Activation and desensitization of N-methyl-D-aspartate receptors in nucleated outside-out patches from mouse neurones. J Physiol 450:643-672.

Sattler R, Tymianski M (2001) Molecular mechanisms of glutamate receptor-mediated excitotoxic neuronal cell death. Mol Neurobiol 24:107-129.

Sattler R, Charlton MP, Hafner M, Tymianski M (1998) Distinct influx pathways, not calcium load, determine neuronal vulnerability to calcium neurotoxicity. J Neurochem 71:2349-2364.

Saudou F, Finkbeiner S, Devys D, Greenberg ME (1998) Huntingtin acts in the nucleus to induce apoptosis but death does not correlate with the formation of intranuclear inclusions. Cell 95:55-66.

Sawa A, Wiegand GW, Cooper J, Margolis RL, Sharp AH, Lawler JF, Jr., Greenamyre JT, Snyder SH, Ross CA (1999) Increased apoptosis of Huntington disease lymphoblasts associated with repeat length-dependent mitochondrial depolarization. Nat Med 5:1194-1198.

Schilling G, Becher MW, Sharp AH, Jinnah HA, Duan K, Kotzuk JA, Slunt HH, Ratovitski T, Cooper JK, Jenkins NA, Copeland NG, Price DL, Ross CA, Borchelt DR (1999) Intranuclear inclusions and neuritic aggregates in transgenic mice expressing a mutant N-terminal fragment of huntingtin. Hum Mol Genet 8:397-407.

Schinder AF, Olson EC, Spitzer NC, Montal M (1996) Mitochondrial dysfunction is a primary event in glutamate neurotoxicity. J Neurosci 16:6125-6133.

Schneggenburger R (1996) Simultaneous measurement of Ca2+ influx and reversal potentials in recombinant N-methyl-D-aspartate receptor channels. Biophys J 70:2165-2174.

Schwarcz R, Foster AC, French ED, Whetsell WO, Jr., Kohler C (1984) Excitotoxic models for neurodegenerative disorders. Life Sci 35:19-32.

Scott DB, Michailidis I, Mu Y, Logothetis D, Ehlers MD (2004) Endocytosis and degradative sorting of NMDA receptors by conserved membrane-proximal signals. J Neurosci 24:7096-7109.

Seo H, Sonntag KC, Isacson O (2004) Generalized brain and skin proteasome inhibition in Huntington's disease. Ann Neurol 56:319-328.

Seong IS, Ivanova E, Lee JM, Choo YS, Fossale E, Anderson M, Gusella JF, Laramie JM, Myers RH, Lesort M, MacDonald ME (2005) HD CAG repeat implicates a dominant property of huntingtin in mitochondrial energy metabolism. Hum Mol Genet 14:2871-2880.

Sharp AH, Loev SJ, Schilling G, Li SH, Li XJ, Bao J, Wagster MV, Kotzuk JA, Steiner JP, Lo A, et al. (1995) Widespread expression of Huntington's disease gene (IT15) protein product. Neuron 14:1065-1074.

Shehadeh J, Fernandes HB, Zeron Mullins MM, Graham RK, Leavitt BR, Hayden MR, Raymond LA (2006) Striatal neuronal apoptosis is preferentially enhanced by NMDA receptor activation in YAC transgenic mouse model of Huntington disease. Neurobiol Dis 21:392-403.

Shelbourne PF, Killeen N, Hevner RF, Johnston HM, Tecott L, Lewandoski M, Ennis M, Ramirez L, Li Z, Iannicola C, Littman DR, Myers RM (1999) A Huntington's disease CAG expansion at the murine Hdh locus is unstable and associated with behavioural abnormalities in mice. Hum Mol Genet 8:763-774.

Sheng M, Cummings J, Roldan LA, Jan YN, Jan LY (1994) Changing subunit composition of heteromeric NMDA receptors during development of rat cortex. Nature 368:144-147.

Shi WX, Rayport S (1994) GABA synapses formed in vitro by local axon collaterals of nucleus accumbens neurons. J Neurosci 14:4548-4560.

Simpkins KL, Guttmann RP, Dong Y, Chen Z, Sokol S, Neumar RW, Lynch DR (2003) Selective activation induced cleavage of the NR2B subunit by calpain. J Neurosci 23:11322-11331.

Slow EJ, Graham RK, Osmand AP, Devon RS, Lu G, Deng Y, Pearson J, Vaid K, Bissada N, Wetzel R, Leavitt BR, Hayden MR (2005) Absence of behavioral

abnormalities and neurodegeneration in vivo despite widespread neuronal huntingtin inclusions. Proc Natl Acad Sci U S A 102:11402-11407.

Slow EJ, van Raamsdonk J, Rogers D, Coleman SH, Graham RK, Deng Y, Oh R, Bissada N, Hossain SM, Yang YZ, Li XJ, Simpson EM, Gutekunst CA, Leavitt BR, Hayden MR (2003) Selective striatal neuronal loss in a YAC128 mouse model of Huntington disease. Hum Mol Genet 12:1555-1567.

Squitieri F, Gellera C, Cannella M, Mariotti C, Cislaghi G, Rubinsztein DC, Almqvist EW, Turner D, Bachoud-Levi AC, Simpson SA, Delatycki M, Maglione V, Hayden MR, Donato SD (2003) Homozygosity for CAG mutation in Huntington disease is associated with a more severe clinical course. Brain 126:946-955.

Standaert DG, Friberg IK, Landwehrmeyer GB, Young AB, Penney JB, Jr. (1999) Expression of NMDA glutamate receptor subunit mRNAs in neurochemically identified projection and interneurons in the striatum of the rat. Brain Res Mol Brain Res 64:11-23.

Starling AJ, Andre VM, Cepeda C, de Lima M, Chandler SH, Levine MS (2005) Alterations in N-methyl-D-aspartate receptor sensitivity and magnesium blockade occur early in development in the R6/2 mouse model of Huntington's disease. J Neurosci Res 82:377-386.

Steffan JS, Kazantsev A, Spasic-Boskovic O, Greenwald M, Zhu YZ, Gohler H, Wanker EE, Bates GP, Housman DE, Thompson LM (2000) The Huntington's disease protein interacts with p53 and CREB-binding protein and represses transcription. Proc Natl Acad Sci U S A 97:6763-6768.

Stine OC, Pleasant N, Franz ML, Abbott MH, Folstein SE, Ross CA (1993) Correlation between the onset age of Huntington's disease and length of the trinucleotide repeat in IT-15. Hum Mol Genet 2:1547-1549.

Stocca G, Vicini S (1998) Increased contribution of NR2A subunit to synaptic NMDA receptors in developing rat cortical neurons. J Physiol 507 (Pt 1):13-24.

Stout AK, Reynolds IJ (1999) High-affinity calcium indicators underestimate increases in intracellular calcium concentrations associated with excitotoxic glutamate stimulations. Neuroscience 89:91-100.

Stout AK, Raphael HM, Kanterewicz BI, Klann E, Reynolds IJ (1998) Glutamate-induced neuron death requires mitochondrial calcium uptake. Nat Neurosci 1:366-373.

Strong TV, Tagle DA, Valdes JM, Elmer LW, Boehm K, Swaroop M, Kaatz KW, Collins FS, Albin RL (1993) Widespread expression of the human and rat Huntington's disease gene in brain and nonneural tissues. Nat Genet 5:259-265.

Sugars KL, Rubinsztein DC (2003) Transcriptional abnormalities in Huntington disease. Trends Genet 19:233-238.

Sugihara H, Moriyoshi K, Ishii T, Masu M, Nakanishi S (1992) Structures and properties of seven isoforms of the NMDA receptor generated by alternative splicing. Biochem Biophys Res Commun 185:826-832.

Sun Z, Wang HB, Deng YP, Lei WL, Xie JP, Meade CA, Del Mar N, Goldowitz D, Reiner A (2005) Increased calbindin-D28k immunoreactivity in striatal projection neurons of R6/2 Huntington's disease transgenic mice. Neurobiol Dis 20:907-917.

Surmeier DJ, Bargas J, Kitai ST (1988) Voltage-clamp analysis of a transient potassium current in rat neostriatal neurons. Brain Res 473:187-192.

Tabrizi SJ, Cleeter MW, Xuereb J, Taanman JW, Cooper JM, Schapira AH (1999) Biochemical abnormalities and excitotoxicity in Huntington's disease brain. Ann Neurol 45:25-32.

Tang TS, Tu H, Chan EY, Maximov A, Wang Z, Wellington CL, Hayden MR, Bezprozvanny I (2003) Huntingtin and huntingtin-associated protein 1 influence neuronal calcium signaling mediated by inositol-(1,4,5) triphosphate receptor type 1. Neuron 39:227-239.

Tang TS, Slow E, Lupu V, Stavrovskaya IG, Sugimori M, Llinas R, Kristal BS, Hayden MR, Bezprozvanny I (2005) Disturbed Ca2+ signaling and apoptosis of medium spiny neurons in Huntington's disease. Proc Natl Acad Sci U S A 102:2602-2607.

Tobin AJ, Signer ER (2000) Huntington's disease: the challenge for cell biologists. Trends Cell Biol 10:531-536.

Toescu EC, Verkhratsky A (2000) Assessment of mitochondrial polarization status in living cells based on analysis of the spatial heterogeneity of rhodamine 123 fluorescence staining. Pflugers Arch 440:941-947.

Tovar KR, Westbrook GL (1999) The incorporation of NMDA receptors with a distinct subunit composition at nascent hippocampal synapses in vitro. J Neurosci 19:4180-4188.

Tovar KR, Westbrook GL (2002) Mobile NMDA receptors at hippocampal synapses. Neuron 34:255-264.

Vallano ML, Lambolez B, Audinat E, Rossier J (1996) Neuronal activity differentially regulates NMDA receptor subunit expression in cerebellar granule cells. J Neurosci 16:631-639.

Van Raamsdonk JM, Pearson J, Slow EJ, Hossain SM, Leavitt BR, Hayden MR (2005) Cognitive dysfunction precedes neuropathology and motor abnormalities in the YAC128 mouse model of Huntington's disease. J Neurosci 25:4169-4180.

Velier J, Kim M, Schwarz C, Kim TW, Sapp E, Chase K, Aronin N, DiFiglia M (1998) Wild-type and mutant huntingtins function in vesicle trafficking in the secretory and endocytic pathways. Exp Neurol 152:34-40.

Vicini S, Wang JF, Li JH, Zhu WJ, Wang YH, Luo JH, Wolfe BB, Grayson DR (1998) Functional and pharmacological differences between recombinant N-methyl-D-aspartate receptors. J Neurophysiol 79:555-566.

Vonsattel JP, DiFiglia M (1998) Huntington disease. J Neuropathol Exp Neurol 57:369-384.

Vonsattel JP, Myers RH, Stevens TJ, Ferrante RJ, Bird ED, Richardson EP, Jr. (1985) Neuropathological classification of Huntington's disease. J Neuropathol Exp Neurol 44:559-577.

Wanker EE, Rovira C, Scherzinger E, Hasenbank R, Walter S, Tait D, Colicelli J, Lehrach H (1997) HIP-I: a huntingtin interacting protein isolated by the yeast two-hybrid system. Hum Mol Genet 6:487-495.

Wellington CL, Hayden MR (1997) Of molecular interactions, mice and mechanisms: new insights into Huntington's disease. Curr Opin Neurol 10:291-298.

Wellington CL, Singaraja R, Ellerby L, Savill J, Roy S, Leavitt B, Cattaneo E, Hackam A, Sharp A, Thornberry N, Nicholson DW, Bredesen DE, Hayden MR (2000) Inhibiting caspase cleavage of huntingtin reduces toxicity and aggregate formation in neuronal and nonneuronal cells. J Biol Chem 275:19831-19838.

Wellington CL, Ellerby LM, Gutekunst CA, Rogers D, Warby S, Graham RK, Loubser O, van Raamsdonk J, Singaraja R, Yang YZ, Gafni J, Bredesen D, Hersch SM, Leavitt BR, Roy S, Nicholson DW, Hayden MR (2002) Caspase cleavage of mutant huntingtin precedes neurodegeneration in Huntington's disease. J Neurosci 22:7862-7872.

Wellington CL, Ellerby LM, Hackam AS, Margolis RL, Trifiro MA, Singaraja R, McCutcheon K, Salvesen GS, Propp SS, Bromm M, Rowland KJ, Zhang T, Rasper D, Roy S, Thornberry N, Pinsky L, Kakizuka A, Ross CA, Nicholson DW, Bredesen DE, Hayden MR (1998) Caspase cleavage of gene products associated with triplet expansion disorders generates truncated fragments containing the polyglutamine tract. J Biol Chem 273:9158-9167.

Wexler NS, Young AB, Tanzi RE, Travers H, Starosta-Rubinstein S, Penney JB, Snodgrass SR, Shoulson I, Gomez F, Ramos Arroyo MA, et al. (1987) Homozygotes for Huntington's disease. Nature 326:194-197.

Wheeler VC, White JK, Gutekunst CA, Vrbanac V, Weaver M, Li XJ, Li SH, Yi H, Vonsattel JP, Gusella JF, Hersch S, Auerbach W, Joyner AL, MacDonald ME (2000) Long glutamine tracts cause nuclear localization of a novel form of huntingtin in medium spiny striatal neurons in HdhQ92 and HdhQ111 knock-in mice. Hum Mol Genet 9:503-513.

White RJ, Reynolds IJ (1995) Mitochondria and Na+/Ca2+ exchange buffer glutamate-induced calcium loads in cultured cortical neurons. J Neurosci 15:1318-1328.

White RJ, Reynolds IJ (1996) Mitochondrial depolarization in glutamate-stimulated neurons: an early signal specific to excitotoxin exposure. J Neurosci 16:5688-5697.

White RJ, Reynolds IJ (1997) Mitochondria accumulate Ca2+ following intense glutamate stimulation of cultured rat forebrain neurones. J Physiol 498:31-47.

Williams K (1993) Ifenprodil discriminates subtypes of the N-methyl-D-aspartate receptor: selectivity and mechanisms at recombinant heteromeric receptors. Mol Pharmacol 44:851-859.

Xiong J, Verkhratsky A, Toescu EC (2002) Changes in mitochondrial status associated with altered Ca2+ homeostasis in aged cerebellar granule neurons in brain slices. J Neurosci 22:10761-10771.

Young AB, Greenamyre JT, Hollingsworth Z, Albin R, D'Amato C, Shoulson I, Penney JB (1988) NMDA receptor losses in putamen from patients with Huntington's disease. Science 241:981-983.

Zeitlin S, Liu JP, Chapman DL, Papaioannou VE, Efstratiadis A (1995) Increased apoptosis and early embryonic lethality in mice nullizygous for the Huntington's disease gene homologue. Nat Genet 11:155-163.

Zeron MM, Chen N, Moshaver A, Lee AT, Wellington CL, Hayden MR, Raymond LA (2001) Mutant huntingtin enhances excitotoxic cell death. Mol Cell Neurosci 17:41-53.

Zeron MM, Hansson O, Chen N, Wellington CL, Leavitt BR, Brundin P, Hayden MR, Raymond LA (2002) Increased sensitivity to N-methyl-D-aspartate receptor-mediated excitotoxicity in a mouse model of Huntington's disease. Neuron 33:849-860.

Zeron MM, Fernandes HB, Krebs C, Shehadeh J, Wellington CL, Leavitt BR, Baimbridge KG, Hayden MR, Raymond LA (2004) Potentiation of NMDA receptor-mediated excitotoxicity linked with intrinsic apoptotic pathway in YAC transgenic mouse model of Huntington's disease. Mol Cell Neurosci 25:469-479.

Zuccato C, Liber D, Ramos C, Tarditi A, Rigamonti D, Tartari M, Valenza M, Cattaneo E (2005) Progressive loss of BDNF in a mouse model of Huntington's disease and rescue by BDNF delivery. Pharmacol Res 52:133-139.

Zuccato C, Tartari M, Crotti A, Goffredo D, Valenza M, Conti L, Cataudella T, Leavitt BR, Hayden MR, Timmusk T, Rigamonti D, Cattaneo E (2003) Huntingtin interacts with REST/NRSF to modulate the transcription of NRSE-controlled neuronal genes. Nat Genet 35:76-83.

Zuccato C, Ciammola A, Rigamonti D, Leavitt BR, Goffredo D, Conti L, MacDonald ME, Friedlander RM, Silani V, Hayden MR, Timmusk T, Sipione S, Cattaneo E (2001) Loss of huntingtin-mediated BDNF gene transcription in Huntington's disease. Science 293:493-498.